

KDU 62:5 (05)

KOSOVA ACADEMY OF SCIENCES AND ARTS
SECTION OF NATURAL SCIENCES

RESEARCH
23
KËRKIME



PRISHTINA
2018

Dear readers,

Research is a scientific journal which is published by Academy of Sciences and Arts of Kosovo since 1979. A considerable number of papers in the field of natural sciences and applied sciences were issued during this period of time in spite of circumstances which were not always favorable. *The Journal* has been published almost continuously, despite its difficult journey. The '*Research*' Journal was among the key bearers of the scientific work of the Section of Natural Sciences which functions within the Academy of Sciences and Arts of Kosovo.

Until now the magazine has been published in Albanian and it was used by many generations of scientific researchers from the University and Academy.

Rapid development of science and technology in recent decades enabled a considerable increase in the exchange of scientific information through electronic platforms of scientific journals at a global level and the vast majority of them use English as a standard language. Therefore, such a situation imposes new approaches, as regards the use and presentation of scientific results, on Albanian-speaking scholars who aim at presenting their scientific achievements in front of a broader audience. This is also the goal of the '*Research*' Journal and it's our pleasure to present the first edition of the journal in English to the readers along with peer reviews prepared by international experts.

Editorial Board of the "*Research*" Journal

Të nderuar lexues,

Kërkime është revistë shkencore e Akademisë së Shkencave dhe e Arteve të Kosovës që botohet prej vitit 1979. Gjatë kësaj periudhe janë nxjerrë një numër i konsiderueshëm i punimeve në kuadër të shkencave të natyrës dhe të atyre të aplikuara, edhe pse rrethanat nuk kanë qenë çdo herë të favorshme. Përkundër këtij rrugëtimi të vështirë, ajo është botuar pothuajse në vazhdimësi. Revista Kërkime ishte një ndër bartëset kryesore të prezantimit të krijimtarisë shkencore të Shkencave të Natyrës të Akademisë së Shkencave dhe Arteve të Kosovës.

Revista deri më tani është botuar në gjuhën shqipe dhe është shfrytëzuar prej shumë gjeneratave të hulumtuesve shkencorë të Universitetit dhe të Akademisë.

Zhvillimi i hovshëm i Shkencës dhe i Teknologjisë në dekadat e fundit ka mundësuar një rritje të konsiderueshme të shkëmbimit të informacionit shkencor përmes platformave elektronike të revistave shkencore në nivel global duke përdorur komunikimin në gjuhën angleze si gjuhë standarde në shumicën dërmuese të tyre. Prandaj situata e tillë imponon qasje të reja të shfrytëzimit dhe prezantimit të rezultateve shkencore edhe për studiuesit shqipfolës në mënyrë që t'i prezantojnë të arriturat e tyre shkencore para një auditori edhe më të gjerë. Ky është edhe synimi i revistës *Research* dhe kemi kënaqësinë që tani t'ua ofrojmë të gjithë lexuesve - numrin e parë të revistës në gjuhën angleze, me vlerësim të punimeve prej ekspertëve homologë ndërkombëtarë.

Këshilli botues i revistës "*Research*"

KDU 62:5 (05)

AKADEMIA E SHKENCAVE DHE E ARTEVE E KOSOVËS
KOSOVA ACADEMY OF SCIENCES AND ARTS

SEKSIONI I SHKENCAVE TË NATYRËS
SECTION OF NATURAL SCIENCES

RESEARCH
23
KËRKIMË

Published/publikohet: Once a year /një herë në vit



PRISHTINË
2018

Editorial Board /Këshilli botues

Editor-in-Chief /

Kryeredaktori: Salih Gashi, KASA-ASHAK, Kosova

Secretary/Sekretari: Fetah Podvorica, KASA-ASHAK, Kosova

Other members: Qamil Haxhibeqiri, KASA-ASHAK, Kosova
Abdel Razik Sebak, Concordia University, Montreal, Canada
Myzafere Limani, KASA-ASHAK, Kosova

Editorial Office/Zyra Editoriale

Kosova Academy of Sciences and Arts

Akademia e Shkencave dhe e Arteve e Kosovës

Rr. "Agim Ramadani", Nr. 305, 10000, Prishtinë, Republika e Kosovës

Tel. +383 38 249 303; E-mail: research@ashak.org

Publisher/Publikuesi

Kosova Academy of Sciences and Arts

Akademia e Shkencave dhe e Arteve e Kosovës

Rr. "Agim Ramadani", Nr. 305, 10000 Prishtinë, Republika e Kosovës

Tel. +383 38 249 303; E-mail: research@ashak.org

KDU 62:5 (05)

AKADEMIA E SHKENCAVE DHE E ARTEVE E KOSOVËS
KOSOVA ACADEMY OF SCIENCES AND ARTS

SEKSIONI I SHKENCAVE TË NATYRËS
SECTION OF NATURAL SCIENCES

RESEARCH
23
KËRKIMË

Published/publikohet: Once a year /një herë në vit



PRISHTINË
2018

Copyright © ASHAK

PËRMBAJTJA

Fetah I. Podvorica

MODIFICATION OF THE SURFACES OF MATERIALS WITH
ARYL DIAZONIUM SALTS 1

Bajram Berisha

THE mRNA EXPRESSION OF SOME INSULIN-LIKE GROWTH
FACTOR (IGF) FAMILY MEMBERS DURING FINALE
FOLLICLE GROWTH IN THE BOVINE OVARY..... 31

Ardian Morina

NANOSCALE INTERFACE PROCESSES AND THEIR EFFECT
ON MACROSCALE TRIBOLOGICAL PERFORMANCE 47

Behxhet Mustafa, Dashnor Nebija, Avni Hajdari

EVALUATION OF ESSENTIAL OIL COMPOSITION, TOTAL
PHENOLICS, TOTAL FLAVONOIDS AND ANTIOXIDANT
ACTIVITY OF MALUS SYLVESTRIS (L.) MILL. FRUITS..... 71

Arbnor Pajaziti, Ilir Doçi, Endrit Toplica

DESIGN AND PROGRAMMING OF 3D PRINTED ROBOTIC
HAND 87

*Vitore Shala-Mayrhofer, Sali Aliu, Valbona Hobdari, Fetah Elezi,
Blerina Rexhepi, Ana Koci, Hans-Peter Kaul, Marc Lemmens*

INVESTIGATIONS ON THE RESISTANCE OF MAIZE
GENOTYPES FROM KOSOVO, ALBANIA AND AUSTRIA
AGAINST FUSARIUM GRAMINEARUM 113

MODIFICATION OF THE SURFACES OF MATERIALS WITH ARYL DIAZONIUM SALTS

Fetah I. Podvorica^{a, b, *}

Abstract

This mini-review deals with the aryl diazonium salts and their use for the modification of material surfaces. In the last two decades, these compounds have been employed to a great extent to decorate different types of carbon including graphene and carbon nanotubes, metals including coinage metals, semi-conductor and polymer materials with organic films. The reason for such expansion lie on the simplicity of preparation of aryl diazonium salts in aprotic, ionic liquid and aqueous solution, the possibility to introduce many functional groups as substituents and the low electroreduction potential of diazonium cation. The accent is pointed mainly on several experimental results that have been of crucial importance in the development of the subject.

Key words: Aryl diazonium salts, electrochemical reduction, aryl radical, monolayer, molecular junctions, biosensors

Introduction

Tailoring the surfaces of materials with organic molecules has shown the great potential of such assemblies to link the bulk properties

^a Akademia e Shkencave dhe e Arteve e Kosovës, Rr. “Agim Ramadani” nr 305, 10000 Prishtinë, Kosovë. fetahpodvorica@ashak.org

^b Departamenti i Kimisë, FSHMN, Universiteti i Prishtinës, Rr. “Nëna Terezë” nr. 5. 10000 Prishtinë, Kosovë.

* fetah.podvorica@uni-pr.edu

of materials (electrical, optical, thermal or mechanical) with that of attached molecules (that can increase hydrophobicity or hydrophilicity, resistance against corrosion, biocompatibility ...). The stability of the modified surfaces depends to a great extent in the type of the interaction between the substrate surface and the organic moiety. If the organic coating is simply deposited on the material surface, the interactions are weak and the layer may be deteriorate quite easily. Such techniques include physical and chemical vapor deposition (PVD, CVD) that permits the adhesion of uniform thin organic film on the material surface of different composition. [1,2]

Organic coatings that have a strong interaction with material surface are created by chemical methods and include the formation of self-assembled monolayers of thiols on gold surface and alcoxysilanes on metal oxides. [3,4] These very thin layers are attached with a chemical bond on the substrate surface. Aryl diazonium salts have received in the last 2 decades a lot of attention as coupling agents for the modification of the material surfaces. The break point in their use as such agents for the modification of carbon surfaces is the pioneer work of Pinson's group in Paris in 1992 when they described for the first time the modification of the carbon electrode surface during the electrochemical reduction of aryl diazonium salts in acetonitrile. [5]

Since that period these compounds has been used currently in many areas as very efficient species that permitted an easy way for the creation of modified material surfaces with thin organic films that are stable over the time under different conditions.

Their extensive use is based in the specific properties that this moiety contain: i) the ability to accept one electron under quite mild conditions, ii) the cleavage of the carbon nitrogen bond immediately after the charge transfer and the formation of the aryl radical, iii) the very high reactivity of such radicals. [6]

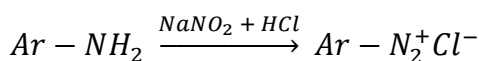
Synthesis of diazonium salts

Aryl diazonium salts are instable organic compounds that contain the benzene ring and the diazo cation with the general formula: $R-C_6H_4-N_2^+ A^-$, where R stands for H or other substituents and A^- is the anion: Cl^- , Br^- , BF_4^- etc. They are prepared by the reaction of primary aryl amines with nitrous acid in aqueous solution. Peter Griess was the first scientist who obtained an aryl diazonium salt in 1858. [7] The diazotization reaction is possible also in aprotic solvents, like

acetonitrile, when the primary amine reacts with isoamyl nitrite. Tetrafluoroborate anion, BF_4^- , is mostly used as counter ion instead of other anions that lead to a high instability that may cause explosions. When heated, aryl diazonium tetrafluoroborates provide fluoro arenes without any explosion. [8] This reaction permits in a very easy way to introduce fluorine atoms into a benzene ring. [9]

Modification of the surfaces of materials with aryl diazonium salts

The reaction of primary aryl amines to give the aryl diazonium salts in the presence of nitrite ion, in aqueous acid medium, is shown in the following scheme:



Scheme 1: The reaction of synthesis of aryl diazonium salts

Nitrous acid that is created instantly during the reaction of nitrite ions and the acid; it is then transformed to nitrosyl ion, NO^+ , that reacts with the amine to give the nitrosoamine. After several rearrangements an aryl diazonium ion is formed. [10] Aryl diazonium salts are stable in: i) aqueous solutions at low pH, at higher pH values are transformed at diazoates; ii) aprotic solvents and iii) ionic liquids. [11-13]

However, the limitations with aryldiazonium salts, such as intrinsic thermal instability, difficult isolation and purification procedures, and their explosive property, have driven researchers back to pursuing the targeted application in the same medium without their isolation. Belanger and co-workers reported in situ generation of an aryldiazonium salt from its corresponding amine by standard diazotization procedures without any purification step. [14,15]

Alkyl diazoniums are very instable compounds that decompose instantly to a nitrogen molecule and a carbocation, even at low temperature, which go on to form different products of elimination and substitution like alcohols, alkenes, alkyl dimers etc. [16,17]

Aryl diazonium salts, short time after their discovery, were used for the synthesis of azo compounds in order to prepare dyes by the industry. [18]

The electrochemical properties of aryl diazonium salts were studied on mercury electrode by polarography. The hanging mercury electrode was immersed in the solution of aryl diazonium salt with different organic solvents. Other electrodes like gold and platinum were used for further investigations. The authors have concluded that these compounds are easily reduced at the potential about 0 V toward SCE (Saturated calomel electrode) and they observed the formation of organomercuric products that contain phenyl units. [19, 20] The dediazotation reactions of aryl diazonium salts were possible in the presence of copper (I) chloride. This reaction that is known as Sandmeyer reaction permitted the creation of the chlorobenzene.

The different procedures for surface the modification

Tethering of metal surfaces with organic moieties ensuing the electrochemical reduction of vinylics and the oxidation of primary alkyl amines has shown the tremendous potential of different organic molecules to create thin polymer coatings that change drastically the properties of the material. [21,22] The reduction of vinylics is done under very negative potential ($E_p \sim -2.5$ V/Ag/AgCl for acrylonitrile and acrylate monomers) in aprotic solvents in glow box (extra anhydrous conditions) and permitted the modification of nickel surface. The key step during this process is the creation of the radical anion which attacks the metal surface and makes a bonded anion. The attached moiety can react with other monomers units in the solution and at this step initiates the polymerization reaction by the creation of a polymer chain. [23] These coatings are applied among others in microelectronics, for the removal of heavy metal ions in aqueous solution, immobilization of biomolecules etc. [24-26]

The oxidation of primary alkyl amines is done at quite positive potentials, higher than 1 V / SCE, so it is only possible on carbon and metal surfaces that withstand such high potentials like platinum. [27] The amine group after the loss of one electron is transformed into a radical cation which after the deprotonation forms the nitrogen centered aminyl radical. [28] This specie is able to bind to the electrode surface and to create a strongly bonded organic film. The composition and the morphology of these grafted layers is characterized with many surface analysis methods like: (XPS (X-Ray Photoelectron Spectroscopy), PMIRRAS (polarization Modulated InfraRed Reflexion Absorption Spectroscopy), AFM (Atomic Force Microscopy) etc. [28,29] The

grafted layers derived from primary alkyl amines with many substituents such as carboxylic groups, aminoacids, thionine, aminobenzidine, dendrimers and many others have been used for different applications: the detection and the attachment of biomolecules, the formation of layer-by-layer multi-layer films, the complexation of heavy metal ions and polyoxometalates etc. [27]

Electrochemical grafting of the aryl diazonium salts

The previous methods for electrochemical grafting of vinylics and amines have been restricted either on the use of very specific conditions (vinylic monomers, anhydrous conditions, high negative potentials) or materials that withstand the oxidation. The team of Pinson in Paris was looking for other compounds that are susceptible to link with a higher number of material surfaces under quite mild conditions. They have shown that aryl diazonium salts in acetonitrile solutions, are able to passivate surface of the glassy carbon electrode when reduced electrochemically. The experiment have done in the following conditions: the carbon electrode was immersed in the solution of 4-nitrobenzenediazonium tetrafluoroborate $c = 2$ mM in the presence of the supporting electrolyte, tetrabutyl ammonium tetrafluoroborate, NBu_4BF_4 . When the electrode potential is shifted from -0.5 V to -0.6 V/SCE; during the the first scan, one can see the appearance of the reduction current which increases progressively until the peak potential at 0.1 V, , see figure 1a. During the second scan the reduction wave have almost completely disappeared due to the electrode passivation, figure 1b. The only way for this phenomena to occur is the production of efficient reactive moieties that passivate the electrode surface during the reduction of the aryl diazonium cation. The facile reduction of aryl diazonium salts in such mild conditions is attributed to the strong withdrawing electron character of N_2^+ group and the high stability of the dinitrogen molecule as a leaving group which enable the easier reduction of these compounds than aryl halogens for example. [6] The presence of nitrophenyl groups attached on the electrode surface was proven with the following test: the passivated glassy carbon electrode was rinsed vigorously with acetone in an ultrasonic bath during 10 min and then is immersed in the solution of acetonitrile and supporting electrolyte.

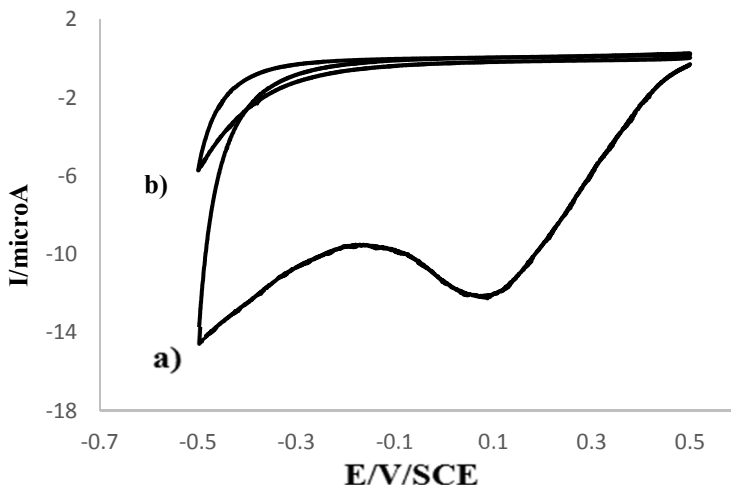
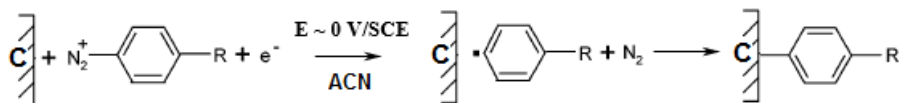


Fig. 1. Cyclic voltammetry of a glassy carbon electrode (diameter $d = 3$ mm) in ACN + 2 mM 4-nitrobenzediazonium tetrafluoroborate + 0.1 M NBu_4BF_4 solution; a) first and b) second scan. Scan rate, $v = 0.1$ V/s.

The modified electrode when biased under negative potential shows a reversible wave at around -1.2 V/SCE; this signal is due to the presence of nitrophenyl groups within the film as the same electrochemical signal is observed with a solution of nitrobenzene. This experiment is considered as the starting point for the use of aryl diazonium salts as efficient reactive for material surface modification. [5] The organic layer derived from the aryl diazonium salt is strongly linked with the carbon surface as it withstands the excursion of the potential between -2 to $+2$ V/SCE when the grafted electrode is used as working electrode. [30] The polyphenyl film resists higher temperatures than 400 °C and it is completely removed near 1000 °C which is very distinct comparing to very low stability of thiol SAMs, CVD and PVD deposited coatings. [31] The organic layer is stable under the ultrasonication in acetonitrile for 1 h. [6] The nitrophenyl groups grafted on glassy carbon surface remain stable without any deterioration at least a period of time of 6 months when exposed to laboratory conditions. [32] In all cases the same aryl radical obtained from the concerted electron transfer and carbon-nitrogen bond cleavage is involved as is shown in the scheme 2. A part of those radicals attack the surface and bind on it. The electrochemical grafting of aryl moieties can be run either in aprotic, in aqueous solution at different pH and ionic liquids. [6,11-13]



Scheme 2. The grafting of aryl groups after the electrochemical reduction of aryl diazonium salts

Other carbon materials were grafted with different aryl diazonium salts consequently like: highly ordered pyrolytic graphite (HOPG) [32,33], carbon fibers, carbon felts, carbon nanotubes, pyrolyzed photoresists (PPF), diamond [34] and graphene. [35,36] Several years after, the grafting of aryl diazonium salts was extended to noble and coinage metals [37-39] and semiconductors, SiH and GaAs, ITO (indium Tin Oxide) and polymer and glass surfaces. [40-44]

The electrochemical signal of the reduction of the aryl diazonium salts, like that in the figure 1, was not always observed on the iron surface and other coinage metal surface due to the oxidation of the coinage metal at lower potential as it is shown in the figure 2a in the case of the iron electrode in acetonitrile solution. [38] One can see that the iron electrode is oxidized at the potential $\sim 0 \text{ V/SCE}$ while the 4-nitrobenzodiazonium salt starts its reduction at higher potential, as it shown in the figure 1a, at around 0.4 V/SCE . This obstacle we overcome by using 4-n-butyl benzodiazonium salt which, due to the presence of the n-butyl group in the para position to the diazo group, has a much lower reduction potential than the 4-nitrobenzen diazonium and the oxidation potential of the iron, see figure 2b.

The grafted organic layer onto different metallic surfaces was characterized with different surface analysis methods (XPS, PMIRRAS, Rutherford BackScattering (RBS), AFM, and contact angle measurements and cyclic voltammetry. [38,45] These techniques permitted the characterization of the grafted film composition, its morphology and thickness and the surface concentration of aryl moieties. The thickness of the films varied from a very thin layer of 1 nm to several micrometers. [43] It depends on the electrolysis time, in the case of the grafting of zinc electrode surface with dodecylbenzen diazonium salt, is shown in the figure 3.

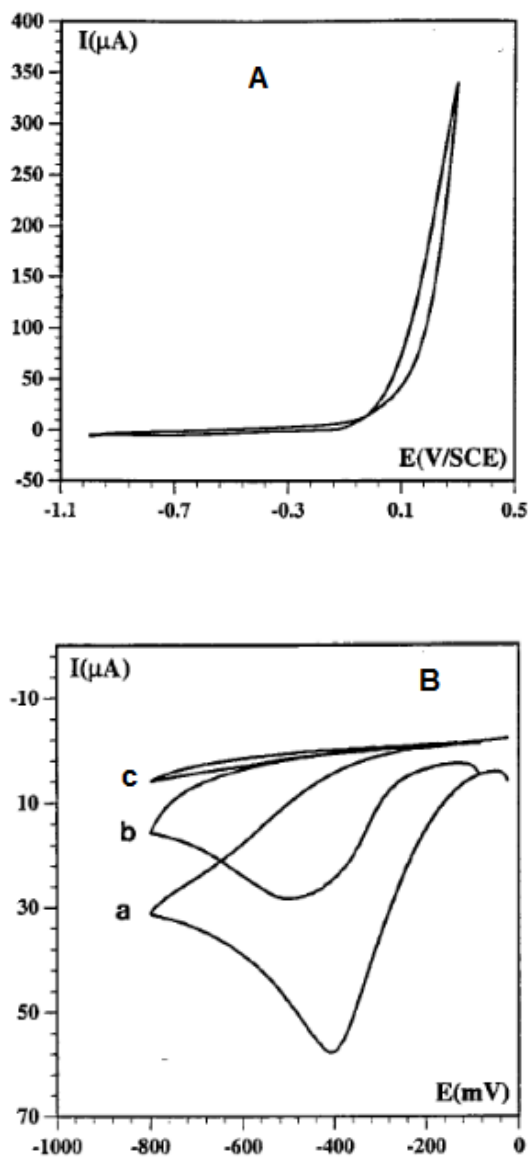


Fig. 2. The electrochemical behavior of the iron electrode in the: A) ACN + 0.1 M NBu₄BF₄ and B) + 5 mM 4-n-butylbenzediazonium tetrafluoroborate ; a) 1st, b) 2nd and c) 3rd scan. Scan rate, $\nu = 0.2$ V/s. Reproduced with permission from ref 38. Copyright 2001 American Chemical Society.

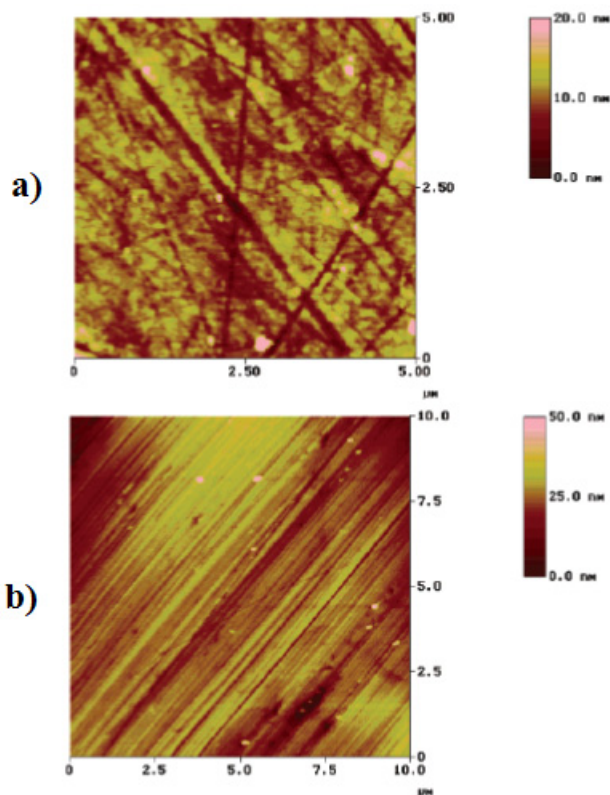


Fig. 3. AFM images of a polished zinc plate: a) bare and b) grafted with dodecylphenyl groups during 30 min at the potential $E = -0.65$ V/SCE.

Reproduced with permission from ref 45. Copyright 2003 American Chemical Society.

Parameters that control the film thickness

The film thickness of the organic layer obtained during the electrochemical reduction of aryl diazonium salts depends on several parameters such the nature of the aryl diazonium salt and its concentration, the grafting potential and the electric charge used during electrolysis. Its impact is shown in Figure 2, the modification of the zinc surface with a “thick” dodecylphenyl layer. By controlling the last parameter, Allongue et al. have confirmed by STM (Scanning Tunnelling Microscopy) and RBS measurements the formation of a monolayer of bromophenyl groups on a Si-H monocrystalline surface.[46] The impact of electrode potential in the film thickness is

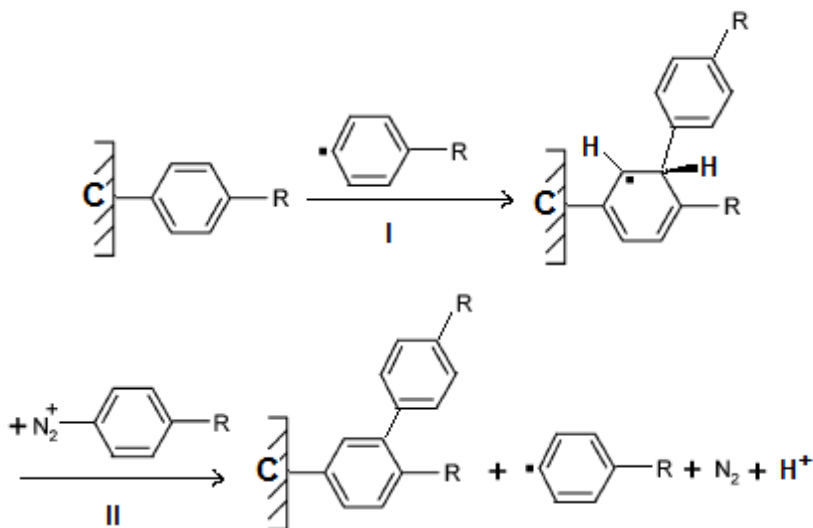
attested by AFM measurements on very flat PPF (Pyrolyzed photoresist carbon film) when it is covered with the organic film containing one or few phenyl layers.[47] The impact of concentration of the diazonium salt during the electrochemical reduction of aryl diazonium salts is seen when very low amounts of 4-nitrobenzediazonium salt are used to modify a carbon surface. [48] particularly during the chemical or spontaneous grafting of aryl diazonium salts on carbon and metal surfaces in aprotic and aqueous solution [49,50] These reducing substrates are able to give one electron to the diazonium cation and after the cleavage of C-N bond, the ensuing aryl radical is grafted on their surface. The open-circuit potential of the carbon and gold electrode immersed in the aprotic solution increased once the 4-nitrobenzenediazonium salt was added. [51,52] This fact evidenced the electron transfer from the electrode surface to the diazonium moiety.

The impact of the nature of the diazonium salts will be described in the next paragraph.

Multi-layer films

As we show just before the thickness of the polyphenyl film is very difficult to control due to the very high reactivity of aryl radicals which are not only reactive toward the electrode surface, as we have already seen in the scheme 2, but are able to form a multi-layer film. The mechanism of the growth of the layer is shown below in the scheme 3. The aryl radical attacks an already attached aryl group, step I, and forms a cyclohexadienyl radical through the homolytic substitution (S_H2) reaction, known also Gomberg reaction. [53,54] In the presence of aryl diazonium cation, the cyclohexadienyl radical behaves as a reducing agent which after its reoxydation creates a grafted dimer on the carbon electrode surface and another aryl radical able to continue further the growth of the layer. [55,56]

Thick aryl conducting layers > 100 nm are obtained with aryl groups containing redox active groups such nitro, anthraquinone groups by using cyclic voltammetry when the electrode potential was swept between the reduction potential of the diazonium cation and that of the redox group. [57] This action is indispensable for the continuous growth of the layer because the electrode is not passivated as during the standard procedure of the electrochemical grafting.



Scheme 3. Proposed mechanism for the formation of a multi-layer with aryl diazonium salts

Characterization of the surface-aryl bond

Since the discovery of the grafting reaction of aryl radicals with the carbon electrode surface the nature of the interaction between the organic moiety and the carbon or metal surface atoms was discussed.

We have already mentioned the stability of grafted layers over the time when exposed in the air or at high temperatures or under vigorous rinsing with different solvents under ultrasonication. A first experimental evidence concerning the existence of a strong adhesion of iron surface atoms and grafted carboxyphenyl groups derived from 4-carboxybenzodiazonium salt was obtained by XPS measurements. [58] The authors observed a peak at 283 eV which was attributed to a carbide compound created after the covalent bonding between iron surface atoms and carbon atoms.

ToFSIMS measurements made with a glassy carbon sample which surface was modified with 4-perfluorohexylphenyl and 4-nitrophenyl groups issued from 4-perfluorobenzodiazonium salt (N₂⁺-C₆H₄-C₆F₁₃) and 4-nitrobenzodiazonium salt respectively, has given several fragments which contained both carbon atoms that were part of glassy carbon and aryl groups: [CH₂-CH₂-C₆H₄-C₆F₁₃]⁺; [CH₂-CH₂-C₆H₃-

$C_6F_{13}-C_6H_4-C_6F_{13}]^+$. [55] These fragments gave, for the first time, an evidence of the existence of the chemical bond between surface carbon atoms and carbon pertaining to the phenyl ring and also the presence of dimers in the grafted film. Surface-enhanced Raman scattering (SERS) spectroscopy is a powerful method that permitted to ascertain the grafting of diazonium salts by observing the Raman signal characteristic of the Au-C(aryl) bond. [59]

By using this technique and Scanning Tunneling Microscopy (STM), De Feyter's group have observed, in situ, the formation of the chemical bond between carbon atoms on HOPG surface and nitrophenyl groups. [60] They have been able to detect the transformation of surface carbon atoms from Csp^2 into Csp^3 hybridization upon grafting the substituted phenyl moiety. They have done the reverse experiment with the help of a nano shaver which cleaved the bond between two carbon atoms at the interface and restored the presence of Csp^2 atoms once the grafted aryl layer was removed.

DFT (Density functional theory) calculations have been achieved by Jiang's group for systems composed of carbon or metallic surfaces modified with organic layers derived from the aryl diazonium salts; they have confirmed the presence of a strong interaction at the interface. [61,62] The adsorption energy of the aryl groups linked with the carbon atoms on the graphene layer is calculated and is quite high up to 265 kJ/mol. When attached to the six membered ring of graphene, the aryl group transforms a sp^2 into a sp^3 carbon atom, this modification gives a particularly stable configuration when the aryl groups are in para position.

They have found that metal surface atoms are able to create a chemical bond with aryl groups that stand upright (normal) with them. This result is of high importance because it proofs that aryl radicals are able to react with metal surfaces and create stable chemical bond instead of alkylthiols that are able to create self-assembled monolayers mostly with gold. The last assemblies have the adsorption energy much lower than aryl-metal bond. [63]

The formation of carbon-metal bond between the phenyl radical (without steric hindrance) and the atop copper surface atom prior to the grafting of organic moiety has been confirmed by comparing the reactivity of phenyl and 2,6-dimethylphenyl radical derived from 2,6-dimethylbenzediazonium salt (2,6-DMBD). [56] The last one cannot be grafted due to the presence of two methyl groups ortho to the phenyl

radical, the steric hindrance of which prevents the intermediate radical from reacting with the copper or carbon surface as presented in Figure 4. In the figure 4A, the absence of the ferricyanide signal on the glassy carbon electrode reflects the presence of an organic film on the surface; this film is obtained from 2,4 and 3,5- dimethylbenzondiazonium salts. In sharp contrast figure 4B presents an unmodified signal upon scanning reflecting the absence of the grafting.

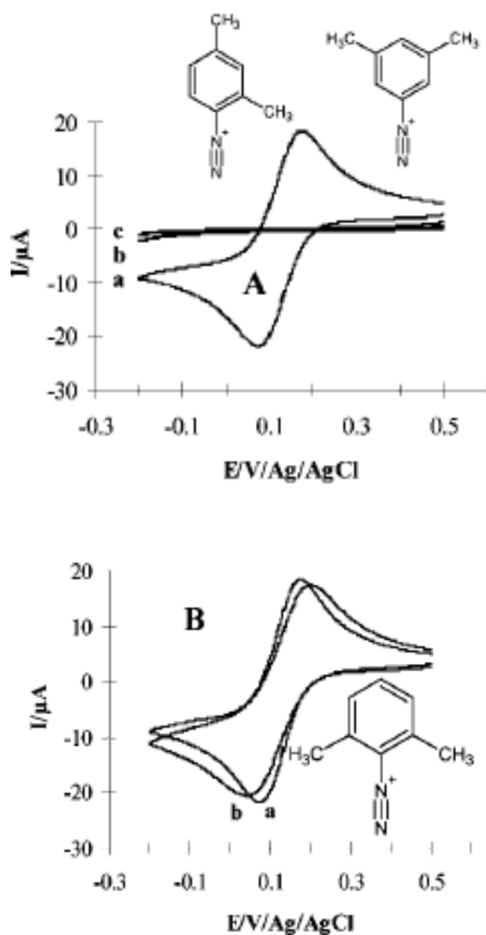


Fig. 4. Electrochemical behavior of ferricyanide redox probe with a glassy carbon electrode: (A)(a) bare and (b) after the modification with 3,5-dimethylbenzondiazonium salt; (B)(a) bare and (b) after the treatment with 2,6-dimethylbenzondiazonium salt. Reproduced with permission from ref 56. Copyright 2009 American Chemical Society.

This lack of surface reactivity of 2,6-DMBD was confirmed by DFT calculations which indicate that the presence of two methyl groups drastically decreases the bonding energy between the copper atom and the carbon of the 2,6-dimethylphenyl radical and obliges the copper atom to move upward (Figure 5c). This phenomenon is not observed in the case of the phenyl and 2-methylphenyl radicals (Figure 5a and b). [56]

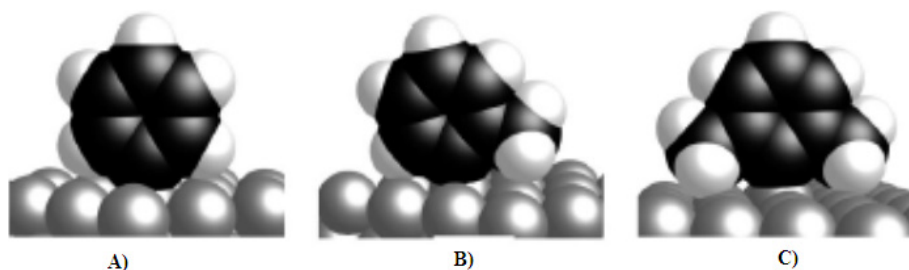


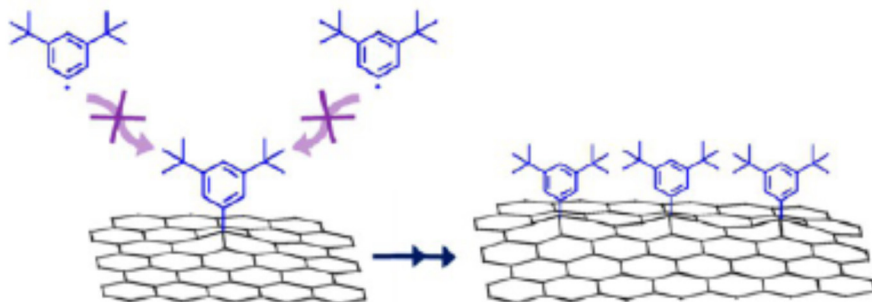
Fig. 5. The attachment of organic layer on the copper atop atoms: A) phenyl; B) 2-MBD and C) 2,6-DMBD. Reproduced with permission from ref 56. Copyright 2009 American Chemical Society.

Formation of monolayers and multi layers

As already mentioned, due to the high reactivity of aryl groups, it is very difficult to control the spatial distribution of these species especially their vertical extension; they form a multilayer film in most of the cases (Scheme 3). By controlling the electric charge and the electrode potential it was possible to create very thin organic layers containing one or few phenyl layers. [46,47] Now we will see the impact of the nature of the aryl diazonium salt on the film thickness. Daasbjerg et al have prepared a diazonium salt derived from a diaryldisulfide that has been successfully grafted and formed a multilayer film. [64] As disulfide groups are electrochemically active when they are biased at negative potentials < -1.3 V/SCE the S-S bond is broken that enabled the cleavage of the entire polymer entities from the carbon surface. The carbon surface remains grafted by a monolayer of thiophenyl groups

The first successful tentative to form a single monolayer by direct electrochemical grafting was achieved with the aryl diazonium salt that had bulky groups (tert-butyl) in the 3,5 positions in the benzene ring, see scheme 4. [65] Those groups hindered the attack of bis-t-

butylphenyl radicals on already attached groups due to steric effects. The thickness of the monolayer was measured by ellipsometry, AFM and STM and is about 1 nm as is shown in the figure 5. [60,65] STM image of an HOPG surface completely covered by the organic layer has the height profile, shown in the inset of the image ~ 1 nm. [60]



Scheme 4. Formation of monolayer during the electrochemical reduction of bis-t-butyl-benzendiazonium salt according the paper. Reproduced with permission from ref 60. Copyright 2015 American Chemical Society.

Another approach involved the control of number of the aryl radicals in the solution during the electrochemical reduction of the aryl diazonium salt. [66] This control is achieved with a radical scavenger DPPH (2,2-diphenyl-1-picrylhydrazyl) introduced in the solution (at higher concentration than the aryl diazonium salt) and that traps the excess of aryl radicals once the monolayer with nitrophenyl moieties is established.

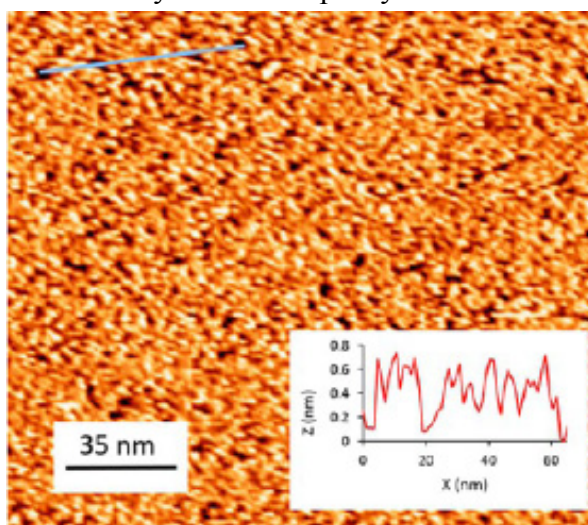


Fig. 6. STM image of a HOPG surface grafted with 3,5-t-butylphenyl groups. The inset shows the film height profile. Reproduced with permission from ref 60. Copyright 2015 American Chemical Society.

Some applications

Aryl diazonium grafted layers have found many applications in many areas: In this short review we will describe few of them: anticorrosive properties, sensors, ATRP (atom transfer radical polymerization) and molecular junctions.

Anticorrosive properties

Aryldiazonium salts containing alkyl or perfluoroalkyl groups in the para position to the diazonium group grafted onto iron and stainless steel surface have shown anticorrosive properties. This effect is measured by two electrochemical methods linear voltammetry and impedance. [67,68] Polarization resistance of the iron electrode, which is reciprocally dependent to the corrosion current, increased linearly when it was covered with organic layer of alkyl substituted aryl groups groups with different chain length (Figure 7). The inhibition efficacy reached 92 % similar to some classic inhibitors but at their difference one does not need to maintain the electrode to immerse in the inhibitor solution.

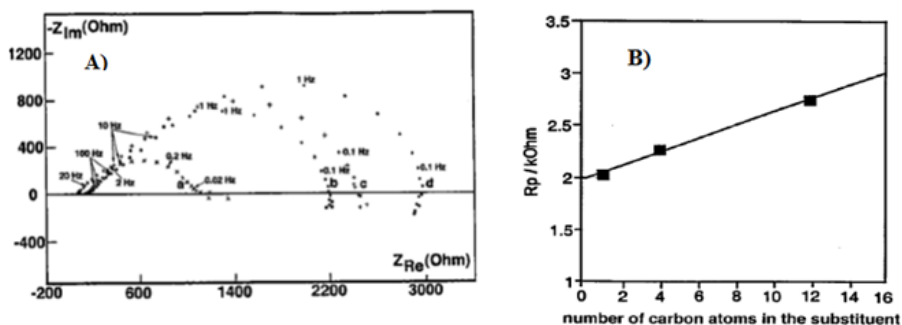


Fig. 7. A) The measurement of the polarization resistance, R_p , of an iron electrode in aqueous acid medium by impedance: a) bare; and modified with b) 4-methylphenyl; c) 4-butylphenyl and d) 4-dodecylphenyl groups. B)

Linear increase of R_p with carbon atoms number. Reproduced with permission from ref 67. Copyright 2002 American Chemical Society.

Sensors

The ability to form thin organic layers strongly attached to the substrate surface at the contrary of thiol SAMs gold, has promoted the aryl diazonium salts as favorite candidates for the creation of chemical sensors and biosensors.

The state of art for the construction of sensors is beyond the scope of the review and we will focus only on some applications. In the case of chemical sensors the aryl layers substituted with specific groups like hydroquinone, carboxylic, amine groups served for the pH sensing, NADH oxidation, metal ion complexation such as cadmium, lead, uranium and copper. [69-72] The organic layer issued from a single or a mixture of diazonium salts attached on the transducer surface may have additional functions: to react with a specific receptor component like an enzyme, antibody a peptide etc. that will serve for the detection of the targeted molecule and to prevent nonspecific interactions with other molecules.

For example, the grafting of electrode surfaces with mixed layers derived from two different diazonium salts containing oligo(ethylene oxide) chain or aryl groups with opposite charges permitted the preparation of the sensor platforms able to avoid the nonspecific protein adsorption such as bovine serum albumin. [73,74] This capacity of aryl diazonium platforms has been used for the preparation of immunobiosensors. The mixed layer was composed with a molecular wire that contain a ferrocene moiety terminated by a biotin and a chain that prevent the specific adsorption, see figure 8. [74] The biotin served to complex the antibody and this interaction is evidenced with the decrease of the current. The immunosensor has been able to detect very low concentrations of the antibody until 30 ng/L.

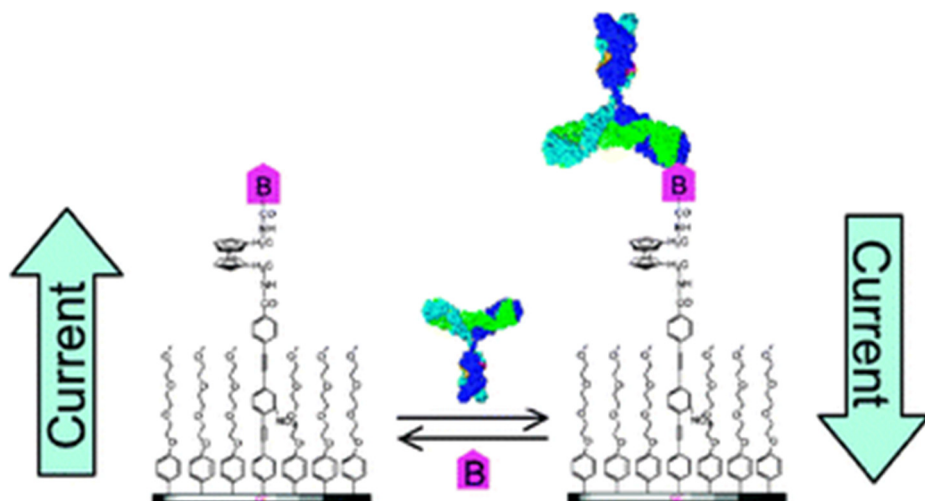


Fig. 8. Scheme of the functioning of an immunobiosensor for the detection of an antibody. Reproduced with permission from ref 74. Copyright 2008 Royal Society of Chemistry.

The grafting of SiH surfaces with 4-nitrophenyl groups, and the ensuing transformation of NO_2 groups to NH_2 have permitted the post modification and the creation of Silicon nanowires that contain the antibody sensible for targeting the prostate cancer risk biomarker, 8-hydroxydeoxyguanosine. [75] The detection limit was very low, about 1 ng/ml .

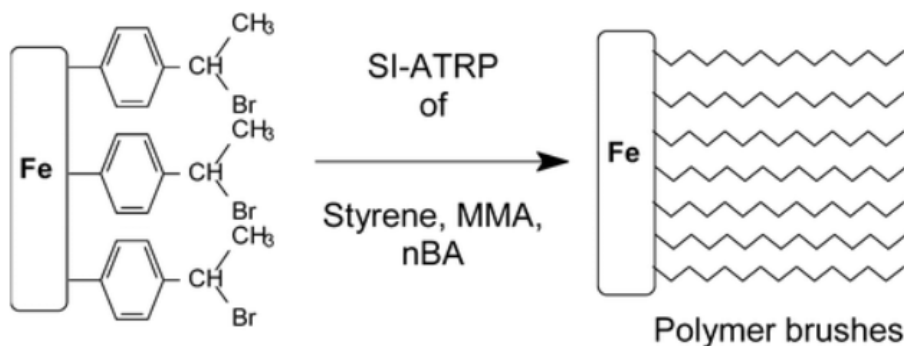
SI-ATRP (Surface Initiated Atom Transfer Radical Polymerization)

Tailoring the material surfaces with polymers of controlled composition and thickness is an important step in the architecture of nanomaterials and in the increase of the stability of these entities toward the environment. Atom Transfer Radical Polymerization (ATRP) is a widely used technique to create polymer brushes that can be attached or deposited on the surface. This method consist in the formation of well-defined polymer chains with precise length thanks to the ability of the radical control. [76,77]

Alkyl halides, RX , are used as initiators of the polymerization and may be activated only in the presence of transition metal complexes at lower state oxidation, ML_1 otherwise are considered as dormant species. The metal complex enables the creation of the alkyl radical R^* , after the oxidation of the metal ion and the ligand transfer from the RX

to the ML_1 give ML_2 . The generated radical reacts with the monomer, mostly alkyl methacrylate, and initiates the polymerization process, which is the propagation step. The process can be stopped at every moment with the reverse reaction between R^* and the ML_2 giving halogen-terminated polymer chain and ML_1 . The process may start again so this kind of polymerization is called also living polymerization.

Surface Initiated ATRP (SI) is an important derivation of the ATRP which permits the growth of polymer brushes from the initiators that are strongly attached on the material surface. [78] The principle of the method is given in the following example, see scheme 8, when first an iron surface was modified by phenyl moieties containing bromine atom at the end of the alkyl chain. [79] Strongly attached layer may serve as a platform for the polymerization reaction in the presence of n-butyl methacrylate monomer and Cu(II) ions, that means to initiate SI-ATRP. Homogeneous polymer brushes are obtained with different thickness according to the reaction time. The advantage of this modification procedure to that of ATRP is the strong adherence of the film on the material surface. The SI-ATRP may be initiated also by the diazonium groups on the electrode surface when phenylacetic diazonium salt is grafted on the electrode by the oxidation of the carboxylate group. [80]



Scheme 8. Principle of the SI-ATRP initiated by bromine atoms at the end of bromopropylphenyl layers. Reproduced with permission from ref 79. Copyright American Chemical Society.

Molecular Junctions

Organic electronics has been developed for many years after the discovery of conducting polymers and now is currently used for many purposes like: organic transistors, photovoltaics, organic light-emitting

diodes (OLED) etc. This progress has made possible to create the so-called hybrid electronics which combines the silicon based microelectronics and unique structural, electronic and functional properties of organic molecules. [81] The thicknesses of these devices are between 40 nm to 100 μm . The electron transfer between two conductors in such high distances is made by “Hopping” by redox exchange inside the electronic device. [82] Molecular junctions are composed typically by a single molecule attached between two electrodes, that are at a very short distance < 10 nm (this is the main difference with organic electronics). At this short range distance the electron transfer is made by tunneling.

In the molecular junctions the connection between the molecule wire and the two electrodes is of crucial importance and directly affects the current-voltage and stability characteristics. The use of diazonium salts has greatly overcome the difficulty of making stable molecular junctions with SAMs and Langmuir-Blodgett monolayers due to their low stability. Molecular junctions with aryl diazonium salts are made with silicon, [83] carbon, [84] and gold surfaces and the bond strength is at least twice that of SAMs. [82,85] The direct evidence of the formation of a single molecular junction between a bisdiazonium salt and gold electrodes shown in Figure 9. By using the STM break junction technique and a bipotentiostat the authors monitored the electrochemical reduction of the bisdiazonium salt, figure 9a. The decrease of the height of the current reduction peak is the direct proof of the gold surface modification with aryl group. When both electrodes are approached at very short distance a molecular junction is formed between them. The creation of the molecular bridge is also evidenced by measurements of the conductance with STM at different potentials, Figure 9b. In the absence of organic layer the conductance shows an exponential decay at atomic distance between two electrodes, for potential values higher than -300 mV due to the lack of the grafting of the aryl radicals. For lower values than -300 mV the gold surfaces are modified with the organic layer derived from the bisdiazonium and a conductance peaks appeared at $0.0025 G_0$, $G_0 = 2e^2/2h$ – quantum conductance, indicating the formation of a single-molecule junction. This kind of the experiment permits the measure of the conductance of a single molecule.

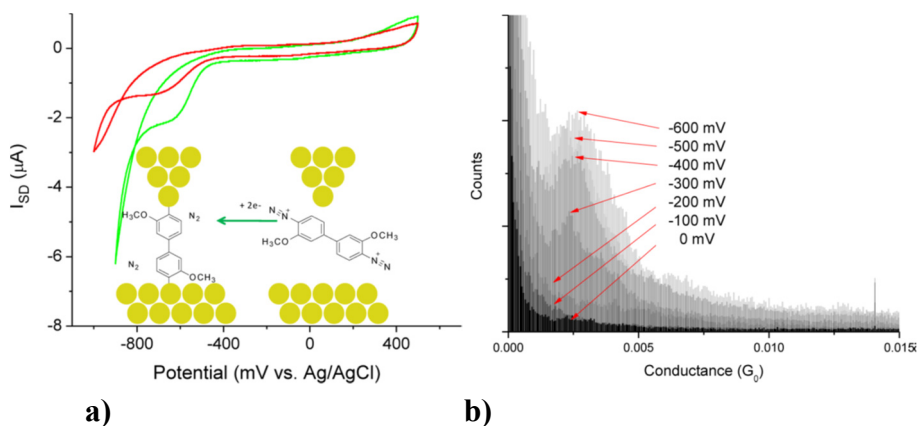


Fig. 9. a) Cyclic voltammogram of the bisdiazonium molecule used for the creation of a molecular junction. b) Conductance histograms in linear scale taken at electrochemical grafting potentials ranging from 0 to -600 mV vs Ag/AgCl. Reproduced with permission from ref 85. Copyright 2013 American Chemical Society.

Conclusion and perspectives

The grafting of strongly attached aryl moieties that contain different substituents in various material surfaces is now a well-established method. It is simple to apply and the production of the aryl radical is done by different ways of activation of diazonium cation. The existence of the covalent bond is demonstrated by experimental methods and theoretical calculations. The expansion of the use of nanomaterials like nanoparticles, nanorods, graphene and carbon nanotubes will put even more in evidence the usefulness of aryl diazonium salts. The use of diazonium salts has been transferred from university laboratories to industry: coating of stents (Sinomedical), microelectronics (Aveni) and music amplifiers (University of Alberta) and more industrial applications are expected.

References

- [1] Matthews, A. and Rohde, S.L. Coatings and Surface Engineering: Physical Vapor Deposition. Book. Ed. Wiley 2015.
- [2] Yanguas-Gil, A. Physical and Chemical Vapor Deposition Techniques. In: Growth and Transport in Nanostructured Materials. Ed. Springer 2017.
- [3] Love, J.C., Estroff, L.A., Kriebel, J.K., Nuzzo, R.G. and Whitesides, G.M. Self-Assembled Monolayers of Thiolates on Metals as a form of Nanotechnology. *Chem. Rev.* 2005, *105*, 1103-1170.
- [4] Bradley, D.C. Metal alkoxides as precursors for electronic and ceramic materials. *Chem. Rev.*, 1989, *89*, 1317-1322.
- [5] Delamar, M, Hitmi, R, Pinson, J. and Savéant J-M. Covalent modification of carbon surfaces by grafting of functionalized aryl radicals produced from electrochemical reduction of diazonium salts. *J. Am. Chem. Soc.*, 1992, *114*, 5883-5884.
- [6] Pinson, J and Podvorica, F. Attachment of organic layers to conductive or semiconductive surfaces by reduction of diazonium salts. *Chem. Soc. Rev.*, 2005, *34*, 429-439.
- [7] Griess, P. Preliminary notice of the reaction of nitrous acid with picramic acid and aminonitrophenol . *Annalen der Chemie und Pharmacie*, 1858, *106*, 123-125.
- [8] Balz, G. and Schiemann, G. Uber aromatische Fluorverbindungen, I.: Ein neues Verfahren zu ihrer Darstellund. *Chem. Ber.*, 1927, *60*, 1186-1190.
- [9] Galli, C. Radical reactions of arenediazonium ions: An easy entry into the chemistry of the aryl radical. *Chem. Rev.*, 1988, *88*, 765-792.
- [10] Hughes, E.D., Ingold, C.K., Ridd, J.H. Nitrosation, diazotization and deamination. Part I. Principles, background, and method for the kinetic study of diazotization. *J. Chem. Soc.*, 1958, 58-65.
- [11] Pazo-Llorente, R., Bravo-Diaz, C. and Gonzalez-Romero, E. pH Effects on Ethanolysis of Some Arenediazonium Ions: Evidence for Homolytic Dediazoniatioon Proceeding through Formation of Transient Diazo Ethers. *Eur. J. of Org. Chem.*, 2004, *15*, 3221-3226.
- [12] Podvorica, F. I.; Kanoufi, F.; Pinson, J.; Combellas, C. Spontaneous Grafting of Diazoates on Metals. *Electrochim. Acta* 2009, *54*, 2164-2170.

-
- [13] Ghilane J., Martin, P., Fontaine, O., Lacroix, J.-C. and Randriamahazaka, H. Modification of carbon electrode in ionic liquid through the reduction of phenyl diazonium salt. Electrochemical evidence in ionic liquid. *Elec. Comm.*, 2008, 10, 1060-1063.
- [14] Baranton, S. and Belanger, D. Electrochemical Derivatization of Carbon Surface by Reduction of in Situ Generated Diazonium Cations. *J. Phys. Chem. B* 2005, 109, 24401–24410.
- [15] Chamoulaud, G. and Belanger, D. Spontaneous Derivatization of a Copper Electrode with in Situ Generated Diazonium Cations in Aprotic and Aqueous Media. *J. Phys. Chem. C.*, 2007, 111, 7501-7507.
- [16] Patai, S. The Chemistry of Diazonium and Diazo Groups. Publisher Wiley, New York, 1978.
- [17] Streitwieser, A. and Schaeffer, W.D. Stereochemistry of the Primary Carbon. VI. The reaction of optically active 1-Aminobutane-1-d nitrous acid. Mechanism of the amine-nitrous acid reaction. *J. Am. Chem. Soc.*, 1957, 79, 2888-2893.
- [18] Merino, E. Synthesis of azobenzenes: the coloured pieces of molecular materials. *Chem. Soc. Rev.*, 2011, 40, 3835-3853.
- [19] Elofson, R.M. and Gadallah, F.F. Substituent effects in the polarography of aromatic diazonium salts. *J. Org. Chem.*, 1969, 34, 854-857.
- [20] Gadallah, F.F and Elofson, R.M. Arylation of aromatic compounds by electrochemical reduction of benzenediazonium tetrafluoroborate in aprotic solvents. *J. Org. Chem.*, 1969, 34, 3335-3338.
- [21] Lecayon, G., Bouizem, Y., Le Gressus, C., Reynaud, C., Boiziau, C. and Juret, C. Grafting and growing mechanisms of polymerised organic films onto metallic surfaces. *Chem. Phys. Lett.*, 1982, 91, 506-510.
- [22] Barbier, B., Pinson, J., Desarmot, G. and Sanchez, M. Electrochemical Bonding of Amines to Carbon Fiber Surfaces toward Improved Carbon-Epoxy Composites. *J. Electrochem. Soc.*, 1990, 137, 1757-1764.
- [23] Bureau, C. and Delhalle, J. Synthesis and Structure of Polymer/Metal Interfaces: a Convergence of Views between Theory and Experiment. *J. Surf. Anal.*, 1999, 6, 159 – 170.
- [24] Charlier, J., Baranton, L., Bureau, C. and Palacin, S. Directed Organic Grafting on locally Doped Silicon Substrates. *ChemPhysChem*, 2005, 6, 70-74.

- [25] Viel, P., Dubois, L., Lyskawa, J., Salle, M. and Palacin, S. New Concept to remove Heavy Metals from liquid waste based on Electrochemical pH-switchable Immobilized Ligands. *Appl. Surf. Sci.*, 2007, 253, 3263-3269.
- [26] Ameer, S., Bureau, C., Charlier, J. and Palacin, S. Immobilization of biomolecules on electrodes modified by electrografted films. *J. of Phys. Chem. B*, 2004, 108, 13042-13046.
- [27] Podvorica, F.I. Chapter: Non-Diazonium Organic and Organometallic Coupling Agents for Surface Modification in the book Aryl Diazonium Salts New coupling agents in Polymer and Surface Scienc. Published by Wiley in 2012, Weinheim Germany.
- [28] Adenier, A., Chehimi, M.M., Gallardo, I., Pinson, J. and Vila, N. Electrochemical Oxidation of Aliphatic Amines and Their Attachment to Carbon and Metal Surfaces. *Langmuir*, 2004, 20, 8243-8253.
- [29] Herlem, M., Fahys, B., Herlem, G., Lakard, B., Reybier, K., Trokourey, A., Diasco, T., Zairi, S. and Jaffrezic,-Renault, N. Surface modificagtion of p-Si by a polyethylenimine coating:influence of the surface pre-treatment. Application to a potentiometric transducer as pH sensor. *Electrochim. Acta*, 2002, 47, 2597-2602.
- [30] D'Amours, M. and Belanger, D. Stability of substituted phenyl groups electrochemically grafted at carbon electrode surface. *J. Phys. Chem. B*, 2003, 107, 4811- 4817.
- [31] Berisha, A., Chehimi, M., Pinson, J. and Podvorica, F. Book Chapter. In: *Electroanalytical Chemistry, A Series of Advances*. Ed. by Allen J. Bard and Cynthia G. Zoski, CRC Press 2015, 26, 115–224.
- [32] Allongue, P., Delamar, M., Desbat, B., Fagebaume, O., Hitmi, R., Pinson, J. and Saveant, J.-M. Covalent Modification of Carbon Surfaces by Aryl Radicals Generated from the Electrochemical Reduction of Diazonium Salts. *J. Am. Chem. Soc.*, 1997, 119, 201 – 207.
- [33] Kariuki, J.K. and McDermott M.T. Formation of Multilayers on Glassy Carbon electrodes via the Reduction of Diazonium Salts. *Langmuir*, 2001, 17, 5947-5951.
- [34] Lud, S.Q., Steenackers, M., Jordan, R., Bruno, P., Gruen, D.M., Feulner, P., Garrido, J.A. and Stutzman, M. Chemical grafting of biphenyl self-assembled monolayers on ultrananocrystalline diamond. *J. Am. Chem. Soc.*, 2006, 128, 16884-16891.
- [35] McCreery, R.L. Advanced Carbon Electrode Materials for Molecular Electrochemistry. *Chem. Rev.*, 2008, 108, 2646-2687.

- [36] Liu, G. Z.; Liu, J.; Böcking, T.; Eggers, P. K.; Gooding, J. J. The Modification of Glassy Carbon and Gold Electrodes with Aryl Diazonium Salt: The Impact of the Electrode Materials on the Rate of Heterogeneous Electron Transfer. *Chem. Phys.* 2005, *319*, 136–146.
- [37] Pinson, J., Fagebaume, O. and Podvorica, F. Metal with modified surface, preparation method, and use, French Patent 2001, PCT/FR2001/000388; US Patent 2005 7,182,822.
- [38] Adenier, A., Bernard, M.C., Desbat, B., Cabet-Deliry, E., Chehimi, M.M., Fagebaume, O., Pinson, J. and Podvorica, F. Covalent Modification of Iron Surfaces by Electrochemical Reduction of Aryldiazonium Salts. *J. Am. Chem. Soc.*, 2001, *123*, 4541-4549.
- [39] Bernard, M. C., Chausse, A., Deliry, E., Chehimi, M.M., Pinson, J., Podvorica, F. and Vautrin-Ul, C. Organic Layers Bonded to Industrial, Coinage and Noble Metals through Electrochemical Reduction of Aryldiazonium Salts. *Chem. Mater.*, 2003, *15*, 3540-3552.
- [40] DeVilleneuve, C.H., Pinson, J., Bernard, M.C. and Allongue, P. Electrochemical formation of close-packed phenyl layers on Si(111). *J. Phys. Chem. B*, 1997, *101*, 2415-2420.
- [41] Stewart, M. P.; Maya, F.; Kosynkin, D. V.; Dirk, S. M.; Stapleton, J. J.; McGuinness, C. L.; Allara, D. L.; Tour, J. M. Direct Covalent Grafting of Conjugated Molecules onto Si, GaAs, and Pd surfaces from Aryldiazonium Salts. *J. Am. Chem. Soc.*, 2004, *126*, 370–378.
- [42] Maldonado, S., Smith, T.J., Williams, R.D., Morin, S., Barton, E. and Stevenson, K.J. Surface modification of indium tin oxide via electrochemical reduction of aryldiazonium cations. *Langmuir*, 2006, *22*, 2884-2891.
- [43] Adenier, A., Combellas C., Kanoufi F., Pinson J. and Podvorica F. I. Formation of Polyphenylene Films on Metal Electrodes by Electrochemical Reduction of Benzenediazonium Salts. *Chem. Mater.*, 2006, *18*, 2021-2029.
- [44] Zheng, W.; van den Hurk, R.; Cao, Y.; Du, R.; Sun, X.; Wang, Y.; McDermott, M. T.; Evoy, S. Aryl Diazonium Chemistry for the Surface Functionalization of Glassy Biosensors. *Biosensors* 2016, *6*, 8.
- [45] Bernard, M.C., Chausse, A., Deliry, E., Chehimi, M.M., Pinson, J. Podvorica, F. and Vautrin-Ul, C. Organic Layers Bonded to Industrial, Coinage and Noble Metals through Electrochemical Reduction of Aryldiazonium Salts. *Chem. Mater.*, 2003, *15*, 3540 – 3552.

- [46] Allongue, P., de Villeneuve, C.H., Cherouvrier, G., Cortes, R. and Bernard, M.-C. Phenyl layers on H-Si(111) by electrochemical reduction of diazonium salts : monolayer versus multilayer formation. *J. Electroanal. Chem.*, 2003, 550, 161-174.
- [47] Anariba, F., DuVall, S.H. and McCreery, R.L. Mono- and Multilayer Formation by Diazonium Reduction on Carbon Surfaces Monitored with Atomic Force Microscopy “Scratching”. *Anal. Chem.*, 2003, 75, 3837-3844.
- [48] Andrieux, C.P. and Pinson, J. The Standard Redox Potential of the Phenyl Radical/Anion Couple. *J. Am. Chem. Soc.*, 2003, 125, 14801-14806.
- [49] Adenier, A., Cabet-Deliry, E., Chausse, A., Griveau, S., Mercier, F., Pinson, J. and Vautrin-UI, C. Grafting of nitrophenyl Groups on Carbon and Metallic Surfaces without Electrochemical Induction. *Chem. Mater.*, 2005, 17, 491-501.
- [50] Combellas C., Delamar M., Kanoufi F., Pinson J. and Podvorica F. I. Spontaneous grafting of Iron Surfaces by Reduction of Aryldiazonium Salts in Acidic Water. Application to the protection against corrosion. *Chem. Mater.*, 2005, 17, 3968-3975.
- [51] Le Floch, F., Simonato, J.-P. and Bidan, G. Electrochemical signature of the grafting of diazonium salts: A probing parameter for monitoring the electro-addressed functionalization of devices. *Electrochim. Acta*, 2009, 54, 3078-3085.
- [52] Lehr, J., Williamson, B.E., Flavel, B.S. and Downard, A. Reaction of Gold Substrates with Diazonium Salts in Acidic Solution at Open-Circuit Potential. *Langmuir*, 2009, 25, 13503-13509.
- [53] Fukurumi, S. and Kochi, J.K. Mechanism of Homolytic Substitution (SH₂) Reactions. Radical Chain Cleavage of Alkylmetals by Photochemically Generated Iodine Atoms. *J. Org. Chem.*, 1980, 45, 2654 – 2662.
- [54] Gomberg, M. and Bachmann, W.E. The synthesis of biaryl compounds by means of the diazo reaction. *J. Am. Chem. Soc.*, 1924, 46, 2339-2343.
- [55] Combellas C., Kanoufi F., Pinson J. and Podvorica F. I. Time-of-flight Secondary Ion Mass Spectroscopy Characterization of the Covalent Bonding between a Carbon Surface and Aryl groups. *Langmuir*, 2005, 21, 280 - 286.
- [56] Combellas, C. Jiang, De-en, Kanoufi, F., Pinson, J. and Podvorica, F. I. Steric effects in the reaction of aryl radicals on surfaces. *Langmuir*, 2009, 25, 286-293.

- [57] Ceccato, M., Bousquet, A., Hinge, M., Pedersen, S.U. and Daasbjerg, K. Using a Mediating Effect in the Electroreduction of Aryldiazonium Salts to Prepare Conducting Organic Films of High Thickness. *Chem. Mater.*, 2011, 23, 1551-1557.
- [58] Boukerma, K., Chehimi, M.M., Pinson, J. and Blomfeld, C. X-Ray Photoelectron Spectroscopy Evidence for the covalent Bond between an Iron Surface and Aryl Groups Attached by the Electrochemical Reduction of Diazonium Salts. *Langmuir*, 2003, 19, 6333-6335.
- [59] Laurentius, L., Stoyanov, S.R., Gusarov, S., Kovalenko, A., Du, R., Lapinski, G.P. and McDermott, M.T. Diazonium-Derived Aryl Films on Gold Nanoparticles: Evidence for a Carbon-Gold Covalent Bond. *ACS Nano*, 2011, 5, 4219-4227.
- [60] Greenwood, J., Phan, T.H., Fujita, Y., Li, Z., Ivashenko, O., Vanderlinden, W., Gorp, H.V., Frederickx, W., Lu, G., Tahara, K., Tobe, Y., Uji-I, H. Mertens, F.L., and De Feyter, S. Covalent Modification of Graphite Using Diazonium Chemistry: Tunable Grafting and Nanomanipulation. *ACS Nano*, 2015, 9, 5520-5535.
- [61] Jiang, D., Sumpster, B.G. and Dai, S. How do Aryl Group Attach to a Graphene Sheet? *J. Phys. Chem. Lett.*, 2006, 110, 23628-23632.
- [62] Jiang, D., Sumpster, B.G. and Dai, S. Structure and Bonding between an Aryl Group and Metal Surfaces. *J. Am. Chem. Soc.*, 2006, 128, 6030-6031.
- [63] Gooding, J.J. Advances in Interfacial Design for Electrochemical Biosensors and Sensors: Aryl Diazonium Salts for Modifying Carbon and Metal Electrodes. *Electroanalysis* 2008, 20, 573-582.
- [64] Nielsen, L.T., Vase, K.H., Dong, M., Besenbacher, F., Pedersen, S.T. and Daasbjerg, K. Electrochemical Approach for Constructing a Monolayer of Thiphenolates from Grafted Multilayers of Diaryl Disulfides. *J. Am. Chem. Soc.*, 2007, 129, 1888-1889.
- [65] Combellas, C., Kanoufi, F., Pinson, J. and Podvorica, F.I. Sterically Hindered Diazonium Salts for the Grafting of a Monolayer on Metals. *J. Am. Chem. Soc.*, 2008, 130, 8576.
- [66] Menanteau, T., Levillain, E. and Breton, T. Electrografting via Diazonium Chemistry: From Multilayer to Monolayer Using Radical Scavenger. *Chem. Mater.*, 2013, 25, 2905-2909.
- [67] Chausse, A., Chehimi, M. M., Karsi, N., Pinson, J., Podvorica, F. and Vautrin-UI, C. The Electrochemical Reduction of Diazonium Salts on Iron Electrodes. The Formation of Covalently Bonded Organic Layers and Their Effect on Corrosion. *Chem. Mater.*, 2002, 14, 392-400.

- [68] Le, X. T.; Doan, N. D.; Dequivre, T.; Viel, P.; Palacin, S. Covalent Grafting of Chitosan onto Stainless Steel Through Aryldiazonium Self-Adhesive Layers. *ACS Appl. Mater. Interfaces* 2014, 6, 9085–9092.
- [69] Yang, X., Hall, S.B., Burrell, A.K. and Officer, D.L. A pH-responsive hydroquinone-functionalised glassy carbon electrode. *Chem. Comm.*, 2001, 2628-2629.
- [70] Ghanem, M.A., Chretien, J.-M., Kilburn, J.D. and Bartlett, P.N. Electrochemical and solid-phase synthetic modification of glassy carbon electrodes with dihydroxybenzene compounds and the electrocatalytic oxidation of NADH. *Bioelectrochemistry*, 2009, 76, 115-125.
- [71] Betelu, S., Vautrin-UI, C., Ly, J. and Chausse, A. Screen-printed electrografted electrode for trace uranium analysis. *Talanta*, 2009, 80, 372-376.
- [72] Bouden, S., Bellakhal, N., Chausse, A. and Vautrin-UI, C. Performances of carbon-based screen-printed electrodes modified by diazonium salts with various carboxylic functions for trace metal sensors. *Elec. Commun.*, 2014, 41, 68-71.
- [73] Gui, A.L, Luais, E., Peterson, J.R. and Gooding, J.J. Zwitterionic phenyl layers: finally, stable, anti-biofouling coatings that do not passivate electrodes, *ACS Appl. Mater. Interfaces*, 2013, 5, 4827-4835.
- [74] Liu, G., Paddon-Row, M.N. and Gooding, J.J. Protein modulation of electrochemical signals: application to immunobiosensing. *Chem. Comm.*, 2008, 3870-3872.
- [75] Mohd Azmi, M.A., Tehrani, Z., Lewis, R.P., Walker, K.-A.D., Jones, D.R., Daniels, D.R., Doak, S.H. and Guy, O.J. Highly sensitive covalently functionalized integrated silicon nanowire biosensor devices for detection of cancer risk biomarker. *Biosens. and Bioelectronics*, 2014, 52, 216-224.
- [76] Wang J-S, Matyjaszewski K. Controlled/“living” radical polymerization. atom transfer radical polymerization in the presence of transition-metal complexes. *J. Am. Chem. Soc.*, 1995, 117, 5614–5.
- [77] Matyjaszewski, K. Atom Transfer Radical Polymerization (ATRP): Current Status and Future Perspectives. *Macromolecules*, 2012, 45, 4015-4039.
- [78] Mahouche Chergui, S., Gam Derouich, S., Mangeney, C., Chehimi, M. M. Aryl Diazonium Salts: a New Class of Coupling Agents for

- Bonding Polymers, Biomacromolecules and Nanoparticles to Surfaces. *Chem. Soc. Rev.*, 2011, 40, 4143–4166.
- [79] Matrab, T., Save, M. Charleux, B., Pinson, J., Cabet-Deliry, E., Adenier, A., Chehimi, M.M. and Delamar, M. Grafting densely-packed poly(n-butyl methacrylate) chains from an iron substrate by aryl diazonium surface-initiated ATRP: XPS monitoring. *Surf. Sci.*, 2007, 601, 2357–2366.
- [80] Hazimeh, H., Pioge, S., Pantoustier, N., Combellas, C., Podvorica, F.I. and Kanoufi, F. Radical Chemistry from Diazonium-Terminated Surfaces. *Chem. Mater.*, 2013, 25, 605-612.
- [81] Tao, N.J. Electron transport in molecular junctions. *Nature Nanotechnology*, 2006, 1, 173-181.
- [82] McCreery, R.L. and Bergren, A.J. Progress with Molecular Electronic Junctions: Meeting Experimental Challenges in Design and Fabrication. *Adv. Mater.* 2009, 21, 4303–4322
- [83] Wenyong Wang, W., Scott, A., Gergel-Hackett, N., Hacker, C., Janes, D.B. and Richter, C.A. Probing Molecules in Integrated Silicon–Molecule–Metal Junctions by Inelastic Tunneling Spectroscopy. *Nano Lett.*, 2008, 8, 478-484.
- [84] Rangathan, S., Steidel, I., Anariba, F. and McCreery, R.L. Covalently Bonded Organic Monolayers on a Carbon Substrate: A New Paradigm for Molecular Electronics. *Nano Lett.*, 2001, 1, 491-494.
- [85] Hines, T., Díez-Perez, I., Nakamura, H., Shimazaki, T., Asai, Y. and Tao, N. Controlling Formation of Single-Molecule Junctions by Electrochemical Reduction of Diazonium Terminal Groups, *J. Am. Chem. Soc.*, 2013, 135, 3319-3322.

Modifikimi me kripëra aril diazonium i sipërfaqeve të materialeve

Fetah I. Podvorica

Përmbledhje

Ky punim i shkurtër revial ka të bëjë me kripërat aril diazonium dhe përdorimin e tyre për modifikim të sipërfaqeve të materialeve. Në dy dekadat e fundit, këto komponime janë përdorur në shkallë të gjerë për mvshje me filma organikë të sipërfaqeve të llojeve të ndryshme të karbonit duke përfshirë grafenin dhe nanotubat e karbonit, metalet fisnike si dhe ato industriale, gjysmëpërçuesit dhe polimeret. Arsyeja për këtë përdorim kaq të gjerë bazohet në: i) mënyrën e thjeshtë të përgatitjes së kripërave aril diazonium në mjedis aprotik, në lëngje jonike dhe në tretësirat ujore, ii) mundësinë e futjes së shumë grupeve funksionale si substituentë dhe iii) potencialin e vogël të reduktimit elektrokimik të kationit diazonium. Në materialin e shtjelluar theksi është vënë kryesisht në disa rezultate eksperimentale të cilat kanë qenë me rëndësi të veçantë për zhvillimin e këtij lëmi. Reduktimi elektrokimik ose kimik i këtyre kripërave në sipërfaqe të materialeve të ndryshme mundëson krijimin e radikaleve arile të cilat janë shumë reaktive dhe menjëherë lidhen kimikisht me atomet në sipërfaqe të materialit. Për shkak të reaktivitetit shumë të madh këto specie reagojnë edhe me grupet arile të cilat lidhen paraprakisht në sipërfaqe të materialit dhe në këtë mënyrë mundësojnë formimin e filmave organikë me trashësi prej 1 nm deri në disa μm të cilët pastaj shërbejnë: për mbrojtje të metaleve prej korrozionit, për krijimin e kontaktit në mes dy materialeve në distanca shumë të shkurtra, për krijimin e sensorëve kimikë dhe biokimikë etj.

THE mRNA EXPRESSION OF SOME INSULIN-LIKE GROWTH FACTOR (IGF) FAMILY MEMBERS DURING FINALE FOLLICLE GROWTH IN THE BOVINE OVARY

Bajram Berisha^{a,*}

Abstract

The objective of this study was to characterize mRNA expression patterns of Insulin-like Growth Factors (IGF-1, IGF-2) and their receptor 1 (IGF-R) in follicles during well defined stages of final growth in the bovine ovary. The classification of follicle in our experiment occurred by estradiol-17beta (E) concentration in the follicular fluid (FF) into 5 groups (<0.5, 0.5-5, 5-40, 40-180 and >180 ng/ml E). For the further analysis the follicle tissue was separated in theca interna (TI) and granulosa cells (GC). Expression of mRNA was evaluated by Reverse Transcription-Polymerase Chain Reaction (RT-PCR) and steroid hormone concentration by Enzyme Immunoassay (EIA). The IGF-1 mRNA expression in TI was high in early follicle groups followed by a significant decrease afterwards in pre-ovulatory follicle class (>180 ng/ml E in FF). The IGF-2 mRNA expression in TI tissue was low in the early follicle class (<0.5 ng/ml E in FF), followed by a significant increase in following classes and a further decrease in pre-ovulatory follicle group (>180ng/ml E in FF). In contrast, no significant changes of IGF-1 and IGF-2 mRNA expression in GC during follicle finale growth were observed. The IGF-R mRNA

^a Faculty of Agriculture and Veterinary, University of Prishtina, Rr. George Bush, p.n., 10000 Prishtinë, Kosova. Faculty of Agriculture and Veterinary, University of Prishtina, Rr. George Bush, p.n., 10000 Prishtinë, Kosova.

* bajram.berisha@uni-pr.edu

expression in TI and GC was relatively low in early follicles class (<0.5 ng/ml E in FF) with a clear and continuous up-regulation in the following classes for both tissues to a higher plateau, and it was shown to be significant only for GC. These results lead to the assumption that the locally produced IGF-1, IGF-2 and IGF-R are involved in the local mechanisms regulating follicle development, selection and final growth in the ovary.

Key Words: IGF-1, IGF-2, IGF-R, mRNA expression, follicles, bovine

Introduction

There are clear evidences that the ovarian function is regulated primarily by the pituitary gonadotropins follicle-stimulating hormone (FSH) and luteinizing hormone (LH). [1] It is also well recognized that locally produced factors, such as steroids, peptides and growth factors have essential modulatory roles in follicle development, selection, dominance and ovulation. [1, 2] A number of growth factors have been demonstrated to affect follicle development and function in large farm animals. [3] The insulin-like growth factor (IGF) family members are known to enhance the actions of gonadotropins and steroids in the ovary. [4,5] Furthermore, IGF-1 and IGF-2 are growth factors that are involved in ovarian cell proliferation, mitogenesis and angiogenesis during follicle final growth, ovulation and corpus luteum (CL) formation. [6,7] The formation of the CL after ovulation involves changes in cellular morphology and ultra-structure, and key alterations in steroid hormone synthesis [6]. The mRNA expression of IGF-1 and IGF-2 in ovarian follicles is developmentally regulated in many species. [8-10] There are clear evidences that IGF-1 stimulates granulosa and theca cell proliferation in *in vivo* and *in vitro* in a number of species. [11-13] Comparable effects on the proliferation and granulosa cell (GC) differentiation have been demonstrated for IGF-2 too. [10, 13] Binding sites and IGF receptor 1 (IGF-R) mRNA expression were found in bovine follicles. [9, 14] In addition, binding proteins for IGFs (IGF-BP) are expressed in specific tissue and cell types of the ovary. The expression of IGF-BPs appears to be independently regulated in different species during the reproductive cycle and they may have different effects on IGF action. [15-17] There are clear evidences for a functional role of IGF family members on luteal tissue. It is

demonstrated that IGF-1 and IGF-2 have stimulatory effects on progesterone secretion and they are important factors for CL formation and function in deferent species. [18, 19] The aim of this study was to evaluate the mRNA expression of IGF-1, IGF-2 and their receptor IGF-R during different well defined follicle stages of development, selection and final follicle growth in the bovine ovary.

Materials and Methods

Collection and preparation of follicles

The entire reproductive tracts from cows (German Fleckvieh) were collected at a local slaughterhouse within 10-20 min after slaughter and were transported on ice to the laboratory as described by Berisha et al. [20]. The stage of the bovine estrous cycle was defined by macroscopic observation of the ovaries as described by Ireland et al. [21] Only follicles which appeared healthy (i.e. well vascularized and having transparent follicular wall and fluid) and whose diameter was ≥ 5 mm were used.

Large follicles (>14 mm) were only collected after CL regression, signs of mucus production in the uterus and cervix and assumed to be pre-ovulatory. The follicles were classified according to the estradiol-17 β (E) content in follicular fluid (FF) as follows; 1) $E < 0.5$; 2) $>0.5-5$; 3) $>5-20$; 4) $>20-180$ and 5) >180 ng/ml FF. The corresponding size of follicles were in the range of 1) 5-7; 2) 8-10; 3) 10-13; 4) 12-14 and 5) >14 mm. For the further investigation the follicle tissue was separated in theca interna (TI) and granulosa cells (GC). Since healthy follicles have relatively constant progesterone (P) levels in FF, only follicles with P below 100 ng/ml in FF were used for evaluation, to exclude atretic follicles. For further characterization of the follicle classes the mRNA expression was tested for the FSH receptor (FSHR) and aromatase cytochrome P450 (ARO) in GC and LH receptor (LHR) in TI and GC. [20]

Hormone determinations

The Progesterone (P) and estradiol-17beta (E) concentrations were determined directly in the FF with an enzyme immunoassay (EIA) using the second antibody technique as described by Berisha et al. [20]

RNA isolation and Reverse Transcription Polymerase Chain Reaction (RT-PCR)

Total RNA from TI tissue and GC was isolated by the single step method as described by Chomczynski and Sacchi [22]. RNA was dissolved in water and spectroscopically quantified at 260 nm. Aliquots were subjected to 1% denaturing agarose gel electrophoresis and ethidium bromide staining to verify the quantity and quality of RNA. [20]

Two micrograms of total RNA were used to generate single-strand cDNA in a 60 μ l reaction mixture as described previously. [20] The optimal amount of total RNA of specific genes for reverse transcription was evaluated by testing different RNA concentrations. The primers were designed using the EMBL database or were used as described elsewhere (Table 1) and were commercially synthesized (Amersham-Pharmacia, Freiburg, Germany). All primer pairs were designed according to known bovine sequences. Primer sequence and resulting fragment size for all examined factors are shown in Table 1. The conditions for enzymatic amplification (RT-PCR) for all examined genes in all examined tissues were established on a gradient cycler (Eppendorf, Hamburg, Germany). For each set of primers, the reaction was optimized for amount of primers, cDNA, and number of cycles. The PCR for all examined factors contained 10 mM Tris-HCl (pH 8.8), 50 mM KCl, 1.5 mM MgCl₂, 0.1% Triton X-100, 0.6 μ M of each primer and 0.5 units of thermostable polymerase PrimeZyme (Biometra, Göttingen, Germany) to 3 μ l cDNA (final volume 25 μ l). Ubiquitin PCR was performed under the same conditions. Number of amplification cycles was for each examined factor individual optimized. All amplifications were done as follows: an initial denaturation step 94 °C for 2 min, each cycle 94 °C for 1 min, 55-67 °C (individual optimized temperature for each examined factor) for 1 min, and afterwards one additional elongation step 72 °C for 2 min. Samples for the house-keeping gene ubiquitin were amplified by 22 cycles: a single denaturation step 94 °C for 2 min, each cycle 94 °C for 45 sec, 55 °C for 45 sec, 72 °C for 45 sec and afterwards one additional elongation step 72 °C for 2 min.

Aliquots of the PCR reaction products (5 μ l) were fractionated by electrophoresis through a 1.5% agarose gel containing ethidium bromide in a constant 60 V field. To determine the length of the products, a Mass Ladder and 100-bp marker (Gibco BRL, MD, U.S.A.) was used. The ethidium bromide-stained gels were evaluated by a video documentation system (Amersham-Pharmacia, Freiburg, Germany).

Band intensities were analyzed by computerized densitometry (arbitrary units) using the Image Master program (Amersham-Pharmacia, Freiburg, Germany). However, RT-PCR and this evaluation technique used is relative and not a strictly quantitative method.

Table 1. Gene transcript of IGF-1, IGF-2 and IGF-R primer sequences and resulting fragment size.

Target	Sequence of nucleotide	Fragment size (bp)	EMBL/Reference*
IGF-1	for 5'- GGA CCC GAG ACC CTC TGC GGG -3' rev 5' - GGC CGA CTT GGC GGG CTT G -3'	210	[23]
IGF-2	for 5' -TAT GCT GCT TAC CGC CCC AG -3' rev 5' -ACA TCC CTC TCG GAC TTG GC -3'	215	[24]
IGF-R	for 5' -TTA AAA TGG CCA GAA CCT GAG -3' rev 5' -ATT ATA ACC AAG CCT CCC AC -3'	314	[24]
Ubiquitin	for 5' -ATG CAG ATC TTT GTG AAG AC -3' rev 5' -CTT CTG GAT GTT GTA GTC -3'	189	[24]

* EMBL accession number or reference of published sequence.

Confirmation of the PCR product identity was obtained by cDNA subcloning into a transcription vector as described by Berisha et al. [20].

Statistical analyses

The statistical significance of differences in mRNA expressions of examined factors was assessed by ANOVA followed by Fisher's LSD as a multiple comparison test. All experimental data are shown as the mean±SEM. Follicles per class (n=5-20) were obtained from at last n=4 cows. Differences between groups were considered statistically significant if $P < 0.05$.

Results

Specificity and validation of RT-PCR data

Initial experiments verified specific transcripts for IGF-1, IGF-2 and IGF-R in bovine follicles tissue (TI and GC) by RT-PCR. Each PCR product (Table 1) showed 100% homology to the known bovine genes after sequencing (see Figure 1 for the different PCR products and the corresponding size). To confirm the integrity of the mRNA templates and RT-PCR protocol, the ubiquitin (housekeeping gene) was examined in all samples. The relative signal intensities for specific PCR products for all examined factors (IGF-1, IGF-2 and IGF-R) were assessed after correction based on the ubiquitin PCR signal intensities. The results of our experiment were expressed as the ratio of densitometric readings for examined factors to ubiquitin, therefore, values indicate relative changes in mRNA level.

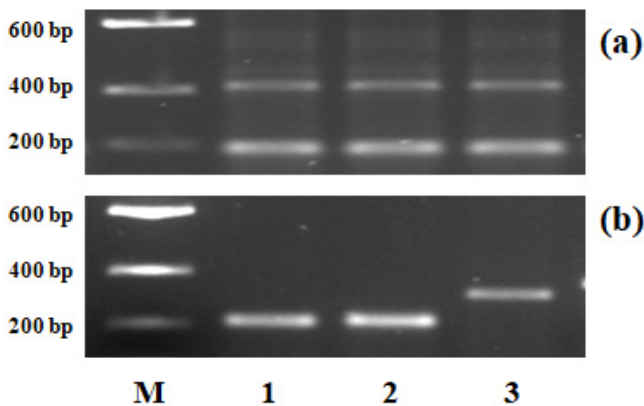


Fig. 1. Specific reverse transcription-polymerase chain reaction (RT-PCR) products for (a) Ubiquitin (189, 417 bp) and (b) IGF-1, IGF-2 and IGF-R from mixed cDNA (4–5 samples) of preovulatory follicle tissue, separated by agarose gel electrophoresis. M: DNA mass ladder (200, 400, 800 bp); lane 1: IGF-1 (210 bp); lane 2: IGF-2 (215 bp) and lane 3 IGF-R (314 bp).

The mRNA expression of IGF family members in follicles

The IGF-1, IGF-2 and IGF-R mRNA expression in TI and GC were analyzed by RT-PCR and the densitometric evaluation is shown in Fig. 2, Fig. 3 and Fig. 4. The IGF-1 mRNA expression in TI was high in early follicle groups followed by statistically significant decrease ($P < 0.05$) afterwards in pre-ovulatory follicles (>180 ng/ml E in FF). In

contrast, no significant change in IGF-1 mRNA expression in TI tissue during follicle development was found (Fig. 2a, Fig. 2b). The IGF-2 mRNA expression in TI tissue was low in early antral follicle group (<0.5 ng/ml E in FF), followed by statistically significant increase ($P<0.05$) in following classes and a further decrease in pre-ovulatory follicle class (>180 ng/ml E in FF). The IGF-2 expression of GC was very low, with no clear regulatory change in all follicles classes examined (Fig. 3a, Fig. 3b). The IGFR-1 expression in TI and GC is relatively low in early antral follicles class (<0.5 ng/ml E in FF) with a clear and continuous up-regulation in the following classes for both tissues to a higher plateau, and was statistically significant ($P<0.05$) only for GC (Fig. 4a, Fig. 4b).

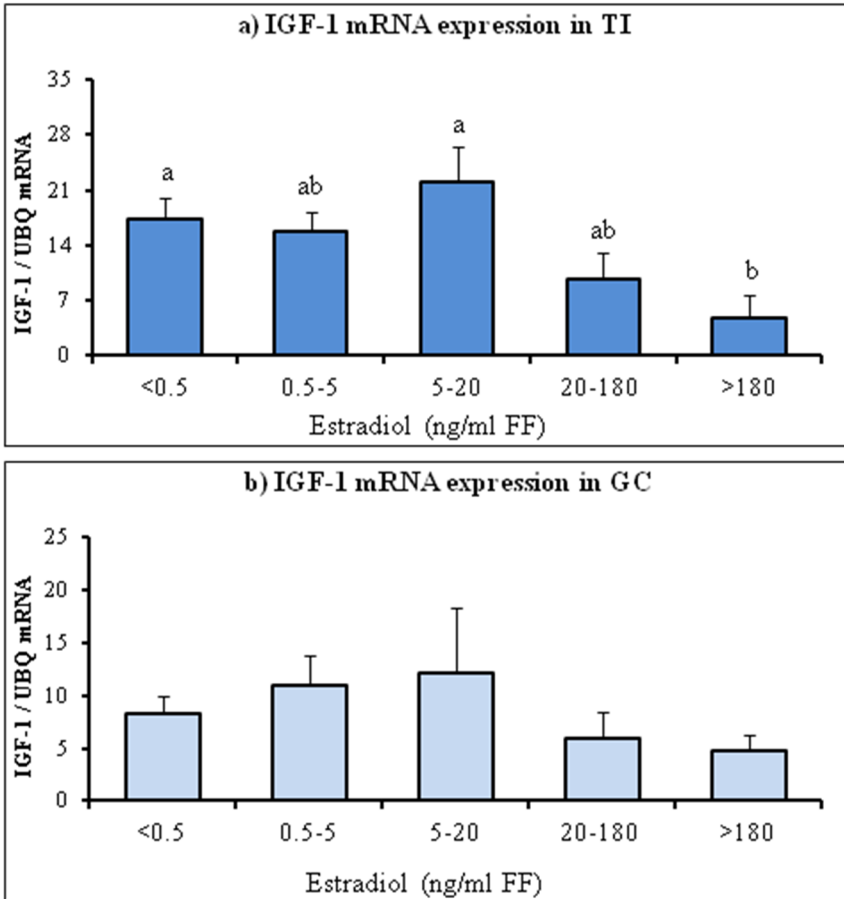


Fig. 2. The mRNA expression (densitometrically analyzed RT-PCR; ratio of examined factor/ubiquitin mRNA; arbitrary units) of IGF-1 in theca interna (TI) and granulosa cells (GC) during different follicular stages. Data are expressed as a means \pm SEM (n=5-20 follicles). Different letters denote statistically significant values ($P<0.05$).

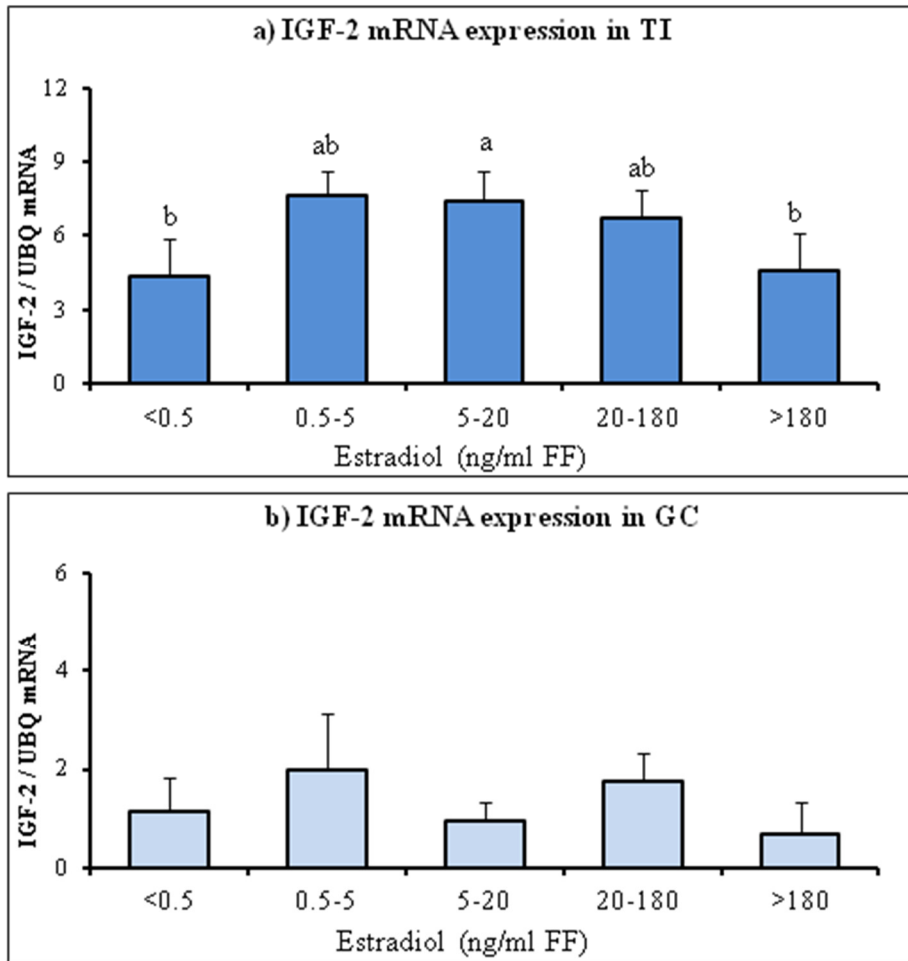


Fig. 3. The mRNA expression (densitometrically analyzed RT-PCR; ratio of examined factor/ubiquitin mRNA; arbitrary units) of IGF-2 in theca interna (TI) and granulosa cells (GC) during different follicular stages. Data are expressed as a means \pm SEM (n=5-20 follicles). Different letters denote statistically significant values (P<0.05).

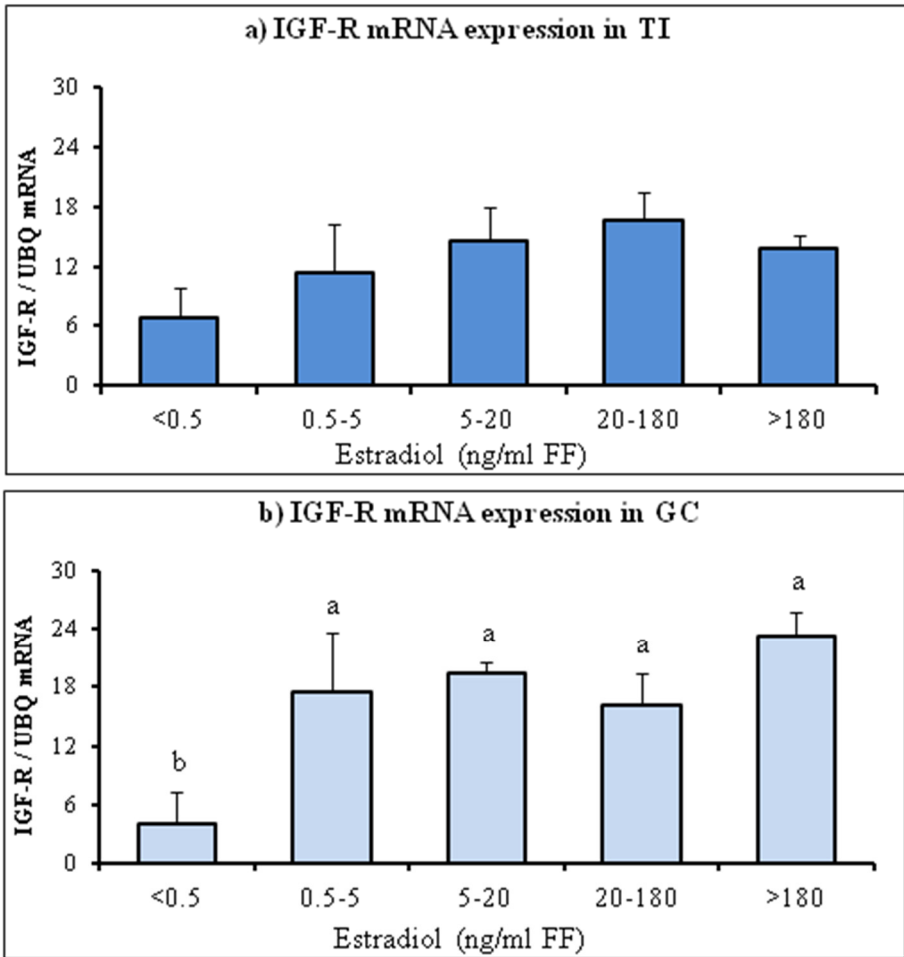


Fig. 4. The mRNA expression (densitometrically analyzed RT-PCR; ratio of examined factor/ubiquitin mRNA; arbitrary units) of IGF-R in theca interna (TI) and granulosa cells (GC) during different follicular stages. Data are expressed as a means \pm SEM (n=5-20 follicles). Different letters denote statistically significant values (P<0.05).

Discussion and Conclusions

The results presented in this study clearly demonstrate that the IGF-1, IGF-2 and their receptor IGF-R mRNA were expressed within GC and TI tissue (Fig. 1). The relatively high and constant mRNA expression of IGF-1 and IGF-2 in TI (Fig. 2a and Fig. 3a) of follicle classes examined in our experiment, suggests physiological functions especially in early antral follicle stages. The GC mRNA expression of IGF-1 in our follicle classes (Fig. 2a) agrees with the data of Yuan et al. [25] in large pre-ovulatory follicles. These results suggest production and secretion of IGF-1 growth factor during distinct periods of follicle development. In addition there are clear evidences for in vitro secretion of IGF-1 by GC of ovine [26], bovine [27, 28] and porcine [29] follicles. The follicle classes in our experiment were characterized by E and P content in FF and by mRNA expression pattern for FSHR, LHR and ARO (aromatase) as described earlier in detail. [20] Recent experiments in rats GC demonstrated that IGF-1 in vitro treatment increase further the FSH stimulated LHR mRNA up-regulation. [30] In addition, it is demonstrated that IGF-1 stimulates the LH receptor expression in bovine theca cells as well. [31] Our IGF-2 data in bovine ovarian follicles (Fig. 3a and Fig. 3b) agree with the observations of Armstrong et al. [9] It seems that the action of IGFs is most effective when acting synergistically with the gonadotropins. [32, 33] During final growth of follicles there were clear changes of IGFR-1 mRNA expression in TI and GC (Fig 4a and Fig. 4b). The IGFR-1 mRNA expression in TI and GC is relatively low in small follicles class (<0.5 ng/ml E in FF) with a clear and continuous up-regulation in the following classes for both tissues to a higher plateau, and was significant only for GC. The binding sites and interaction of IGF-R with IGF-1 and IGF-2 were demonstrated in the developing and pre-ovulatory bovine follicles. [9,14,34] There are clear evidences that ovarian follicles produce and secrete IGF-BPs in different species. [32, 35, 36] Our earlier results indicate that the GC expresses less IGF-BPs than TI tissue. [6, 37] These changes may influence the bioavailability of IGF which is not reflected in significant differences of IGF-1 and IGF-2 in follicles during finale development and maturation. [38, 39] In conclusion, our results lead to the assumption that the locally produced IGF-1, IGF-2 and IGF-R are involved in the local mechanisms regulating development, selection and finale follicle growth in the bovine ovary.

Acknowledgement

This work was supported by the German Research Foundation (DFG BE 3189)

References

- [1] Fortune JE. Ovarian follicular growth and development in mammals. *Biol. Reprod.* 1988, *50*, 225-232.
- [2] Armstrong, DG.; Webb, R. Ovarian follicular dominance: The role of intraovarian growth factors and novel proteins. *Rev. Reprod.* 1997, *2*, 139-146,
- [3] Berisha, B.; Schams, D. Ovarian function in ruminants. *Domest Anim Endocrinol.* 2005, *29*, 305-317.
- [4] Spicer, LJ.; Aad, PY. Insulin-like growth factor (IGF) 2 stimulates steroidogenesis and mitosis of bovine granulosa cells through the IGF1 receptor: role of follicle-stimulating hormone and IGF2 receptor. *Biol. Reprod.* 2007, *77*, 18-27.
- [5] Rawan, AF.; Yoshioka, S.; Abe, H.; Acosta, TJ. Insulin-like growth factor-1 regulates the expression of luteinizing hormone receptor and steroid production in bovine granulosa cells. *Reprod. Domest. Anim.* 2015, *50*, 283-291.
- [6] Schams, D.; Berisha, B.; Kosmann M.; Amselgruber, WM. Expression and localization of IGF family members in bovine antral follicles during final growth and in luteal tissue during different stages of estrous cycle and pregnancy. *Domest. Anim. Endocrinol.* 2002, *22*, 51-72.
- [7] Berisha B.; Schams D.; Rodler D.; Pfaffl, MW. Angiogenesis in The Ovary - The Most Important Regulatory Event for Follicle and Corpus Luteum Development and Function in Cow - An Overview. *Anat. Histol. Embryol.* 2016, *45*, 124-130.
- [8] Spicer, LJ.; Echternkamp, SE. The ovarian insulin and insulin-like growth factor system with an emphasis on domestic animals. *Domest. Anim. Endocrinol.* 1995, *12*, 223-245.
- [9] Armstrong, DG.; Gutierrez, CG.; Baxter, G.; Glazyrin, AL.; Mann, GE.; Woad, KJ.; Hogg, CO.; Webb, R. Expression of mRNA encoding IGF-I, IGF-II and type 1 IGF receptor in bovine ovarian follicles. *J. Endocrinol.* 2000, *165*, 101-113.
- [10] Hammond, JM.; Mondschein, JS.; Samaras, SE.; Smith, SA.; Hagen, DR. The ovarian insulin-like growth factor system. *J. Reprod. Fertil. Suppl.* 1991. *43*, 199-208.
- [11] Gutierrez, CG.; Campbell, BK.; Webb, R. Development of a long-term bovine granulosa cell culture system: induction and maintenance of estradiol production, response to follicle-

- stimulating hormone, and morphological characteristics. *Biol. Reprod.* 1997, 56, 608-616.
- [12] Campbell, BK.; Scaramuzzi, RJ.; Webb, R. Control of antral follicle development and selection in sheep and cattle. *J. Reprod. Fertil.* 1995, 49, 335-350.
- [13] Rebouças, EL.; Costa, JJ.; Passos, MJ.; Silva, AW.; Rossi, RO.; van den Hurk, R, Silva JR. Expression levels of mRNA for insulin-like growth factors 1 and 2, IGF receptors and IGF binding proteins in in vivo and in vitro grown bovine follicles. *Zygote* 2014, 22, 521-532.
- [14] Zhou, J.; Chin, E.; Bondy, C. Cellular pattern of insulin-like growth factor-I (IGF-I) and IGF-I receptor gene expression in the developing and mature ovarian follicle. *Endocrinology* 1991, 129, 3281-3288.
- [15] Nakatani, A.; Shimasaki, S.; Erickson, GF.; Ling, N. Tissue specific expression of four insulin-like growth factor-binding proteins (1,2,3, and 4) in the rat ovary. *Endocrinology* 1991, 129, 1521-1529.
- [16] Spicer, LJ.; Stewart, RC.; Avarey, P.; Francisco, CC.; Keefer, BE. Insulin-like growth factor-binding protein-2 and -3: their biological effects in bovine thecal cells. *Biol. Reprod.* 1997, 56, 1458-1465.
- [17] Wang, H-S.; Chard T. IGFs and IGF-binding proteins in the regulation of human ovarian and endometrial function. *J. Endocrinol* 1999, 161, 1-13.
- [18] McArdle, CA.; Holtorf, AP. Oxytocin and progesterone release from bovine corpus luteal cells in culture: effects of insulin-like growth factor I, insulin, and prostaglandins. *Endocrinology* 1989, 124,1278-1286.
- [19] Sauerwein, H.; Miyamoto, A.; Günther, J.; Meyer, HD.; Schams, D. Binding and action of insulin-like growth factors and insulin in bovine luteal tissue during the oestrous cycle. *J. Reprod. Fertil.* 1992, 96, 103-115.
- [20] Berisha, B.; Schams, D.; Kosmann, M.; Amselgruber, W.; Einspanier, R. Expression and localisation of vascular endothelial growth factor and basic fibroblast growth factor during the final growth of bovine ovarian follicles. *J. Endocrinology* 2000, 167, 371-382.

- [21] Ireland, J.; Murphee, R.; Coulson, P. Accuracy of predicting stages of the estrous cycle by gross appearance of the corpus luteum. *J. Dairy Sci.* 1991, *63*, 155-160.
- [22] Chomczynski, P.; Sacchi, N. Single-step method of RNA isolation by acid guanidinium thiocyanate-phenol-chloroform extraction. *Anal. Biochem.* 1987, *162*, 156-159.
- [23] Schmidt, A.; Einspanier, R.; Amselgruber, W.; Sinowatz, F.; Schams, D. Expression of insulin-like growth factor 1 (IGF-1) in the bovine oviduct during the oestrous cycle. *Exp. Clin. Endoc.* 1994, *102*, 364-369.
- [24] Plath-Gabler, A.; Gabler, C.; Sinowatz, F.; Berisha, B.; Schams, D. The expression of the IGF family and GH receptor in the bovine mammary gland. *J. Endocrinol.* 2001, *168*, 39-48.
- [25] Yuan, W.; Bao, B.; Garverick, HA.; Youngquist, RS.; Lucy, MC. Follicular dominance in cattle is associated with divergent patterns of ovarian gene expression for insulin-like growth factor I (IGF-I), IGF-II, and IGF binding protein-2 in dominant and subordinate follicles. *Domest. Anim. Endocrinol.* 1998, *15*, 55-63.
- [26] Khalid, M.; Haresign, W.; Luck, MR. Secretion of IGF-1 by ovine granulosa cells: effects of growth hormone and follicle stimulating hormone. *Anim. Reprod. Sci.* 2000, *58*, 261-272.
- [27] Sirotkin, AV.; Makarevich, AV. GH regulates secretory activity and apoptosis in cultured bovine granulosa cells through the activation of the cAMP/protein kinase A system. *J. Endocrinol.* 1999, *163*, 317-327.
- [28] Spicer, LJ.; Chamberlain, CS. Production of insulin-like growth factor-I by granulosa cells but not thecal cells is hormonally responsive in cattle. *J. Anim. Sci.* 2000, *78*, 2919-2926.
- [29] Samaras, SE.; Canning, SF.; Barber, JA.; Simmen, FA.; Hammond, JM. Regulation of insulin-like growth factor I biosynthesis in porcine granulosa cells. *Endocrinology* 1996, *137*, 4657-4664.
- [30] Hirakawa, T.; Minegishi, T.; Abe, K.; Kishi, H.; Ibuki, Y.; Miamoto, K. A role of insulin-like growth factor I in luteinizing hormone receptor expression in granulosa cells. *Endocrinology* 1999, *140*, 4965-4971.
- [31] Stewart, RE.; Spicer, LJ.; Hamilton, TD.; Keefer, BE. Effects of insulin-like growth factor I and insulin on proliferation and on basal and luteinizing hormone-induced steroidogenesis of bovine

- thecal cells: involvement of glucose and receptors for insulin-like growth factor I and luteinizing hormone. *J. Anim. Sci.* 1995, *73*, 3719-3731.
- [32] Adashi, EY. Growth factors and ovarian function: the IGF-I paradigm. *Horm. Res.* 1994, *42*, 44-48.
- [33] Adashi, EY. The IGF family and folliculogenesis. *J. Reprod. Immunol.* 1998, *39*, 13-19.
- [34] Spicer, LJ.; Stewart, RE. Interaction among bovine somatotropin, insulin, and gonadotropins on steroid production by bovine granulosa and theca cells. *J. Dairy Sci.* 1996, *79*, 813-821.
- [35] Besnard, N.; Pisselet, C.; Monniaux, D.; Locatelli, A.; Benne, F.; Gasser, F.; Hatey, F.; Monget, P. Expression of messenger ribonucleic acids of insulin-like growth factor binding protein-2, -4, and -5 in the ovine ovary: localization and changes during growth and atresia of antral follicles. *Biol. Reprod.* 1996, *55*, 1356-1367.
- [36] Echterkamp, SE.; Howard, HJ.; Roberts, AJ.; Grizzle, J.; Wise, T. Relationships among concentrations of steroids, insulin-like growth factor-I, and insulin-like growth factor binding proteins in ovarian follicular fluid of beef cattle. *Biol. Reprod.* 1994, *51*, 971-981.
- [37] Schams, D.; Berisha, B.; Kosmann, M.; Einspanier, R.; Amselgruber, WM. Possible role of growth hormone, IGFs and IGF-binding proteins in the regulation of ovarian function in large farm animals. *Dom. Anim. Endocrinol.* 1999, *17*, 279-285.
- [38] De la Sota, RL.; Simmen, FA.; Diaz, T.; Thatcher, WW. Insulin-like growth factor system in bovine first-wave dominant and subordinate follicles. *Biol. Reprod.* 1996, *55*, 803-812.
- [39] Stewart, RE.; Spicer, LJ.; Hamilton, TD.; Keefer, BE.; Dawson, LJ.; Morgan, GL.; Echterkamp, SE. Levels of insulin-like growth factor (IGF) binding proteins, luteinizing hormone and IGF-1 receptors, and steroids in dominant follicles during the first follicular wave in cattle exhibiting regular estrous cycles. *Endocrinology* 1996, *137*, 2842-2850.

Ekspresioni i ARNi të disa pjesëtarëve të familjes së Faktorit të Rritjes i ngjashëm me Insulinën (IGF) gjatë rritjes përfundimtare të folikulave në vezoren e gjedhit

Bajram Berisha

Përmbledhje

Qëllimi i këtij studimi ishte të karakterizonim modelet e ekspresionit të ARNi të disa pjesëtarëve të familjes së Faktorit të Rritjes të ngjashëm me Insulinën “Insulin like Growth Factor” (IGF-1, IGF-2) dhe receptorit të tyre 1 (IGF-R) në folikula, gjatë fazave të zhvillimit dhe të rritjes përfundimtare në vezoren e gjedhit. Klasifikimi i folikulave antrale është bërë bazuar në përqendrimin e estradiolit-17beta (E) në lëngun folikular në 5 grupe (<0.5, 0.5-5, 5-40, 40-180 dhe >180 E2 ng/ml). Madhësia e folikulave në grupet eksperimentale ka qenë përkatësisht 5-7, 8-10, 10-13, 12-14 dhe >14 mm. Për hulumtime të mëtejshme, indet e folikulave janë ndarë në indet teka interna (TI) dhe qelizat granuloze. Ekspresioni i ARNi është analizuar me anë të metodës “Reverse Transcription-Polymerase Chain Reaction” (RT-PCR), ndërkaq përqendrimi i hormoneve steroidale me anë të metodës “Enzyme Immunoassay” (EIA). Ekspresioni i ARNi të IGF-1 në TI në grupet e folikulave të hershme ishte konstatuar i lartë, pasuar nga një rënie e konsiderueshme në grupin e folikulave para-ovulacionit (>180 ng/ml E në FF). Ekspresioni i ARNi të IGF-2 në TI në grupin e folikulave të hershëm (<0.5 ng/ml E në FF) ishte i ulët, pasuar nga një rritje e ndjeshme në grupet pasuese dhe një rënie të mëtejshme në grupin e folikulave para-ovulacionit (>180 ng/ml E në FF). Në të kundërtën, asnjë ndryshim i rëndësishëm i ekspresionit të ARNi të IGF-1 dhe IGF-2 në qelizat granuloze nuk është vërejtur gjatë rritjes përfundimtare të folikulave. Ekspresioni i ARNi të IGF-R në TI dhe qelizat granuloze në grupin e folikulave të hershme (<0.5 ng/ml E në FF) ishte relativisht i ulët, me një ngritje të qartë dhe të vazhdueshme në grupet vijuese të folikulave për të dyja indet, ndërkaq me një ndryshim signifikant vetëm për qelizat granuloze. Këto rezultate çojnë në supozimin se IGF-1, IGF-2 dhe IGF-R, janë faktorë të rëndësishëm të përfshirë në mekanizmat lokalë (autokrine - parakrine) që rregullojnë zhvillimin, seleksionimin dhe rritjen përfundimtare të folikulave në vezoren e gjedhit.

NANOSCALE INTERFACE PROCESSES AND THEIR EFFECT ON MACROSCALE TRIBOLOGICAL PERFORMANCE

Ardian Morina^{a,*}

Abstract

A remarkable example in which the atomic scale processes affect larger scale performance is friction in dry and boundary lubricated sliding systems. However, development of tribological systems with designed friction and wear performance so far has been mainly empirical, largely due to the limited understanding of atomic-level processes at interfaces. Ability to analyse the chemical and physical interactions within the interface enables accessing information that can lead to better understanding of the origin of friction, and as a result to the design of optimised and reliable tribological systems. The current paper provides an overview of how the interface processes affect the friction and wear performance of two tribological systems relevant to power and transport industries. It then introduces two novel analytical methodologies, based on Raman and X-ray Absorption Spectroscopy, and discusses their potential for in-situ analysis of chemical interactions occurring in a boundary lubricated tribological interface.

Keywords: friction, wear, lubrication, in-situ interface characterization

^a School of Mechanical Engineering, University of Leeds, UK.

* a.morina@leeds.ac.uk

Introduction

Tribology focuses on friction, wear and lubrication of interacting surfaces in relative motion. Its scientific principles relate to several conventional scientific fields, underlining the interdisciplinary nature of tribology. For example, the research on understanding the origin of friction and wear in boundary lubricated system is underpinned by the fundamental science of materials, fluid mechanics, contact mechanics, chemistry and physics and requires use of high resolution spectroscopy- (such as X-ray Photoelectron, X-ray Absorption Near Edge, Raman Spectroscopy techniques) and microscopy-based analytical techniques (such as Scanning Electron, Atomic Force and Transmission Electron Microscopy techniques).

Tribology research has led to the development of a range of novel technologies used in power generation, transportation, manufacturing up to healthcare industries. The first report which documented the significance of tribology impact to economy and overall society is the landmark Jost report published around 50 years ago. In the Jost report it was shown that application of advanced tribology technologies could lead to 515 million UK pound saving, corresponding to 1.36% of UK's GNP at that time. The significant impact of tribology research and innovation to industry and economy was then later confirmed by several other similar reports for countries such as Germany, USA, Japan and China, with China reporting up to 7% of GNP savings with optimised tribological systems. The latest reports show that even after a half century of increased focus on the tribology research, there are still significant gains that can be achieved with optimised tribological systems. [1-3] For example, it is considered that up to 23% of world's total energy consumption originates from tribological contacts, with 20% of that used to overcome friction. In this scale, it can be easily seen that even a slight reduction of friction energy losses would lead to enormous energy savings worldwide. In addition to these savings, reduction of friction would have a considerable impact on environment through reduction of CO₂ emissions. [4, 5]

Although friction has been studied since Leonardo Da Vinci, there is still no universal theory developed that would describe how the interface processes determine friction and wear performance. The fundamental and impactful research of tribological systems, being that in energy, transport, healthcare or manufacturing industries, is being hugely limited by the *lack of detailed understanding of the origin of*

friction and wear at the contact interface. Understanding the kinetics of interface processes is of great relevance to several industries, as illustrated in Fig. 1.

The difficulty of observing and understanding the sliding lubricated interfaces has limited (i) the predictive engineering to improve the performance of tribological systems and (ii) tailoring lubricants and surfaces for generating low friction and wear interface films. *Directly seeing and analysing within a moving contact* is a powerful approach to understanding how the interface layers that form as a result of materials interaction with the environment and lubricants affect friction, wear and adhesion [6, 7]. The *in-situ* study of tribological interfaces requires analyses within the contact, ideally while the tribological test is running. Kinetics of interface processes refer to overall processes that define film properties at the interface (film thickness, nano-bubble measurements, formation and removal rate, lateral distribution, contact area development, debris development etc.). [8,9]

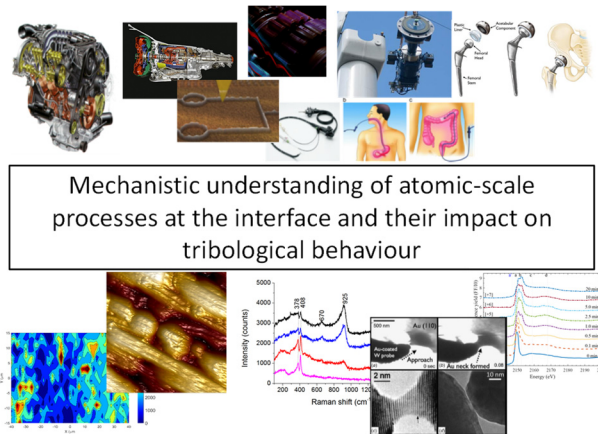


Fig. 1. Interface processes and their impact on macroscale friction and wear

The aim of the current paper is twofold:

- 1) to give an overview of the research done on studying the interface processes in two different tribological systems, and
- 2) to introduce two techniques for in-situ study of lubricated interfaces, based on Raman Spectroscopy and X-ray Absorption Spectroscopy.

Interface processes and tribological performance

Wind turbine gearbox bearing

In the updated Renewable Energy Directive [10] published in 2016, the European Commission has set a target of at least 27% of renewables in the final energy consumption by 2030, with wind turbines being one of the key renewable energy technologies to achieve this target. However, wind turbine gearbox bearings are seen to fail prematurely, impacting the reliability and cost of energy produced from wind.

In wind turbine gearboxes, especially offshore, bearings are seen to experience a fatigue type of failures in the form of white structure brittle flaking, micropitting surface fatigue and smearing. [11,12] Micropitting is a surface fatigue mechanism occurring on components lubricated under Elasto-Hydrodynamic or mixed/boundary lubrication regimes when the minimum lubricant film thickness (h_{\min}) becomes thinner than surface roughness leading to solid-solid contacts of asperities. In addition, lubricant chemical additives usually added to reduce wear could potentially have an opposite effect on the performance, especially when the lubricant is contaminated with water which is quite common for offshore wind turbines. Therefore, it is very important to understand the influence of lubricant additives and lubricant contamination with water on micropitting surface damage to be able to develop new lubricant and material technologies that can extend the lifetime of wind turbine gearbox bearings.

One of the most common anti-wear additives used in lubricants is the zinc dialkyldithiophosphate (ZDDP) additive. Although the exact mechanism by which this additive protects the lubricated surfaces from excessive wear is still debatable [13, 14], there is a consensus that its performance comes from the tribofilm it forms at the boundary lubricated interface which then separates the two surfaces in contact. [15-17] However, high contact pressure rolling/sliding experiments have shown that ZDDP in fact accelerates the micropitting surface damage. [18, 19]

Fig. 2 shows that micropitting surface damage from a ZDDP-containing lubricant can be accelerated when testing at high relative humidity and minimised if there is an organic friction modifier such as N-tallow-1,3-diaminopropane (TDP) additive in the lubricant.

Higher relative humidity will cause ingress of water in the lubricant which could potentially cause a) surface corrosion, in the case water is free in the lubricant and adsorbs on the surface, b) lubricant oxidation and hydrogen embrittlement, c) antagonistic effect on formation of protective lubricant tribofilms and d) lubricant viscosity reduction.

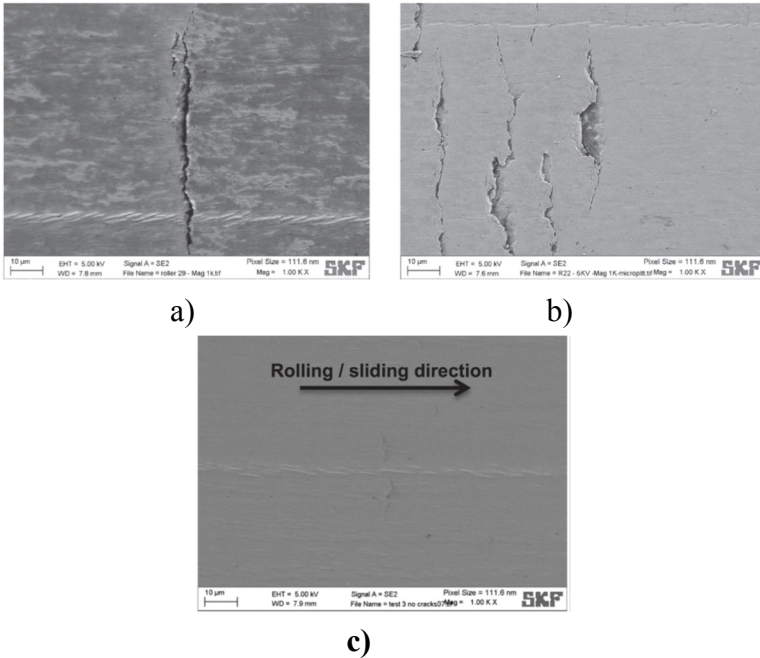


Fig. 2. Scanning Electron Microscope Images of the roller wear scars lubricated with a) Base oil (BO) + ZDDP, b) BO + ZDDP (Relative Humidity RH 60%) and c) BO + ZDDP + N-tallow-1,3-diaminopropane (TDP) at 75 °C. [20, 21]

Post-test surface analyses of the formed tribofilms with the Mini-Traction Machine Surface Layer Imaging Method (MTM SLIM) (Fig. 3) show that the ZDDP tribofilm thickness reduces significantly when there is water dissolved in the lubricant.

This effect of water on ZDDP tribofilm thickness has also been confirmed with X-ray Photoelectron Spectroscopy (XPS) analyses of the wear scar. Fig. 4 results show the chemical composition of the tribofilm as a function of tribofilm sputtering time. Sputtering is a mechanical etching process by using inert Ar ions. From Fig. 4a and b results it can be seen that intersection between Fe and Zn curves occur at 300 s and 100 s, respectively. Assuming that the formed tribofilms have similar etching rate, these results indicate that the tribofilm formed with BO + ZDDP at 60% RH is much thinner than the BO + ZDDP tribofilm.

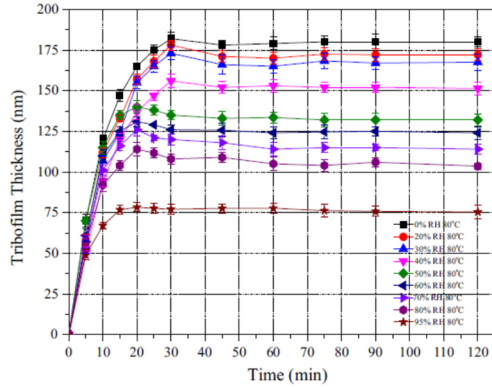


Fig. 3. BO + ZDDP tribofilm thickness from experiments run at increasing relative humidity. [22]

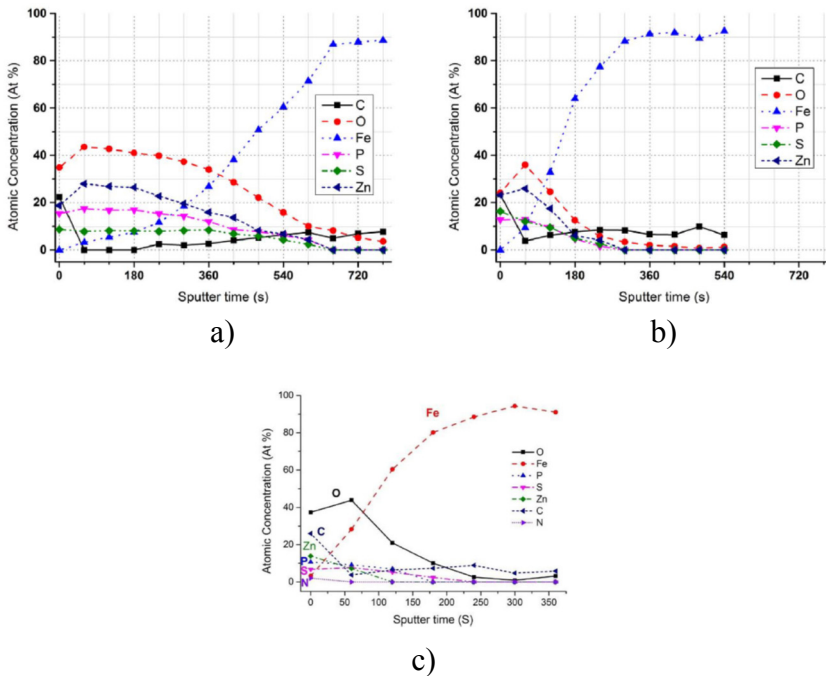


Fig. 4. Sputter depth profiles of the reaction layers on the roller surfaces lubricated with (a) BO + ZDDP, b) BO + ZDDP (60% RH) and (c) BO + ZDDP + TDP. [20]

Comparing the results in Fig. 4a and c, the intersection between Fe and Zn curves occur at 300 s and 25 s, indicating that the tribofilm formed from BO + ZDDP + TDP lubricant is much thinner than ZDDP tribofilm. These results indicate that the tribofilm thickness is not the

only parameter which affects the wear performance but its chemical structure, topographical and mechanical properties are also important.

The key chemical structures which would form from ZDDP additives are the phosphate glasses, however the chain length of these phosphates would affect their mechanical properties and anti-wear performance. [23, 24] Characterising the chain length of phosphates formed in an inhomogeneous and patchy surface films of around 100 nm thickness is not a trivial task, but with the use of surface sensitive techniques such as XPS and XANES [25-27] a good indication of this can be obtained. One way to obtain the phosphate chain length is through the ratio between bridging oxygen (P-O-P) and non-bridging oxygen (-P=O and P-O-M, M stands for metal). Detailed analysis of the O 1s XPS peak can determine the intensity of both bridging oxygen and non-bridging oxygen which then can be used to calculate the phosphate chain length. A key assumption here is that oxygen detected from the wear scar is coming completely from the phosphate tribofilm, which is not necessarily accurate. Hence, other methods are used to complement this method. [28, 29] Nevertheless, fig. 3 clearly shows that non-bridging oxygen (NBO) peak in relation to the bridging oxygen peak is much larger, confirming the different phosphate chain length as a result of the water in the lubricant.

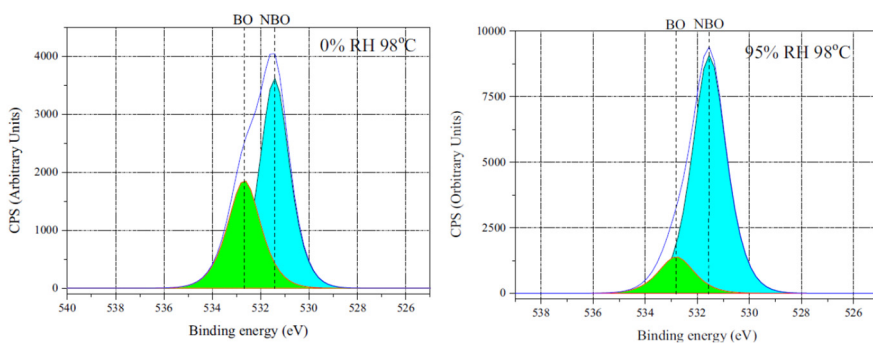


Fig. 5. Chemical structure of the ZDDP tribofilm, effect of relative humidity

Another aspect of tribofilms which would affect the micropitting performance is its lateral distribution and roughness. Atomic Force Microscopy (AFM) is a very helpful technique to image the formed tribofilms in high resolution as well as measure their surface roughness. Fig. 6. shows that the amines present in the ZDDP-containing lubricant

(BO+ZDDP+TDP) result formation of a much more uniform and smoother tribofilm.

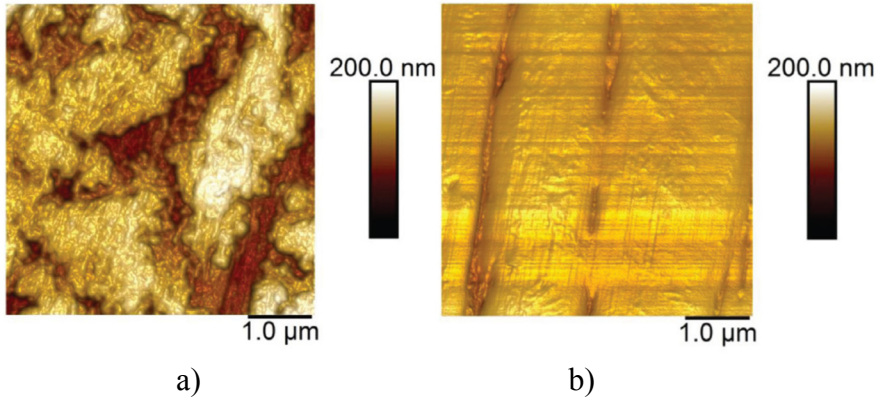


Fig. 6. Atomic Force Microscope images of tribofilms formed from a) BO + ZDDP and b) BO + ZDDP+ TDP lubricants. [21]

Low roughness of the tribofilm is another beneficial aspect as it will reduce the contact stresses at the asperity level which in turn will lead to less local plastic deformations and ultimately surface damage. Understanding the processes by which these tribofilms form in industrial components is of paramount importance for developing reliable energy efficient systems.

Friction reduction from engine lubricants containing MoDTC Additive

Road transport is a big contributor to world's greenhouse gas emissions, as well as being responsible for increasingly severe air pollution in congested city areas, affecting both developed and developing countries. Transport is the main cause of reduced air quality in cities, which poses a serious threat to public health. Road transport alone is responsible for almost a fifth of total EU emissions and 73 per cent of emissions from transport [30]. The automotive industry is under a lot of pressure to introduce transport technologies with higher fuel efficiency, but at the same time with superior driving performance. By 2021, the average fuel consumption of a new car will be around 4.1 l/100 km of petrol or 3.6 l/100 of diesel [31]. Hence, engine manufacturers are

responding by introducing engine downsizing technologies, such as start/stop, low density materials, turbocharging etc., as well as by reducing to minimum all parasitic energy losses in engines.

A recent study on passenger car engine energy consumption done in Japan [32], has concluded that around 35% of total fuel consumption is due to friction losses (Fig. 7) while only around 22% of the fuel energy is used to move the car [33]. Hence, an important approach to improve the car engine efficiency is by reducing the frictional losses to minimum. One way to achieve that is by using lubricant additives which would form low friction tribofilms in contacts such as piston ring/liner and valve train systems.

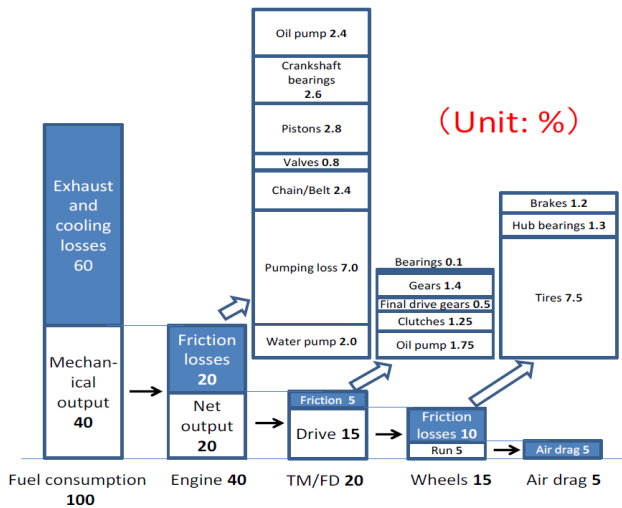


Fig. 7. Fuel energy distribution in a passenger car. [32]

An important additive used as a friction modifier is the molybdenum dialkyldithio carbamate (MoDTC). This additive is added to the base oil in a typical concentration of 0.05 to 0.9 wt%, depending on the region. Fig. 8 shows that a MoDTC containing lubricant reduces friction significantly compared to a base oil and dry test, as well as it protects the contact from seizure. All the lubricated tests in this study were run in boundary lubrication regime, using the high speed pin-on-disk tribometer at 0.5 wt% MoDTC, 100 °C, 0.3 m/s and 2.12 GPa contact pressure. The test run in dry condition, i.e. not lubricated, had to be stopped after around 5 minutes test due to cold welding of the samples in contact. In the lubricated test with MoDTC

containing lubricant, friction was initially high and then after an induction time of around 3 minutes the friction instantaneously dropped to a friction of 0.05-0.06, typical for this additive. [34, 35] It is obvious that even with only 0.5wt% MoDTC additive in the base oil, huge reduction of friction has been achieved.

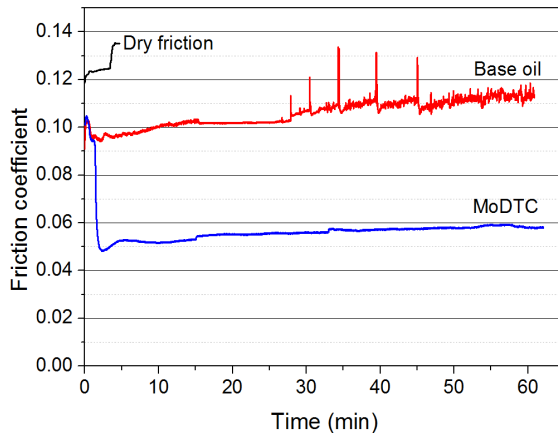


Fig. 8. Friction performance of a MoDTC containing lubricant

It is important lubricants provide low friction without affecting the surface durability. Fig. 9 shows optical images of tribopair wear scars after tests under no lubrication, with mineral base oil and MoDTC lubricant. As expected, the highest wear was observed for the sample run in a dry friction test. In these conditions, the wear scar is characterised by large grooves and localised surface damage indicating abrasive and adhesive wear mechanism. Although tests under dry friction were carried out for only 5 minutes, the ball wear scar diameter was the largest (1227 μm) compared to tests with mineral base oil (808 μm) and MoDTC (372 μm). The presence of MoDTC additive in mineral base oil not only reduced friction but also reduced wear of the steel ball.

Considering the low amount of the MoDTC additive in the base oil will not change the viscosity of the lubricant, the low friction performance can be achieved mainly as a result of additive interaction with the lubricated interface forming low friction tribofilms. To characterise the chemical composition of the surface films formed, the Raman spectroscopy was used and the results are shown in Fig. 10. Raman spectroscopy is a surface analytical technique which is concerned with the phenomenon of a change of frequency when light is scattered by molecules. It is based on an inelastic

scattering or Raman scattering of monochromatic light, usually from a laser source. The laser light interacts with molecular vibrations, photons or other excitations in the system, resulting in the Raman Effect where the energy of the laser photons is shifted up or down in comparison with original monochromatic frequency. This shift in the energy provides information about vibrational, rotational and other low frequency transitions in molecules which are then used to identify them.

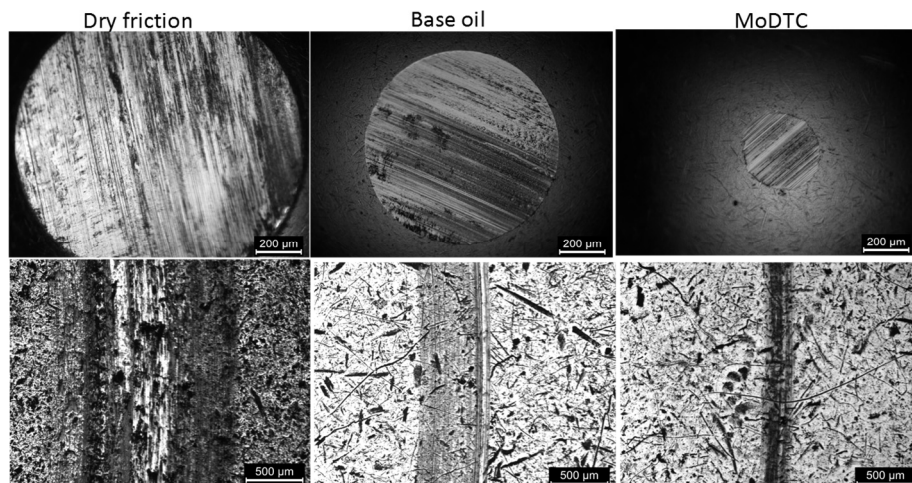


Fig. 9. Wear scar images after tests in dry conditions, and lubricated with mineral base oil and mineral base oil containing MoDTC lubricants

The Raman peaks at 222 cm^{-1} , 291 cm^{-1} , 404 cm^{-1} , 495 cm^{-1} and 1322 cm^{-1} indicate formation of haematite (Fe_2O_3), while peaks at 310 cm^{-1} , 540 cm^{-1} and 666 cm^{-1} are assigned to magnetite (Fe_3O_4) [36]. The peak doublet at 411 cm^{-1} and 382 cm^{-1} observed in spectra obtained from tests with MoDTC correspond to A_{1g} and E^{1}_{2g} vibrational modes within the MoS_x ($x > 2$) layer [37, 38]. The peak observed at 750 cm^{-1} can be assigned to $\nu(\text{Mo-O-Mo})$ vibration in oxygen bridged molybdenum (V) species [39]. These results clearly show that the MoDTC additive has been decomposed and has formed a molybdenum sulphide layer on the interface.

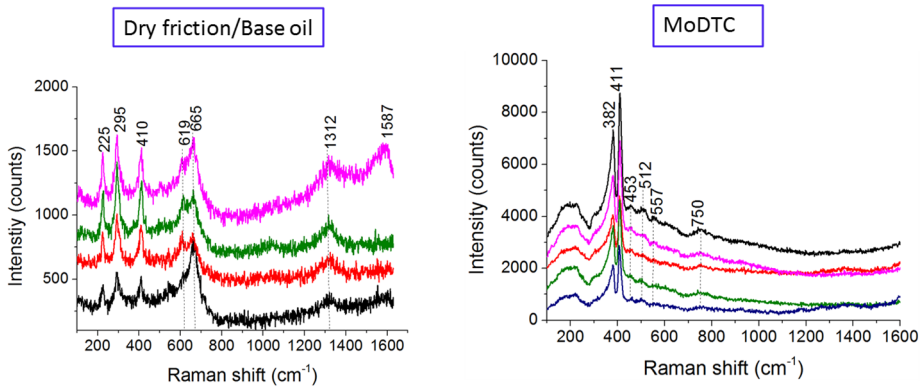


Fig. 10. Surface chemical composition following a dry/base oil and lubricated tests. The spectra are taken from different positions in the wear scar.

Fig. 11 shows a schematic diagram describing the mechanism of friction reduction in MoS₂. Onodera et al. [40], using molecular dynamics, reported that coulombic repulsion between sulphur atoms on adjacent MoS₂ sheets was responsible for low friction. The adsorbed MoS₂ sheets on steel surfaces receive electrons from the surface becoming more negatively charged. Consequently, the repulsive forces between sulphur atoms increase, leading to low friction.

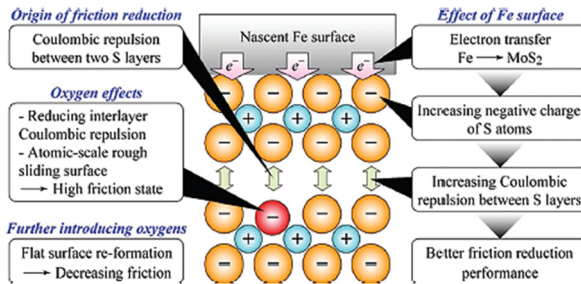


Fig. 11. Low friction in MoS₂ sheets. [40]

While the formation of MoS₂ from the MoDTC additive is now well documented, the current research is focusing on quantifying the effect of different parameters on the tribochemical reactions and their effect on the growth and durability of tribofilms. [41, 42]

In-situ study of boundary lubricated interfaces

Formation of low friction and durable tribofilms is enabled by the rubbing process; only heating the lubricant cannot lead to formation of MoS₂ from MoDTC and phosphates from ZDDP additive. The mechanical energy input through the sliding and rolling process is essential to lower the thermodynamic reaction barrier and promote the activation of chemical reaction. Considering that additives in the lubricant can form tribofilms of different chemistries, the effect of mechanical energy input in the system through sliding and/or rolling would differ for different tribochemical reactions. Recently, research using the Atomic Force Microscopy [6] and the MTM Surface Layer Imaging Method [43] have studied the ZDDP tribofilm thickness to obtain its growth rate dependency on mechanical stress. The following sections introduce two methods to study the growth rate of tribofilms by analysing the chemical composition. These methods have the potential to complement the research with other techniques to obtain the growth rate of tribofilms of certain chemistries, in relation to the overall tribofilm growth rate.

Low friction tribofilm study using the Raman Spectroscopy

Fig. 12 shows the schematic layout of the tribometer and its coupling with the Raman microscope for in-situ characterisation of formed tribofilms. The designed in-situ tribometer utilises the flexible sampling arm provided with the Raman system, and analyses are conducted without removing the samples from the system.

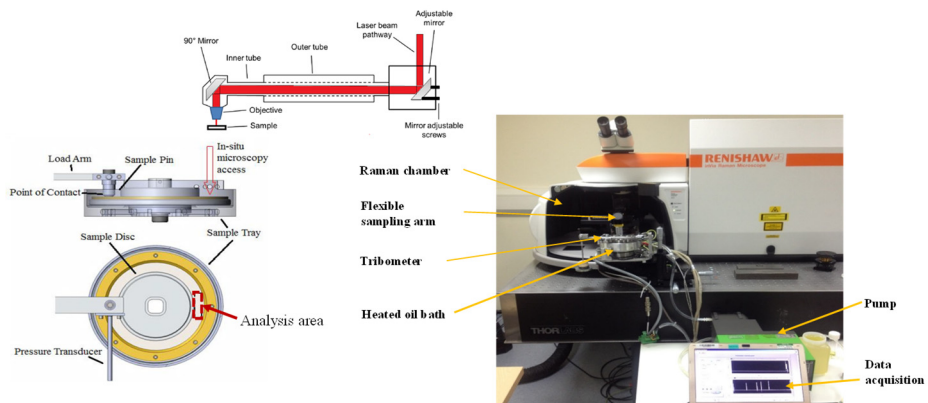


Fig. 12. In-situ Raman tribometer

The in-situ tribometer has been recently used to investigate the transient removal of MoS₂ with sliding time. [44] The tests were initially performed in boundary lubrication regime for one hour, using a lubricant containing both MoDTC and ZDDP additives. After one hour test, the tribometer was halted to replace the lubricant with a lubricant containing only ZDDP additive. This way, there was no MoDTC additive to replenish the tribofilm and the rate of friction increase with sliding indicated the removal of MoS₂ low friction tribofilm. The test was then stopped every few minutes to analyse the wear scar using the Raman microscope. In-situ Raman spectra were carried out using the flexible sampling arm with a laser excitation of 488 nm at 50% laser power and 20 s exposure time. The same experimental procedures were conducted at three different temperatures.

Fig. 13 shows that after one hour test with the lubricant containing ZDDP and MoDTC, friction has been reduced to the level typical for the MoS₂ tribofilm. Removing the MoDTC from the lubricant resulted in friction increase, which indicates that without MoS₂ tribofilm replenishment the low friction performance will be lost. The rate by which the friction increased was seen to be affected by the lubricant temperature with the rate increasing with temperature increase.

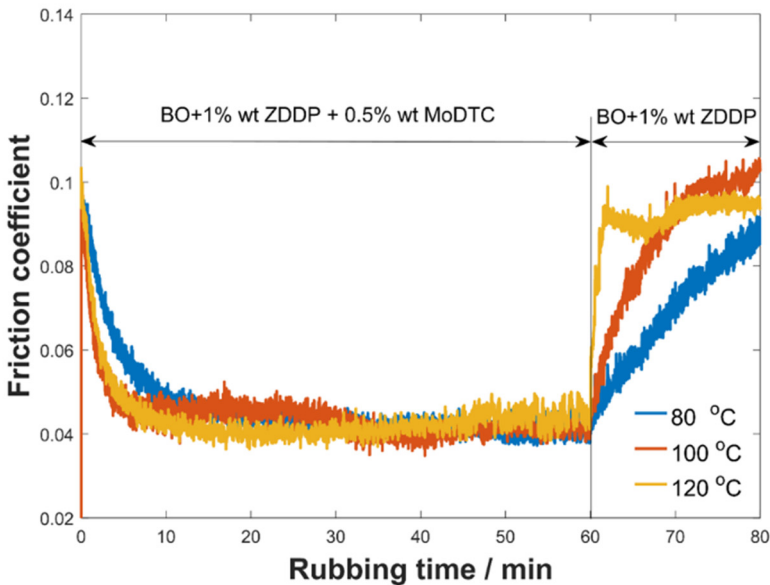


Fig. 13. Friction coefficient as a function of time, temperature and lubricant. [44]

Analyses of the tribofilm chemical composition after the lubricant change, Fig 14a, confirm the MoS₂ composition of the tribofilm but they also show the intensity of MoS₂ A_{1g} peak decreasing with sliding time. With further analysis of the A_{1g} peak intensity with sliding time, the rate of MoS₂ tribofilm removal could be obtained (Fig. 14b).

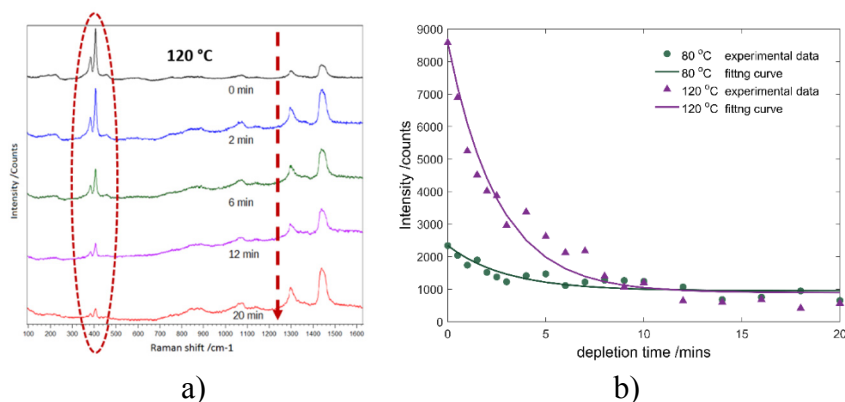


Fig. 14. a) Normalized Raman single spectra as a function of removal time at 120 °C and b) Intensity of the A_{1g} peak as a function of removal time at 80 °C and 120 °C. [44]

Anti-wear film study using the synchrotron X-ray Absorption Spectroscopy (XAS)

The second technique focuses on the study of physical and chemical processes related to ZDDP tribofilm formation. To obtain structural information of lubricant films formed during the friction test, a purpose-built tribometer coupled with the hard X-ray absorption spectroscopy ReflEXAFS was developed. [45, 46] In this methodology, shown schematically in Fig. 15, the tribometer is mounted on the precision positioning stage enabling in-situ tribofilm formation and characterisation. The pin is loaded with a dead weight and slides on a rotating disk covered with lubricant. The XAS experiments are then performed using the I18 microfocuss spectroscopy beamline at Diamond Light Source in Oxfordshire, UK. The I18 has an X-ray beam of a high spatial resolution of 2 μm x 2 μm and energy range between 2.05 keV and 20.5 keV. The high spatial resolution of this beamline allows the analysis of heterogeneous samples such as ZDDP tribofilms by providing insight into the local variations in

composition. In this study, the P and S k-edges were acquired using the fluorescence yield (FY) mode. The experiments were performed under helium environment as the low atomic number of helium reduces absorption of low-energy phosphorus and sulphur fluorescence signal.

The location of the wear scar on the disc was identified by elemental mapping of P and S using scanning micro-X-ray fluorescence (XRF) mapping. This was performed using a $4\ \mu\text{m} \times 4\ \mu\text{m}$ beam size scanning lines of 1.8 mm length at different sample heights. The sample was then positioned at the location of the most intense pixel to achieve the best signal to noise ratio and limit the detected signal to the wear scar. Subsequently, the XAS spectra of P and S k-edges were acquired.

Fig. 16 shows the P and S spectra obtained by analysing the ZDDP film developed from heating the sample as well as developed over increasing sliding time.

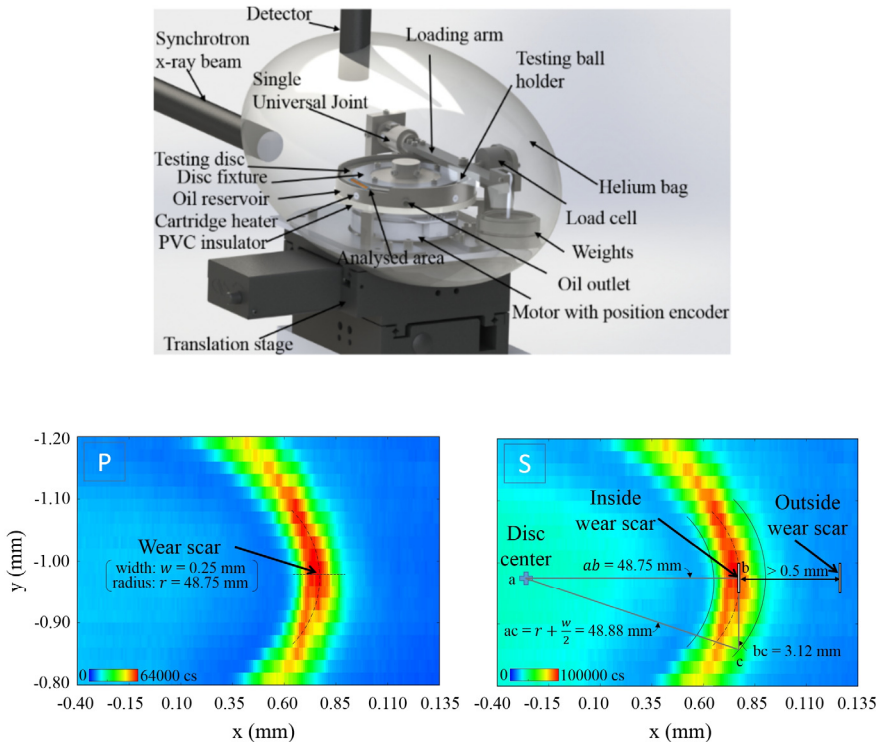


Fig. 15. a) Schematic representation of the synchrotron *in-situ* tribofilm analysis and b) micro X-ray fluorescence maps of P and S k-edges. [45]

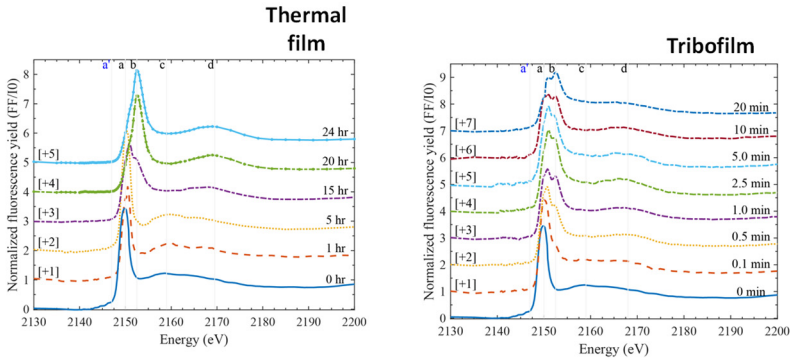


Fig. 16. Spectra evolution of the ZDDP P k-edge normalized fluorescence yield as a result of heating (thermal film) and sliding test (tribofilm). [47]

The typical P k-edge spectrum is characterised by the edge (a) and post-edge peaks (b, c, d), as shown in Fig. 16. The post-edge peaks provide information regarding the oxidation state and arrangements of the different elements within the phosphate glass structure composing the tribofilm [48].

The first peak (a) at 2150.0 eV corresponds to unreacted ZDDP adsorbed to the steel surface, while the second peak (b) at 2152.5 eV can be assigned to zinc phosphate whether of short or long phosphate chains. [46] Peaks (c) and (d), at 2159.0 eV and 2169.5 eV, respectively, indicate the structure of the formed phosphate species. From Fig. 6 results it is clear that the quantity of adsorbed additive on the surface goes down with heating and sliding, while it is opposite with the phosphate peak. This is not surprising as it is well documented that ZDDP additive forms a phosphate film. However, what the XAS techniques enables is the ability to quantify the rate of phosphate formation from the adsorbed ZDDP additive. Figure 17 shows the results of P k-edge peak deconvolution, indicating the area under the peak (a) and area under the peak (b).

From these results, it is evident that the formation of phosphates from ZDDP can be done with only heating but this process is significantly accelerated in a tribological contact, i.e. the sliding process accelerates the formation of phosphate from ZDDP. It takes only 10 minutes of a sliding test for the phosphate to dominate the tribofilm chemical composition while with only heating it takes more than 15 hours.

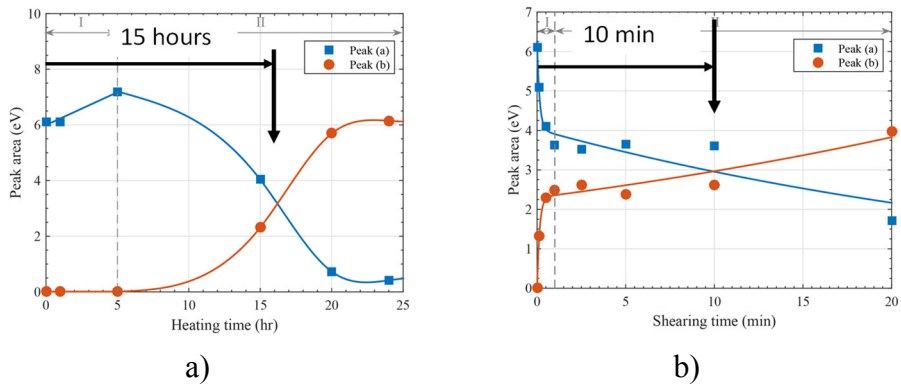


Fig. 17. Normalized heights of P k-edge adsorbed ZDDP and phosphate peaks for a) ZDDP thermal film and b) ZDDP tribofilm. [47]

The fact that sliding accelerates formation of phosphates from ZDDP has been observed before, but with the current XAS technique the quantification of phosphate formation rate can now be obtained. Fig. 17b shows that phosphate tribofilm formation occurs in two phases, during the initial phase of couple of minutes the formation rate is very high but it then reduces significantly. This could be due to a continuous consumption of the unreacted ZDDP to form phosphate species, Fig 17 results confirm that the ZDDP decomposition and tribofilm formation are thermally and mechanically assisted processes in which rubbing acts as a catalyst.

Conclusions

The paper highlights the need for understanding the atomic-level processes in lubricated surfaces and introduces two spectroscopy methods as appropriate research tools for in-situ analysis of lubricated interfaces. The interface processes between the lubricant, environment and surfaces determine not only the chemical composition of surface films but also the kinetics of its formation and removal. While the temperature effect on kinetics of surface film formation can be modelled using Arrhenius model, quantifying the effect of contact pressure and sliding is much more complicated. The two spectroscopy methods introduced here have the potential to provide experimental information on the growth and removal of tribofilms, enabling development of tribochemistry models capable to predict friction and wear performance.

References

- [1] Holmberg, K. and Erdemir, A., Influence of tribology on global energy consumption, costs and emissions. *Friction*, 2017, 5(3), 263-284.
- [2] Holmberg, K., Andersson, P., Siilasto, R., and Erdemir, A. Global impact of friction on energy consumption, environment, and economy. in 5th *World Tribology Congress, WTC 2013*. 2013.
- [3] Holmberg, K., Andersson, P., Nylund, N.O., Mäkelä, K., and Erdemir, A., Global energy consumption due to friction in trucks and buses. *Tribology International*, 2014, 78, 94-114.
- [4] Energy Technology Perspectives 2016, OECD/IEA, 2016, <http://www.iea.org/publications>.
- [5] "SWD(2012) 260 final, Preliminary Descriptions of Research and Innovation Areas and Fields, Research and Innovation for Europe's Future Mobility, {COM(2012) 501 final};
- [6] Gosvami, N.N., et al., Mechanisms of antiwear tribofilm growth revealed in situ by single-asperity sliding contacts. *Science*, 2015, 348(6230), 102-106.
- [7] Erdemir, A., et al., Carbon-based tribofilms from lubricating oils. *Nature*, 2016. 536(7614): p. 67-71.
- [8] Sawyer, W.G., Argibay, N., Burris, D.L., and Krick, B.A., Mechanistic studies in friction and wear of bulk materials. *Annual Review of Materials Research*, 2014, 44, 395-427.
- [9] Wahl, K.J., Macroscale to microscale tribology, in *Micro- and nanoscale phenomena in tribology*, Y.-W. Chung, Ed., ed Boca Raton, FL: CRC Press, 2011, 5-22.
- [10] Directive of the European Parliament and the Council on the promotion of the use of energy from renewable sources (recast); COM(2016) 767 final/2 2016/0382(COD).
- [11] Doll, G.L., Kotzalas, M.N., and Kang, Y.S. Life-limiting wear of wind turbine gearbox bearings: Origins and solutions. in *Proceedings of European wind energy conference exhibition (EWEC 2010)*. 2010.
- [12] Wood, R.J.K., Bahaj, A.S., Turnock, S.R., Wang, L., and Evans, M., Tribological design constraints of marine renewable energy systems. *Philosophical Transactions of the Royal Society A: Mathematical, Physical and Engineering Sciences*, 2010, 368(1929), 4807-4827.

-
- [13] Tysoe, W., On Stress-Induced Tribochemical Reaction Rates. *Tribology Letters*, 2017. 65(2).
- [14] Zhang, J. and Spikes, H., On the Mechanism of ZDDP Antiwear Film Formation. *Tribology Letters*, 2016. 63, 24.
- [15] Morina, A., Neville, A., Priest, M., and Green, J.H., ZDDP and MoDTC interactions in boundary lubrication—The effect of temperature and ZDDP/MoDTC ratio. *Tribology International*, 2006. 39, 1545-1557.
- [16] Barnes, A.M., Bartle, K.D., and Thibon, V.R.A., A review of zinc dialkyldithiophosphates (ZDDPs): characterisation and role in the lubricating oil. *Tribology International*, 2001. 24: p. 389-395.
- [17] Spikes, H., The history and mechanisms of ZDDP. *Tribology Letters*, 2004. 17(3): p. 469-489.
- [18] Laine, E., Olver, A., and Beveridge, T., Effect of lubricants on micropitting and wear. *Tribology International* 2008. 41(11): p. 1049-1055.
- [19] Brizmer, V., Pasaribu, H., and Morales-Espejel, G.E., Micropitting performance of oil additives in lubricated rolling contacts. *Tribology Transactions*, 2013. 56(5): p. 739-748.
- [20] Soltanahmadi, S., Morina, A., van Eijk, M.C.P., Nedelcu, I., and Neville, A., Tribochemical study of micropitting in tribocorrosive lubricated contacts: The influence of water and relative humidity. *Tribology International*, 2017. 107: p. 184-198.
- [21] Soltanahmadi, S., Morina, A., Van Eijk, M.C.P., Nedelcu, I., and Neville, A., Investigation of the effect of a diamine-based friction modifier on micropitting and the properties of tribofilms in rolling-sliding contacts. *Journal of Physics D: Applied Physics*, 2016. 49(50).
- [22] Parsaeian, P., Van Eijk, M.C.P., Nedelcu, I., Neville, A., and Morina, A., Study of the interfacial mechanism of ZDDP tribofilm in humid environment and its effect on tribochemical wear; Part I: Experimental. *Tribology International*, 2017. 107: p. 135-143.
- [23] Morina, A., Neville, A., Green, J.H., and Priest, M., Additive/additive interactions in boundary lubrication - A study of film formation and tenacity, in *Tribology and Interface Engineering Series*. 2005. p. 757-767.
- [24] Morina, A. and Neville, A., Tribofilms: Aspects of formation, stability and removal. *Journal of Physics D: Applied Physics*, 2007. 40(18): p. 5476-5487.

-
- [25] Li, Y.R., Pereira, G., Kasrai, M., and Norton, P.R., Studies on ZDDP anti-wear films formed under different conditions by XANES spectroscopy, atomic force microscopy and ^{31}P NMR. *Tribology Letters*, 2007. 28(3): p. 319-328.
- [26] Li, Y.R., Pereira, G., Kasrai, M., and Norton, P.R. Studies on ZDDP anti-wear films formed under the different conditions by XANES spectroscopy, atomic force microscopy and ^{31}P NMR. in 2007 Proceedings of the ASME/STLE International Joint Tribology Conference, IJTC 2007. 2008.
- [27] Martin, J.M., Grossiord, C., Le Mogne, T., Bec, S., and Tonck, A., The two-layer structure of Zn dtp tribofilms, Part I: AES, XPS and XANES analyses. *Tribology International*, 2001. 34(8): p. 523-530.
- [28] Crobu, M., Rossi, A., Mangolini, F., and Spencer, N.D., Tribochemistry of bulk zinc metaphosphate glasses. *Tribology Letters*, 2010. 39(2): p. 121-134.
- [29] Crobu, M., Rossi, A., Mangolini, F., and Spencer, N.D., Chain-length-identification strategy in zinc polyphosphate glasses by means of XPS and ToF-SIMS. *Analytical and Bioanalytical Chemistry*, 2012. 403(5): p. 1415-1432.
- [30] COM(2017) 675 final; Communication from the Commission to the European Parliament, the Council, the European Economic and Social Committee and the Committee of the Regions.
- [31] European Commission. Regulation (EC) no 443/2009 of the European parliament and of the council setting emission performance standards for new passenger cars as part of the community's integrated approach to reduce CO₂ emissions from light-duty vehicles . 2009
- [32] Nakamura, T., Improvement of fuel efficiency of passenger cars by taking advantage of tribology. *Tribology Online*, 2017. 12(3): p. 76-81.
- [33] Holmberg, K., Andersson, P., and Erdemir, A., Global energy consumption due to friction in passenger cars. *Tribology International*, 2012. 47: p. 221-234.
- [34] Morina, A., Neville, A., Priest, M., and Green, J.H., ZDDP and MoDTC interactions in boundary lubrication-he effect of temperature and ZDDP/MoDTC ratio. *Tribology International*, 2006. 39(12): p. 1545-1557.
- [35] Morina, A., Neville, A., Priest, M., and Green, J.H., ZDDP and MoDTC interactions and their effect on tribological performance

- Tribofilm characteristics and its evolution. *Tribology Letters*, 2006. 24(3): p. 243-256.
- [36] Berkani, S., Dassenoy, F., Minfray, C., Martin, J.-M., Cardon, H., Montagnac, G., and Reynard, B., Structural Changes in Tribo-Stressed Zinc Polyphosphates. *Tribology Letters*, 2013. 51(3): p. 489-498.
- [37] Weber, T., Muijsers, J.C., and Niemantsverdriet, J.W., Structure of Amorphous MoS₃. *The Journal of Physical Chemistry*, 1995. 99(22): p. 9194-9200.
- [38] Wang, Y., He, P., Lei, W., Dong, F., and Zhang, T., Novel FeMoO₄/graphene composites based electrode materials for supercapacitors. *Composites Science and Technology*, 2014. 103(0): p. 16-21.
- [39] Ott, V.R., Swieter, D.S., and Schultz, F.A., Di- μ -oxo, μ -oxo- μ -sulfido, and di- μ -sulfido complexes of molybdenum(V) with EDTA, cysteine, and cysteine ester ligands. Preparation and electrochemical and spectral properties. *Inorganic Chemistry*, 1977, 16(10), 2538-2545.
- [40] Onodera, T., Morita, Y., Suzuki, A., Koyama, M., Tsuboi, H., Hatakeyama, N., Endou, A., Takaba, H., Kubo, M., Dassenoy, F., Minfray, C., Joly-Pottuz, L., Martin, J.-M., and Miyamoto, A., A Computational Chemistry Study on Friction of h-MoS₂. Part I. Mechanism of Single Sheet Lubrication. *The Journal of Physical Chemistry B*, 2009. 113(52): p. 16526-16536.
- [41] Ghanbarzadeh, A., Wilson, M., Morina, A., Dowson, D., and Neville, A., Development of a new mechano-chemical model in boundary lubrication. *Tribology International*, 2016. 93: p. 573-582.
- [42] Ghanbarzadeh, A., Parsaeian, P., Morina, A., Wilson, M.C.T., Van Eijk, M.C.P., Nedelcu, I., Dowson, D., and Neville, A., A Semi-deterministic Wear Model Considering the Effect of Zinc Dialkyl Dithiophosphate Tribofilm. *Tribology Letters*, 2016. 61(1).
- [43] Zhang, J. and Spikes, H., On the mechanism of ZDDP antiwear film formation. *Tribology Letters*, 2016. 63(2): p. 1-15.
- [44] Xu, D., Wang, C., Wang, J., Espejo, C., Neville, A., and Morina, A., Modelling of low friction tribofilm growth and removal. Submitted for publication, 2018
- [45] Dorgham, A., Neville, A., Ignatyev, K., Mosselmans, F., and Morina, A., An in situ synchrotron XAS methodology for surface

-
- analysis under high temperature, pressure, and shear. *Review of Scientific Instruments*, 2017. 88(1).
- [46] Morina, A., Zhao, H., and Mosselmans, J.F.W., In-situ reflection-XANES study of ZDDP and MoDTC lubricant films formed on steel and diamond like carbon (DLC) surfaces. *Applied Surface Science*, 2014. 297: p. 167-175.
- [47] Dorgham, A., In-situ synchrotron XAS study of the mechanochemistry of ZDDP triboreactive interfaces, University of Leeds, PhD thesis, 2018.
- [48] D., I.E., J.A., B., JM, D., M, d.J., D, P., I, M., WC, E., and P, N., Phosphorus k-edge XANES spectroscopy of mineral standards. *Journal of synchrotron radiation*, 2011. 18(2): p. 189-197.

Proceset nanometrike tek sistemet tribologjike dhe ndikimi i tyre në performancën makrometrike

Ardian Morina

Përmbledhje

Dizajnimi i sistemeve tribologjike industriale me fërkim dhe konsumim optimal deri më tani kryesisht ka qenë empirik, i bazuar në teori të zhvilluara nga studimet eksperimentale. Kjo është për shkak se proceset fiziko/kimike që zhvillohen në nivel atomik dhe molekular në sistemet tribologjike nuk janë ende plotësisht të shtjelluara. Studimi i bashkëveprimeve kimike dhe fizike përbrenda një kontakti tribologjik mundëson një kuptim më të plotë të proceseve që e përcaktojnë fërkimin dhe konsumimin e materialeve në kontakt. Ky punim fillimisht pasqyron se si proceset fiziko/kimike e përcaktojnë performancën e dy sistemeve tribologjike, pjesë e industrisë së energjisë dhe transportit. Në pjesën e dytë, punimi paraqet dy metoda të reja analitike që bazohen në teknologjinë e spektroskopisë Raman dhe të absorbimit të rrezeve X, si dhe shtjellon potencialin e tyre për studimin in-situ të reaksioneve kimike dhe fizike që paraqiten në një kontakt tribologjik.

Punimi synon të promovon qasjen multidisiplinare për studimin e sistemeve tribologjike, si dhe të potencialit të kësaj qasjeje në zhvillimin e teknologjive të reja tribologjike, si në industrinë e energjisë e po ashtu edhe në industrinë e transportit.

EVALUATION OF ESSENTIAL OIL COMPOSITION, TOTAL PHENOLICS, TOTAL FLAVONOIDS AND ANTIOXIDANT ACTIVITY OF MALUS SYLVESTRIS (L.) MILL. FRUITS.

Behxhet Mustafa^a, Dashnor Nebija^b, Avni Hajdari^{a,*}

Abstract

The principal aim of this study was to investigate the chemical composition of volatile and phenolic compounds obtained from ripe fruits of European wild apple (*Malus sylvestris* (L.) Mill.) originating from Kosovo, as well as their antioxidant activity. Gas chromatograph equipped with Flame Ionisation Detector (GC/FID) and Gas chromatograph coupled with Mass Spectrometer Detector (GC/MS) were used for the analysis of the volatile compounds whereas determination of total phenolic content (TPC) and total flavonoid content (TFC), as well as antioxidant activities was done spectrophotometrically (UV/VIS). Antioxidant activities of extracts were assessed using Ferric Reducing Antioxidant Power (FRAP) and 2,2-diphenyl-1-picrylhydrazyl (DPPH) scavenging activity. GC analysis of volatile compounds delivered totally 41 compounds were, sesquiterpenes being the principal constituents. In addition, sample analysis showed that European wild apple is rich in phenolic compounds. FRAP antioxidant capacity was 518.7 ± 42.9 mg TE/g dry

^a Department of Biology. Faculty of Mathematical and Natural Science. University of Prishtina. Mother Theresa St. 10000 Prishtinë. Kosova

^b Department of Pharmaceutical Chemistry, Faculty of Medicine, University of Prishtina, Mother Theresa Street, 10000 Prishtinë, Kosova.

* Corresponding author: avni.hajdari@uni-pr.edu

mass, and DPPH radical scavenging capacity, 56.7 ± 10.2 DPPH mg TE/g dry mass or $53.6 \pm 9.7\%$ inhibition.

Key words: European wild apple, GC/MS, volatile compounds, phenolic compounds, antioxidant activity.

Introduction

European wild apple, also known as Crab Apple (*Malus sylvestris* (L.) Mill.), Rosaceae, is a deciduous fruit tree, with expended crowns often appearing like bushes. It grows as a native species, found in broad range of latitudes, in European forests, especially in deciduous and mixed forest habitats and on soil environmental conditions [1-3]. Most individuals grow up to 10 m. [4. European wild apple is an insect pollinated species with flowering time from April to May and fruit ripening time from September to October. [5] The most suitable morphological characteristics to distinguish species wild apple from domestic apple are considered to be the pubescence of leaves and flowers, fruit size and color. [6] Wild apple fruits are rich in pectins and can be consumed raw or cooked. They are used for the production of the apple cider, vinegar, jellies, jams etc. Teas can be made from the leaves and fruits. [3] Furthermore, Wild apple fruits have been traditionally used against various ailments, principally owing to their astringent and laxative properties. Due to the pectin content they are used to obviate the constipation, and the crushed fruit pulp can be used externally to heal inflammations or small flesh wounds. In addition, they are used for respiratory problems (colds, flu), treatment of other symptoms such as fever and headache and externally for the treatment of wounds and sunburns. [7] In Kosovo traditional medicine, the fruits of European wild apple are used to treat different disorders such: warts, earache, skin infections, headache, hypertension, diarrhoea, caught, hyper-cholesterol, diabetes, as expectorant and mucolytic. [8,9] Furthermore, in Kosovo it is used to prepare: jams, compote (first sliced and dried (ahaf), then boiled in water prior to drink (wintertime food) and tea, as well. [10]

The role of apples and their constituents in human health has been thoroughly reviewed. Different mechanisms such as antioxidant, antiproliferative, and cell signalling effects could be responsible for their health benefits such as prevention of cancer, cardiovascular disease, asthma, Alzheimer's disease, improved outcomes related to

cognitive impairment, diabetes, weight loss, bone health, pulmonary function, and gastrointestinal protection. [11-23] It has been documented that *Malus* wild species are rich sources of phenolic compounds with high antioxidant activity. [24] Wild apple fruit contain different components such as polyphenols, condensed tannins (procyanidins), chlorogenic acid, and epicatechin. The most important constituents are caffeic acid derivatives, p-coumaric acid derivatives, flavan-3-ols, flavonols, dihydrochalcones. [25]

Polyphenolic profile of crab-apple fruits and its hybrids with domestic apple showed characteristic polyphenol profile characteristic for genus *Malus*, however low content of flavan-3-ols and derivatives of cinnamic acid and high content of procyanidin B1, phloridzin, anthocyanes, and quercetin glycosides. Procyanidin B2 was not found in both peel and flesh of Siberian crabapple. [26] Chlorogenic acid was the main polyphenol detected in the flesh, whereas phloridzin was the main phenolic compound detected in seeds and steams of crab apple pomace. [27] In the case of domestic apple *Malus domestica* Borkh, experimental data revealed that the most abundant phenolic compounds were quercetin glycosides, procyanidin B2, chlorogenic acid, epicatechin, phloretin glycosides. Vitamin C and phenolic compounds concentrations correlate with antioxidant capacity. [28] It was shown that the peels of apples, in particular, contain high amount of phenolic compounds. Due to the higher concentration of phenolics and flavonoids, the peels have significantly higher total antioxidant activities than the flesh of the apple varieties examined. [29] In the study of Jakobek, et al. [30] flavanols, dihydrochalcones and phenolic acids were identified in the flesh of apple varieties studied (including the crab apple) and flavanols, dihydrochalcones, phenolic acids, flavonols and anthocyanins were identified in peels. Comparing to other apples, wild apple contained much higher amounts of flavanol and phenolic acids in the flesh, while the amount of these compounds in peel was similar. Antioxidant and antiproliferative activity of extracts and juices obtained from crab apples was reported and experimental data revealed that antiproliferative effect was more correlated to the amount of polyphenol than of anthocyanins [31-32]. Polyphenols profile and antioxidant activity of skin and pulp of *Malus pumila* Mill., originating from Italy was studied too. [33]

Literature data showed that only a small number of papers address the composition of volatile compounds of European wild apple, although, some studies of this nature have been reported for mature

fruits (whole fruit, peel and flesh) and flowers of *Malus pumila* Mill originating from Italy [34, 35], from fresh leaves of *Malus domestica* growing in Western Himalaya (India) [36], from leaves of apple-tree (*Malus domestica* Borkh.) growing in Lithuania [37]. Solid-phase microextraction or liquid–liquid extraction coupled with GC-FID and/or GC-MS analysis European wild apple fruit distillates revealed complex volatile profile. The main classes of compounds were alcohols, shikimate metabolites, esters, terpenes, aldehydes and acetals, fatty acids and carotenoid-derived compounds. [38]

The principal aim of this study was to analyse the chemical composition of volatile and phenolic compounds of wild apples originating from Kosovo and to study their antioxidant and radical scavenging activity.

Experimental Section

Collection and extraction of European wild apple samples

Plant material of European wild apple (skin and flesh fruits) was procured from local markets in Prizren (Kosovo), from five different sellers. In total 5 samples were distilled, samples were analysed separately. Fruits were air-dried in shade at room temperature and cut into small pieces (<0.5 cm). For distillation, 50 g of dry tissue were placed into 0.5 liter of water in a 1 liter flask and distilled at a rate of 3 mL/min in a Clevenger apparatus for 3 h. The volatiles were collected with n-Hexane and stored in the dark at -18°C in the freezer pending further analysis.

GC and GC/MS analyses

Chromatographic analyses were made using an Agilent 7890A gas chromatography system equipped with flame ionisation (FID) detector (Agilent Technologies). The separation was conducted on a HP-5MS column 30 m x 0.25 mm with 0.25 mm film thickness. Helium was used as the carrier gas with an initial flow rate of 0.6 mL/min and subsequently at a constant pressure of 16.6 psi. The front inlet was maintained at 250°C in a split ratio of 50:1. The GC oven temperature increased from 60°C to 260°C at a rate of 5°C/min, and the FID operated at 250°C with an air flow of 350 mL/min and a hydrogen flow of 35 mL/min. The injection

volume was 1.0 μL . Gas chromatography/mass spectrometry analyses were performed using an Agilent 7890A gas chromatograph system coupled to a 5975C mass spectrometer detector (MSD) (Agilent Technologies). The ionization energy was 70 eV with a mass range of 40 - 400 m/z. The separation was conducted with the same column and temperature program as for the analytical GC.

Identification of each component of the essential oil was made by comparing their Kovats retention indexes with those in literature [39]. The calculation of the Kovats index was made based on a linear interpolation of the retention time of the homologous series of n-alkanes (C9 - C28) under the same operating conditions. The components were also identified by comparing the mass spectra of each constituent with those stored in the MS library search (NIST 08.L and WILEY MS 9th) and with mass spectra from the literature. [39]

Determination of Total Phenolics and Total Flavonoids.

For the analysis of total phenols, total flavonoids and antioxidant activity (DPPH and FRAP), fruits were dried, ground and 150 mg of dried fruits were extracted with 25 ml of methanol (50%) in water bath for 90 minutes at 75°C and stored at -18°C in a freezer until further analyses.

The total flavonoids in the extracts were determined using a photometric method according to. [40] Catechin (0-10 mg/ml) was used as a standard to establish the calibration curve. Absorbance was measured at a wavelength of 510 nm. The total content of flavonoids was expressed as mg catechin equivalent/g plant dry weight.

The total phenolic content in the extracts was determined using the Folin-Ciocalteu method in an alkaline environment. [41] Caffeic acid (0-25 mg/ml) was used as a standard to establish the calibration curve, and absorbance was measured at 725 nm against the blank. The results were expressed as mg caffeic acid equivalent/g plant dry weight.

Evaluation of Antioxidant Activity

The DPPH (2,2-diphenyl-1-picrylhydrazyl) radical scavenging assay and Trolox (2.5 mM in methanol) were used as reference substances following the protocol of [41]. Trolox (0-50 mg/ml) was used to construct the calibration curve. The absorbance of the decolorizing process was measured at 515 nm against the blank. The

results are expressed as the percent scavenging of DPPH free radicals and were measured using the following equation: % DPPH radical scavenging = [(absorbance of control - absorbance of test sample) / (absorbance of control)] x 100.

The ferric reducing antioxidant power (FRAP) assay measures the ability of antioxidants to reduce the ferric 2,4,6-tripyridyl-s-triazine complex $[\text{Fe(III)}]^{3+}$ to the intensely blue-colored ferrous complex $[\text{Fe(II)}]^{2+}$ in acidic medium. The FRAP assay was performed as described by (Chizzola 2008). The calibration curve was constructed using calibration standards of Trolox from (0 to 400 mg/ml) in ethanol, and absorbance was measured at a wavelength of 593 nm. The results were estimated as mg Trolox equivalent/g plant dry weight.

All spectrophotometric measurements in the following analyses were performed using a UV-Vis (ultra-violet/visible) spectrophotometer (Thermo Scientific™ GENESYS 10S UV-Vis spectrophotometer), and the results represent the average of 5 measurements.

Results and discussion

Experimental results, using GC and GC/MS analysis, documented that volatile oil obtained from European wild apple is a complex mixture of constituents, composed by various volatile compounds classes. There were identified totally 41 compounds, and, as presented in the Table 1, the principal classes of chemical constituents were sesquiterpenes and oxygenated sesquiterpenes, with 50.6% and 30.7%, respectively. The concentration of (E)-spiroether (en-yn-dicycloether) was 9%. Other classes of compounds such monoterpenes, hydrocarbons, phenylpropanoids etc. were present at lower percentages. In the Figure 1 chemical formulas of the most prominent compounds in the volatile oils of European wild apple are presented.

E- β -Farnesene (35.03%), E-Caryophyllene (7.17%) and Germacrene D (5.76%) were the principal sesquiterpenes, whereas α -Bisabolol oxide B (4.82 %), Spathulenol (4.78%), α -Eudesmol (4.52%), Caryophyllene oxide (4.46%), 2Z, 6 E-Farnesol (4.34%) and Z-dihydro-Apofarnesol (2.22) were the most prominent sesquiterpene oxides. In lower concentrations appeared hydrocarbons (2.01%) monoterpenes (1.04%) and other compounds, including fatty acids and phenylpropanoids etc. (1.09%).

Table 1. Chemical composition of volatile compounds of European wild apple

1	Rt	Compounds	KI	%
2	6,45	cis-Crysanthenyl acetate	1265	0.25
3	8,27	Carvacrol ethyl ether	1298	0.16
4	8,99	Eugenol	1359	0.35
5	10,99	Decanoic acid	1366	0.20
6	11,48	β -Patchoulene	1381	0.29
7	13,31	α -Isocomene	1388	0.29
8	19,90	β -Isocomene	1408	0.40
9	22,89	E-Caryophyllene	1419	7.17
10	24,89	E- β -Farnesene	1456	35.03
11	25,70	dehydro-Sesquicineole	1471	1.33
12	25,84	Germacrene D	1481	5.76
13	26,14	β -Selinene	1490	1.00
14	26,64	Z-dihydro-Apofarnesal	1498	0.30
15	26,38	Bicyclogermacrene	1500	0.21
16	26,85	Piperonyl acetate	1503	0.40
17	27,33	E,E- α -Farnesene	1505	0.05
18	27,57	10-epi-Cubebol	1535	0.30
19	28,53	Geranyl butanoate	1564	0.63
20	29,45	Z-dihydro-Apofarnesol	1572	2.22
21	29,61	Spathulenol	1578	4.78
22	30,24	Caryophyllene oxide	1583	4.46
23	30,62	Isolongifolan-7- α -ol	1619	0.44
24	30,81	β -Acorenol	1636	0.41
25	31,41	α -Muurolol	1646	1.26
26	33,08	α -Eudesmol	1653	4.52
27	36,52	α -Bisabolol oxide B	1658	4.82
28	41,29	Unknown 1	1671	0.75
29	43,46	Khusinol	1680	0.42
30	45,56	Elemol acetate	1680	1.57
31	47,57	α -Bisabolene oxide A	1685	1.75
32	48,19	2Z,6Z-Farnesol	1698	0.23
33	49,51	2Z,6E-Farnesol	1723	4.34
34	50,97	Unknown 2	1733	0.45
35	51,19	Camazulene	1731	0.42
36	51,37	α -Bisabolol oxide A	1754	1.61
37	52,02	Unknown 3	1769	0.29
38	52,80	E-Spiroether	1890	8.99

39	53,18	Oleic acid	2142	0.14
40	53,64	n-Docosane	2200	0.05
41	54,28	n-Tricosane	2300	0.06
42	54,48	n-Tetracosane	2400	0.41
43	54,64	n-Pentacosane	2500	0.04
44	54,92	Hexacosane	2600	1.45
<i>Total identified (%)</i>				98.51
Sesquiterpenes				50.62
Oxygenated sesquiterpenes				34.76
Spiroketal				8.99
Hydrocarbons				2.01
Monoterpenes				1.04
Others				1.09

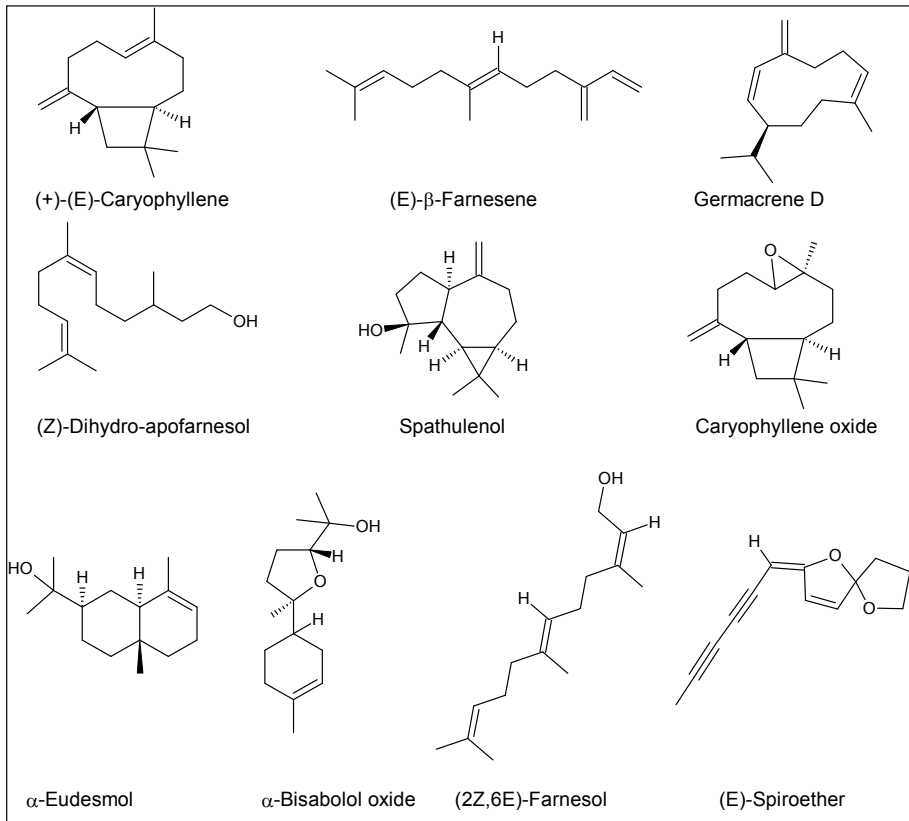


Fig. 1. Chemical formulas of the principal volatile compounds

Comparing to our data, the study of volatile compound in mature fruits (whole fruit, peel and flesh) of *Malus pumila* Mill. originating in Italy, revealed that there were identified 30 compounds and terpenes were the main volatiles, from whole fruits and peels, whereas aliphatic esters were the most abundant constituents of flesh. The most prominent constituent in all samples was sesquiterpene (E,E)- α -farnesene. Other monoterpenes and typical esters were present in smaller amounts [34]. On the other hand, in flower samples of other cultivar of red Italian apple, linalool was the most abundant constituent, followed by (E, E)- α -farnesene [36]. In extracts obtained from fresh leaves of *Malus domestica* growing in Western Himalaya (India) volatile oils were mostly composed by mono-, sesqui-, di-terpenes, phenolics, and aliphatic hydrocarbons. Seventeen compounds of the oil were characterized and principal compounds of the oil were eucalyptol (43.7%), phytol (11.5%), α -farnesene (9.6%), and pentacosane (7.6%) [36]. Sesquiterpenoids, monoterpenoids, diterpenes and aliphatic hydrocarbons were the main constituents of essential oils obtained from leaves of apple-tree (*Malus domestica* Borkh.) growing in Lithuania. The most prominent constituents were (iso)phytol ($\leq 27.3\%$), (E, E)- α -farnesene ($\leq 22.0\%$), n-hexyl benzoate ($\leq 13.5\%$), tridecane (11.0%), and α -cadinol (10.5%) [37]. In contrast to others studies, our samples were rich in (E)-spiroether (9%), which was not previously reported to be present in fruits of European wild apple. (E)-spiroether were reported to be present in other plant species, such *Matricaria recutita* L. which shows that inhibited the production of mycotoxins AFG1 (produced by *Aspergillus parasiticus*) and 3-ADON (*Fusarium graminearum*) [45]. Thus, presence of (E)-spiroether will reduce the mycotoxins contamination of European wild apple fruits and reduce the human health risk caused by those toxins.

Except volatile compounds, total phenolics and total flavonoid concentration, as well as the antioxidant activity (FRAP and DPPH) of methanolic extracts were evaluated too. The concentration of total phenolics was 63.5 ± 6.7 mg caffeic acid equivalent/g of plant dry mass, while the total flavonoid was 40.3 ± 5.8 mg catechin equivalent/g of plant dry mass. Regarding antioxidant activity, the FRAP antioxidant capacity were 518.7 ± 42.9 mg TE/g dm, while DPPH radical scavenging capacity was 56.7 ± 10.2 DPPH mg TE/g dm or $53.6 \pm 9.7\%$ inhibition.

Total phenolics and total flavonoid concentration as well as the antioxidant activity (FRAP and AOA) of the wild apple fruit extracts originated from Serbia were evaluated too, thus total phenolics ranged from 172.91–1556.99mg GAE/100g dry weight; total flavonoid ranged

from 3.97 to 182.22 mg RE/100g d.w., while FRAP value ranged from 2.13 to 7.65mM Fe²⁺ and %AOA from 57.73% to 95.32 %AOA [42]. In fruit extracts originated from Malaysia the total content of phenolic was 216.11± 7.72 (expressed as mg GAE/g extract weight); EC50 was 0.606 ± 0.008mg/ml (DPPH assay) and 14.48 ± 1.423 mM/100g (FRAP value) [43]. Total flavonoid content of aqueous extracts of the fruits peel of European wild apple was 44.62 ± 1.39 mg (expressed as mg Quercetin equivalent per gram extract weight (mg QE/g extract weight); total phenolic content 199.26 ± 8.15(mg GAE/g EW); DPPH antioxidant scavenging capacity was 0.665 ± 0.032 EC50 (mg/ml) and FRAP reducing capacities was 13.91 ± 2.135 (mM/100g) [44].

Conclusion

In this study, the chemical composition of volatile constituents obtained from fruits of European wild apple, growing in Kosovo has been elucidated. Furthermore the total flavonoides and phenolic compounds were assessed and their antioxidant and radical scavenging capacities have been determined. Concerning the volatile compounds, the sesquiterpene hydrocarbons were dominant constituents. In addition this study revealed that European wild apple is very reach source of bioactive phenols and flavonoids and these related data may encourage new studies in the future.

References

- [1] Schnitzler, A.; Arnold, C.; Cornille, A.; Bachmann, O.; and Schnitzler C. Wild European Apple (*Malus sylvestris* (L.) Mill.) Population Dynamics: Insight from Genetics and Ecology in the Rhine Valley. Priorities for a Future Conservation Program. *PLoS ONE* 2014, 9(5): e96596. <https://doi.org/10.1371/>
- [2] Stephan B. R.; Wagner, I.; and Kleinschmit, J. EUFORGEN Technical Guidelines for genetic conservation and use for wild apple and pear (*Malus sylvestris* and *Pyrus pyraster*). International Plant Genetic Resources Institute, Rome, Italy. 2003, 6 pages. Available from: <http://www.euforgen.org>. Accessed on 2017.
- [3] <http://www.pfaf.org/user/plant.aspx?LatinName=Malus+sylvestris>. Accessed on 2017.
- [4] Wagner, I. Zusammenstellung morphologischer Merkmale und ihrer Ausprägungen zur Unterscheidung von Wild- und

- Kulturformen des Apfel- (*Malus*) und des Birnbaumes (*Pyrus*). Mitteilungen der Deutschen Dendrologischen Gesellschaft 1996, 82: 87–108.
- [5] Gregor, A. Der Wildapfel –Biologie und Ökologie einer gefährdeten Baumart. LWF Wissen 73. 2013, Bayerisches Staatsministerium für Ernährung, Landwirtschaft und Forsten (StMELF). Freising, Germany
- [6] Drvodelić, D.; Jemrić, T.; Oršanić, M. and Paulić, V. Fruits Size Of Wild Apple (*Malus sylvestris* (L.) Mill.): Impact On Morphological And Physiological Properties Of Seeds. Izvorni znanstveni članci – Original scientific papers *Šumarski list* 2015, 3–4, 145–153.
- [7] Arnal-Olivares, A.; Tardío, J. and Lázaro, Almudena. Traditional uses of the crab apple tree (*Malus sylvestris* Mill., Rosaceae) in Spain. 58 Annual meeting of the society for Economic Botany. Bragança-Portugal. June 4-9 2017.
- [8] Mustafa B., Hajdari A., Pajazitaj Q., Sylva B., Quave C.L. and Pieroni A. An ethnobotanical survey of the Gollak region, Kosovo. *Genet Resour Crop Ev.* 2011; 59 (5): 739–54.
- [9] Mustafa B., Hajdari A., Krasniqi F., Hoxha E., Ademi H., Quave CL, et al. Medical ethnobotany of the Albanian Alps in Kosovo. *J Ethnobiol Ethnomed.* 2012; 8:6.
- [10] Mustafa B., Hajdari A., Pieroni A., Pulaj B, Koro X and Quave CaL. A cross-cultural comparison of folk plant uses among Albanians, Bosniaks, Gorani and Turks living in south Kosovo, Mustafa et al. *Journal of Ethnobiology and Ethnomedicine* 2015 11:39
- [11] Hyson D.A. A comprehensive review of apples and apple components and their relationship to human health. *Adv Nutr.* 2011, 2(5):408-20. doi: 10.3945/an.111.000513. Epub 2011 Sep 6.
- [12] Yue, Z.; Jie Z.; Ya L.; Dong-Ping, X.; Sha, L.; Yu-Ming, C. and Hua-Bin, L. Natural Polyphenols for Prevention and Treatment of Cancer. *Nutrients.* 2016, 8(8): 515.
- [13] Shih-Hsin, T.; Li-Ching, C. and Yuan-Soon, H.. An apple a day to prevent cancer formation: Reducing cancer risk with flavonoids. *J Food Drug Anal.* 2017, 25(1)119-124
- [14] Weichselbaum, E.; Wyness, L.; and Stanner, S. Apple polyphenols and cardiovascular disease – a review of the evidence. *Nutrition Bulletin* 2010, 35 (2) 92–101
- [15] Tanaka, T. and Takahashi, R. Flavonoids and Asthma. *Nutrients.* 2013, 5(6): 2128–2143. Published online 2013 Jun 10. doi: 10.3390/nu5062128

- [16] Toshihiko, T.; Tadahiro, S.; Tomomasa, K.; Motoyuki, T.; Takuji, S. and Takahiko S. Apple Procyanidins Suppress Amyloid β -Protein Aggregation. *Biochem Res Int*. 2011: 784698. Published online 2011 Aug 2. doi: 10.1155/2011/784698
- [17] Cheng D, Xi Y.; Cao, J. Cao, D.; Ma, Y. and Jiang, W. Protective effect of apple (Ralls) polyphenol extract against aluminum-induced cognitive impairment and oxidative damage in rat. *Neurotoxicology*. 2014, 45,111-20. doi: 10.1016/j.neuro.2014.10.006. Epub 2014 Oct 17.
- [18] Manzano, M.; Giron, M.D.; Vilchez, J.D.; Sevillano, N.; El-Azem, N.; Rueda,R. et al. Apple polyphenol extract improves insulin sensitivity in vitro and in vivo in animal models of insulin resistance *Nutrition & Metabolism* 2016 13:32. <https://doi.org/10.1186/s12986-016-0088-8>
- [19] Conceição de Oliveira M.; Sichieri, R.; Moura, A. Weight loss associated with a daily intake of three apples or three pears among overweight women. *Nutrition*. 2003,19:253–6
- [20] Puel, C.; Quintin, A.; Mathey, J.; Obled, C.; Davicco, M.J.; Lebecque, P. et al. Prevention of bone loss by phloridzin, an apple polyphenol, in ovariectomized rats under inflammation conditions. *Calcif Tissue Int*. 2005,77 (5):311-8. Epub 2005 Nov 16.
- [21] Boyer, J. and Liu, R.H. Apple phytochemicals and their health benefits. *Nutr J*. 2004, 3: 5. Published online 2004 May 12. doi: 10.1186/1475-2891-3-5
- [22] Carrasco-Pozo, C.; Speisky,H.; Brunser, O.; Pastenell, E. and Gotteland, M. Apple Peel Polyphenols Protect against Gastrointestinal Mucosa Alterations Induced by Indomethacin in Rats. *J. Agric. Food Chem.*, 2011, 59 (12), 6459–6466 DOI: 10.1021/jf200553s
- [23] Usta, C.; Bedel,A.; Kurtoğlu, A.U. and Kurtoğlu, E. Effects of Crabapple (*Malus sylvestris*) on Blood Glucose and Lipid Levels in Diabetic Rats. *Journal of Food and Nutrition Research* 2016, 4(3)148-151. doi: 10.12691/jfnr-4-3-3
- [24] Li, N.; Shi, J. AND Wang, K. Profile and antioxidant activity of phenolic extracts from 10 crabapples (*Malus wild species*). *J Agric Food Chem*. 2014 22; 62(3) 574-81. doi: 10.1021/jf404542d. Epub 2014 Jan 13.
- [25] Shoji, T. Crab apple fruit polyphenol and production process thereof. Google Patents. CA Patent 2,421,761. Publication date: Sep 1, 2009.
- [26] Rudikovskaya, E.G.; Dudareva, L.V.; Shishparenok, A.A. and Rudikovskii, V. Peculiarities of polyphenolic profile of fruits of

- Siberian crab apple and its hybrids with *Malus* × *Domestica* Borkh *Acta Physiol Plant* 2015 37: 238. <https://doi.org/10.1007/s11738-015-1993-6>.
- [27] Górnaś, P.; Mišina, I.; Olšteine, A. and Seglina, D. Phenolic compounds in different fruit parts of crab apple: Dihydrochalcones as promising quality markers of industrial apple pomace by-products. *Ind Crops Prod.* 201574, 607–612 DOI10.1016/j.indcrop.2015.05.030
- [28] Lee, K.W.; Kim, Y.J.; Kim, D.O.; Lee, H.J. and Lee, C.Y. Major Phenolics in Apple and Their Contribution to the Total Antioxidant Capacity *J. Agric. Food Chem.*, 2003, 51 (22), 6516–6520 DOI: 10.1021/jf034475w
- [29] Wolfe, K.; Wu, X. and Liu, R.H. Antioxidant Activity of Apple Peels *J. Agric. Food Chem.*, 2003, 51 (3), pp 609–614 DOI: 10.1021/jf020782a Publication Date (Web): January 1, 2003
- [30] Jakobek, A.R. Barron Ancient apple varieties from Croatia as a source of bioactive polyphenolic compounds. *J. Food Comp. Anal.*, 2016, 45, 9–15
- [31] Liaudanskas, M.; Viškelis, P.; Raudonis, R.; Kviklys, D.; Uselis, N. and Janulis, V. Phenolic Composition and Antioxidant Activity of *Malus domestica* Leaves *Sci. World J.* 2014, Article ID 306217, 10 pages <http://dx.doi.org/10.1155/2014/306217>
- [32] Yoshizawa, Y.; Sakurai, K.; Kawaii, S.; Soejima, J. and Murofushi, N. Antiproliferative and Antioxidant Properties of Crabapple Juices. *Food Sci. Technol. Res.*, 2004, 10 (3), 278-281
- [33] Giomaro, G.; Karioti, A.; Bilia, A.R.; Bucchini, A.; Giamperi, L.; Ricci, D. et al. Polyphenols profile and antioxidant activity of skin and pulp of a rare apple from Marche region (Italy) *Chem Cent J.* 2014; 8: 45
- [34] Fraternali, D.; Ricci, D.; Flamini, G. and Giomaro, G. Volatiles Profile of Red Apple from Marche Region (Italy). *Rec. Nat. Prod.* 2011, 5:3, 202-207
- [35] Fraternali, D.; Flamini, G.; Ricci, D. and Giomaro, G. Flowers Volatile Profile of a Rare Red Apple Tree from Marche Region (Italy). *J. Oleo Sci.* 63, 2014, (11) 1195-1201 doi: 10.5650/jos.ess14088
- [36] Walia, M.; Mann, T.S.; Kumar, D.; Agnihotri, V.K. and Singh, B. Chemical Composition and In Vitro Cytotoxic Activity of Essential Oil of Leaves of *Malus domestica* Growing in Western Himalaya (India) *Evid Based Complement Alternat Med.* 2012; 2012: 649727. Published online 2012 Apr 29. doi: 10.1155/2012/649727

- [37] Judžentienė, A. and Misiūnas, A. Chemical composition of apple-tree (*Malus domestica* Borkh.) leaf essential oils. *Chemija*. 2017. vol. 28. No. 3. P. 172–176 2017
- [38] Mihajilov-Krstev, T.M.; Denic, M.S.; Zlatkovic, B.K. Stankov-Jovanovic, V.P.; Mitic, V.D.; Stojanovic G.S. et al. Inferring the origin of rare fruit distillates from compositional data using multivariate statistical analyses and the identification of new flavor constituents. *J Sci Food Agric* 2015; 95: 1217–1235
- [39] R. Adams, Identification of Essential Oil Components by Gas Chromatography/Mass Spectrometry, Allured, Carol Stream, Ill, USA, 4th edition, 2007.
- [40] Leontowicz, H.; Leontowicz, M.; Gorinstein, S.; Martin-Belloso, O. and Trakhtenberg, S. Apple peels and pulp as a source of bioactive compounds and their influence digestibility and lipid profile in normal and atherogenic rats, *Medycyna Wet.* 2007, 63 (11) Supplement 1434–1436.
- [41] Chizzola, R., Michitsch, H. and Franz, C. Antioxidative properties of *Thymus vulgaris* leaves: Comparison of different extracts and essential oil chemotypes, *J. Agric. Food. Chem.* 2008 56, 6897–6904.
- [42] Stojiljković, D.; Arsić, I. and Tadić, V.; Extracts of wild apple fruit (*Malus sylvestris* (L.) Mill., Rosaceae) as a source of antioxidant substances for use in production of nutraceuticals and cosmeceuticals. *nd Crops Prod.* 2016, 80. 165-176
- [43] Zulkifli, K.S.; Abdullah, N.; Abdullah, A.; Aziman, N. and Wan Kamarudin, W.S.S. Bioactive Phenolic Compounds and Antioxidant Activity of Selected Fruit Peels. 012 International Conference on Environment, Chemistry and Biology IPCBEE vol.49 (2012) (2012) IACSIT Press, Singapore DOI: 10.7763/IPCBEE. 2012. V49. 14
- [44] Abdullah, N.; Zulkifli, K.S.; Abdullah, A.; Aziman, N. and Wan Kamarudin, W.S.S. Assessment on the Antioxidant and Antibacterial Activities of Selected Fruit Peels. *International Journal of Chem Tech Research* 2012, 4, 4 1534-1542
- [45] Yoshinari, T.; Yaguchi, A.; Takahashi-Ando, N.; Kimura, M.; Takahashi, H.; Nakajima, T.; Sugita-Konishi, Y.; Nagasawa, H.; Sakuda, S. Spiroethers of German chamomile inhibit production of alatoxin G1 and trichothecene mycotoxin by inhibiting cytochrome P450 monooxygenases involved in their biosynthesis. *FEMS Microbiol Lett.* 2008, 284(2) 184-90.

Vlerësimi i përbërjes së vajit esencial, fenolet dhe flavonidet e tërësishme dhe aktiviteti antioksidant i mollës së egër

Behxhet Mustafa, Dashnor Nebija, Avni Hajdari

Përmbledhje

Qëllimi kryesor i këtij studimi ishte analizimi i përbërjes kimike të komponimeve të avullueshme, komponimeve fenolike, si dhe vlerësimi i aktiviteti antioksidues i ekstrakteve të përftuara nga frutat e pjekura të mollës së egër (*Malus sylvestris* (L.) Mill.) me origjinë nga Kosova. Kromatografi i gaztë i shoqëruar me detektor jonizues me flakë (GC/FID) dhe kromatografi i gaztë i shoqëruar me spektrometër të masës (GC/MS) janë përdorur për analizimin e komponimeve të avullueshme, ndërsa përcaktimi i përqendrimit të fenoleve totale (TPC) dhe flavonoideve totale (TFC), si dhe vlerësimi i aktivitetit antioksidues është bërë me spektrofotometër UV/VIS. Aktiviteti antioksidues i ekstrakteve është bërë duke përdorur kapacitetin reduktues të joneve ferrike (FRAP) dhe aktivitetin zbërthyes të 2,2-difenil-1-pikrilhidrazil (DPPH). Analizat nga kromatografi i gaztë ka rezultuar në identifikimin e 41 komponimeve të avullueshme në total, prej të cilave seskuiterpenet ishin përbërësit kryesorë. Përpos komponimeve të avullueshme, te frutat e mollës së egër është analizuar edhe përqendrimi i fenoleve totale (63.5 ± 6.7 mg acid kafeik/g në masën e thatë të frutave), flavonoideve totale (40.3 ± 5.8 mg katekinës/g në masën e thatë të frutave), si dhe aktiviteti antioksidues FRAP (518.7 ± 42.9 mg TE /g në masën e thatë të frutave), dhe kapaciteti zbërthyes i DPPH (56.7 ± 10.2 DPPH mg TE/g në masën e thatë të frutave ose $53.6 \pm 9.7\%$ inhibimit).

DESIGN AND PROGRAMMING OF 3D PRINTED ROBOTIC HAND

Arbnor Pajaziti^{a,*} Ilir Doçi^a, and Endrit Toplica^a

Abstract

Paper describes design process of robotic hand and programming of several tasks. Robotic hand with all its part is 3D printed with moulded plastic materials, and is developed and controlled in a coordinated manner as a system with many mechanical, electronic, hardware and software components. Motion dynamics of robotic hand is analysed through modelling and simulation with software. Motion of fingers and hand is programmed with ATMEGA2560 Arduino microcontroller and C++ programming. The aim is to create artificial hand that can be implemented by handicapped persons. The need for finding the right balance between modularization and coordination was essential.

Key words: Prosthetic Hand, Control, EMG (ElectroMyoGraphy), Motor Design.

Introduction

Modern artificial limbs are typical examples of mechatronic systems with actuators, sensors, mechanisms and electronics. In terms of control, coordination of the multi-axis system is necessary to minimize the complexity of the system. In this case, the need to find a proper balance between modular systems and coordination of modules

^a University of Prishtina “Hasan Prishtina”, Faculty of Mechanical Engineering, Str. Kodra e Diellit, p.n. Prishtina, Republic of Kosova.

* *Corresponding author:* arbnor.pajaziti@uni-pr.edu

is essential. Loading processing functions need to be distributed in independent modules. [1]

Prosthetic hands were one of the first applications fields envisaged for anthropomorphic hands, for obvious aesthetic and functional reasons. [2] Research is addressing control algorithms, and some of them are based on neural approaches [3], i.e., the control action is often taken as proportional to the superficial ElectroMyoGraphy (EMG) signals extracted by surface electrodes applied to muscles.

In robot hand design aiming at application to a myoelectric prosthetic hand and recognition of finger operation via surface EMG are discussed. [4]

The development of prosthetic hand system for amputees that estimates his/her desired finger angle from biosignals, such as EMG signals, and operates with the same motion as the user's intention is described in. [5]

A complete learning scheme for EMG based interfaces is used to discriminate between different reach to grasp movements in 3D space. The proposed scheme is able to decode human kinematics, using the myoelectric activity captured from human upper arm and forearm muscles. [6]

Today, prosthetic hands and arms are more complex. Hand represents a large number of nerves, ligaments, related muscles and bones to form a precise instrument. Recreating it through implants is one of the biggest challenges of medical engineering. [7,8]

Researchers and companies of the World have worked in the Development of prosthetic hands. Notable are:

E-Nable is a web portal that helps developers and engineers to get in touch and share ideas. It was founded by Jon Schull of the Rochester Institute of Technology, after he realized that many engineers around the world are working on this topic. All hand prostheses of E-Nable work according to the same principle. The fingers and the thumb are connected to the connector for the prosthesis attachment by cables. The fingers close mechanically by moving the stump. This allows to grip and release object. However, only two hand positions are possible. [9]

The *InMoove* robot hand is part of the Open Source project InMoove by Gael Langevin. The hand and the forearm itself do not function as prosthesis, but the hand can be modified by modifications. The controller and the power supply are located in the robot itself. The Robot hand cannot be operated without an external power supply. [10]

The *Handiii* is hand prosthesis of the Japanese company Exiii. Most components of the hand are made using 3D printing. Likewise, the replacement of the components should be easy according to the manufacturer. Hand control is myoelectric. The data are then evaluated, interpreted and converted into the movement of the hand using a commercially available smart

phone. The hand and fingers are completely mobile, with each finger having a separate motor. The *Handiii* allows the wearer a variety of pre-programmed handles. [11]

The Dextrous hand has emerged from the kick starter company Open Hand Project of the developer Joel Gibbard 2013. This is an open source project, whereby anyone can download the files for 3D printer and rebuild the hand. There is no description about the design methodology of robotic hand based on simulations with the software of the field. [12]

Open Bionics is company from Joel Gibbard developed another 3D printed robot hand called Brunel Hand. This 3D printed robot hand is more similar to the size and shape of the human hand. The robot hand is also available as hand prosthesis. Open Bionics also deals with the replacement of a complete upper arm. However, this is an individual project, and one cannot be able to design the small sized robot hand, for children under 10 years. [13]

This paper shows an actual example for accessing and building a bionic hand with high value at low cost that is able to meet human requirements.

The idea of the research is to design and simulate a robotic hand to do different gripping movements based on brain machine interface control. Several modules have been developed for assisting the bionic hand to support the motion by measuring the level and direction of the gripping force. It is deemed that sensors, placed in the muscles, would make possible the achievement of more complex movements with prostheses.

Goals of the research are to design and simulate the robotic hand that will be able to perform different moves like lifting items etc. The project objectives are the research and design of prototype of robotic hand, including the development of complex algorithms for intelligent systems.

3D printed hand and arm prostheses

Prosthetics largely enable the replacement of severed limbs, but the production of conventional prostheses using conventional manufacturing methods is complex, time-intensive and expensive. The invention of 3D printing provides new alternatives for the manufacture of prostheses, which are fast and accurate.

The production of prostheses is fast, cost-effective and can be customized by a 3D printer. There must be only a 3D data record of the model to be printed.

In Figure 1 is shown the 3D printer developed at the Laboratory of Mechatronics at the Faculty of Mechanical Engineering, University of Prishtina.

Hand prostheses

Various hand prostheses with their properties from 3D printing have been developed from different authors. It is evident that all presented models move the fingers through ropes. The rope or tendon is moved either mechanically or by a motor. If the tendon is under tensile load, the finger bends; the cord is released again, the finger moves back to the initial position.

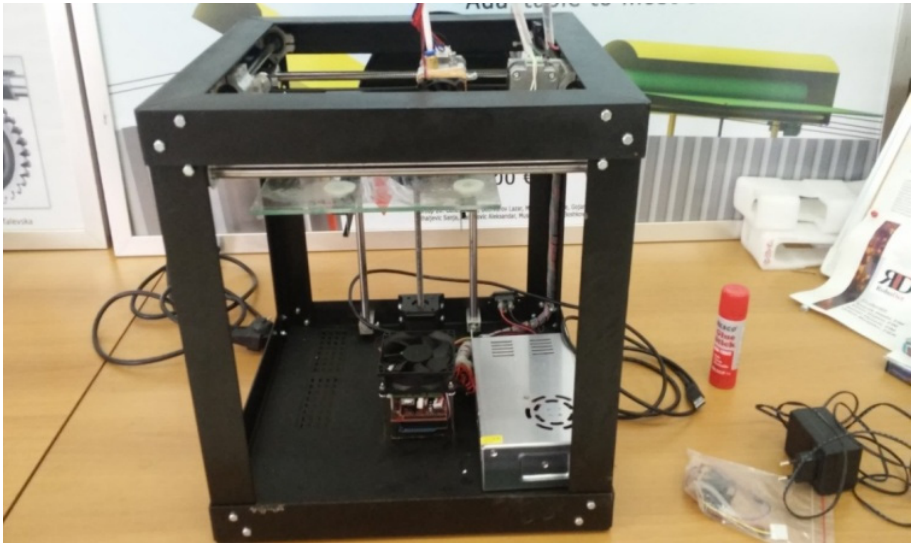


Fig.1. 3D printer constructed at the Laboratory of Mechatronics.

The robot hand called *Dextrus Hand*, from the Open Bionics has been taken as a model for research, Figure 2. [4] All the mechanical parts of the model have been printed at the above mentioned 3D printer.

This 3D printed robot hand is more similar to the size and shape of the human hand.

The exact specifications of the robotic hand are shown in the following table.

Table 1. Ada Hand characteristics [13]

Drive	Linear actuator in the hand
Hand material	Ninjaflex /ABS/PBS plastic
Power supply	12 V DC power supply
Control	ATMEGA2560 Microcontroller
Movement	Fingers can be individually controlled via the fishing
Connection	No prosthesis connection, in progress
Carrying mass	Max. 5 kg

Components selection and design

The components need to be designed and selected in order to determine the exact installation space for the construction or to adapt the existing design. In the following, some of important components which contribute to the finger movement are considered.

3.1. Tendon calculation

The following load case, which is depicted in Figure 2, is considered for the design of the tendon.

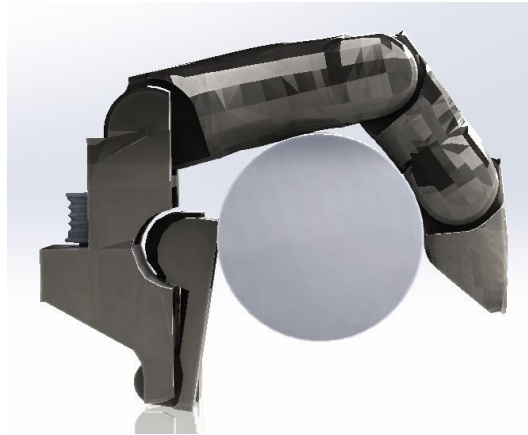


Fig.2. Load hand with weight.

The yellow cylinder symbolizes the weight to be held. In the following, a simplified function diagram is created with all the forces that occur, and a free cut is then created on the finger, see Figure 3.

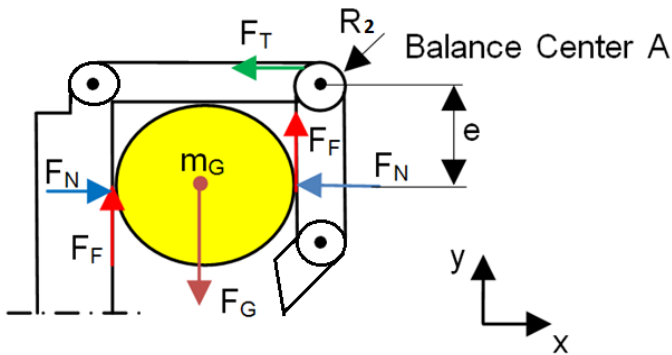


Fig. 3. Schematic finger grasping a cylinder.

$$m_G = \text{Mass weight} = 1.5 \text{ kg}$$

$$F_G = \text{Weight}$$

$$F_T = \text{Tendon force}$$

$$F_F = \text{Friction force}$$

$$F_N = \text{Normal force}$$

$$R_1 = \text{Radius at the last joint} = 8 \text{ mm}$$

$$e = \text{Distance of normal force to center of rotation A} = 18 \text{ mm}$$

$$\mu = \text{Coefficient of friction} = 0.20$$

$$g = \text{Gravity acceleration} = 9.81 \frac{\text{m}}{\text{s}^2}$$

The moment equilibrium around the balance center A:

$$\sum M = 0 = F_T * R_2 - F_N * e - F_F * R_2 \quad (1)$$

Then changed to F_T

$$F_T = F_N * \frac{e}{R_2} + F_F \quad (2)$$

Equilibrium of forces in y – direction:

$$\sum F_Y = 0 = 2 * F_F - F_G \quad (3)$$

The weight force F_G is calculated from the acceleration due to gravity of the mass:

$$F_G = m * g$$

$$F_G = m_G * g \quad (4)$$

Since F_F is equal to:

$$2 * F_F = F_G \quad (5)$$

$$F_F = \frac{F_G}{2}$$

$$\text{where } F_F = F_N * \mu \quad (6)$$

And then normal force F_N in obtained from Eq. (5):

$$F_N = \frac{m * g}{2 * \mu}$$

$$F_N = \frac{m_G * g}{2 * \mu} \quad (7)$$

Tendon force:

F_T is obtained by replacing Eq. (8) in Eq.(2):

$$F_T = \frac{m * g}{2 * \mu} * \frac{e}{R_2} + \frac{m * g}{2} * \left(\frac{e}{\mu * R_2} + 1 \right)$$

$$F_T = \frac{1.5 \text{ kg} * 9.81 \frac{\text{m}}{\text{s}^2}}{2} * \left(\frac{0.018 \text{ m}}{0.0085 * 0.20} + 1 \right) = 8 \text{ N}$$

$$F_N = \frac{m_G * g}{2} * \left(\frac{e}{\mu * R_2} + 1 \right)$$

Per finger, assuming that the fingers carry the weight without the thumb, a tendon force is 2 N.

In model construction or in other areas, the load bearing capacity of a tendon is given in kg. If the tendon force is converted, the tendon must have a load bearing capacity of 1.69 kg.

A commercially available fishing line is chosen as a tendon for the fingers, since the thinnest has a carrying force of at least 5 kg and this is more than sufficient. The tendon is selected with a thickness of 0.19 mm and a load capacity of 10 kg.

Tendon path.

The required tendon path to stretch or flex the fingers is calculated afterwards. Subsequently, the drum is designed for the servo motor, which allows the movement of the fingers. Figure 4 shows the section of a finger.



Fig. 4. Cross-section of a finger.

For simplicity, a function sketch, as shown in Figure 5, is made. It shows the forces occurring at the motor.

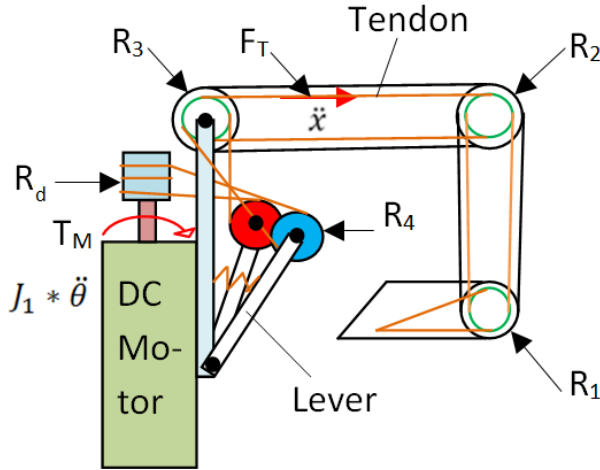


Fig. 5. Functional drawing tendon path, finger flexed.

In the calculation of the tendon path, it is to be assumed that, when stretching the finger, the tendon rolls over a quarter of the circumference of the rollers with the radii R_1 , R_2 , R_3 . Thus, the tendon path to be covered is the sum of the circumferences.

R_1 = Roller finger joint = 8 mm

R_2 = Roller finger joint = 8.5 mm

R_3 = Roller finger joint = 9 mm

R_4 = Pulley = 5 mm

R_5 = Lever = 27 mm

U_1 = Scope of roller R_1

U_2 = Scope of roller R_2

U_3 = Scope of roller R_3

U_4 = Scope of pulley R_4

U_5 = Scope of lever R_5

s_{tw} = Tendon path

U_d = Circumference of drum

R_d = Radius of drum

Calculation of the tendon distance over the circumference of the rollers:

$$s_{tw} = \frac{U_1}{4} + \frac{U_2}{4} + \frac{U_3}{4} + \frac{U_4}{18} + \frac{U_5}{20} \quad (9)$$

$$\begin{aligned}
 U &= \pi * R * 2 s_{tw} = \frac{1}{4} * (2 * \pi * R_1 + 2 * \pi * R_2 + 2 * \pi * R_3) \\
 &+ \frac{1}{18} (2 * \pi * R_4) + \frac{1}{20} * (2 * \pi * R_5) s_{tw} = \frac{\pi}{2} * (8 + 8.5 + 9) mm \\
 &+ \frac{\pi}{9} (5 mm) + \frac{\pi}{10} (27 mm) = 50.257 mm \\
 U &\triangleq 360^\circ s_{tw} = 2 * U_d U_d = \frac{s_{tw}}{2} R_d = \frac{U_d}{2 * \pi} R_d = \frac{s_{tw}}{4 * \pi}
 \end{aligned}$$

The radius of the drum is equal to:

$$R_d = \frac{s_{tw}}{4 * \pi} \quad (10)$$

$$R_d = \frac{50.257}{4 * \pi} = mm$$

It is assumed that the tendon path for flexing and stretching the fingers is the same. The drum is created using a 3D printer with the diameter of 9.5 mm.

Motor design

When designing the motor, care must be taken that the servomotors have sufficient motor torque to hold different objects. Furthermore, a compact design of the servomotor is important in order to carry the forearm weight itself and the object.

A pre-selection has been made before, which has been applied to the DC Gearbox Motor Combo (see Figure 6).

The mini servo ES08AII SERIES motor has been selected to actuate the thumb (Figure 7). This servo motor is compact and high-quality processed. Subsequently, it is to be checked whether the specified motor torque is sufficient. The table below shows the technical data of the servomotor.



Output Speed	100 rpm
Supply Voltage	3 → 12 V DC, 12 V nominal
Maximum Output Torque	~79 Ncm
DC Motor Type	Brushed
Shaft Diameter	3
Power Rating	0.394 W
Gear-head Type	Planetary
Length	49 mm
Width	16 (Dia.) mm
Current Rating	85 mA
Core Construction	Iron Core
Output Speed	100 rpm
Series	941D

Fig. 6. Gearbox Motor Combo.

The same load case is considered for the motor design (see Figure 4).

T_M = Motor torque

T_L = Load moment

J_1 = Replacement moment of inertia

$\ddot{\theta}$ = Angular acceleration

θ = Angle

g = Gravity acceleration = $9.81 \frac{m}{s^2}$

The following equation results:

$$\Sigma M: T_M = T_L + J_1 * \ddot{\theta}_1 \quad (11)$$



Operating Voltage	4.8 ~ 6.0V
STD Direction	Counter Clockwise/Pulse Traveling 1500 to 1900 usec
Stall Torque: 4.8 V	1.5 Kgf.cm (21 oz. in)
Operating Speed: 4.8 V	0.12 Sec/60 ⁰ at no load
Stall Torque: 6.0 V	1.8 Kgf.cm (25.2 oz. in)
Operating Speed: 6.0 V	0.10 Sec/60 ⁰ at no load
Size:	23X11.5X24 mm
Weight:	8.5 g (0.31 oz)
Plug Available	FUT; JR
Other	Analog, Plastics

Fig. 7. Mini servo ES08AII SERIES.

The load moment is composed of the tendon force and the radius of the drum. The momentum moment of inertia consists of the moment of inertia of a finger and that of the drum.

Determine the relative inertia moment:

J_{Finger} = Replaceable moment of inertia of finger

J_{Drum} = Moment of inertia of drum

m_F = Mass finger weighed = 33 g

m_{Drum} = Mass of drum weighed = 2.2 g

l_F = Length of a finger = 95 mm

The equation for the replaceable mass of moment of inertia is as follows:

$\ddot{\theta}_1$ = Angular acceleration of drum and motor

$\ddot{\theta}_2$ = Angular acceleration of fingers

$$\frac{1}{2}J_1 * \ddot{\theta}_1^2 = \frac{1}{2}J_{Finger} * \ddot{\theta}_2^2 + \frac{1}{2}J_{Drum} * \ddot{\theta}_1^2 \quad (12)$$

For the purpose of determining the amount of replaceable mass inertia of a finger, it is regarded as a rigid rod for the sake of simplicity. Figure 8 shows the rod with its pivot. Thus, the formula for the moment of inertia of a rod is added to the Steiner fraction.

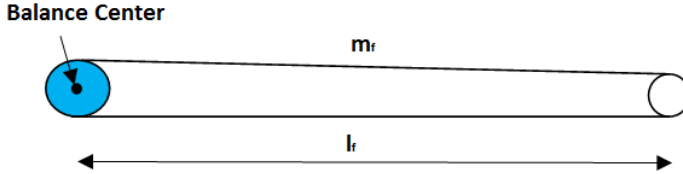


Fig. 8. Simplification of finger.

$$J_{Finger} = \frac{1}{12} * m_F * l_F^2 + m_F * \left(\frac{l_F}{2}\right)^2 = \frac{1}{3} * m_F * l_F^2 \quad (13)$$

$$J_{Finger} = \frac{1}{3} * 0.033 \text{ kg} * (0.095 \text{ m})^2 = 9.9275 * 10^{-5} \text{ kgm}^2$$

The drum is calculated with the formula for mass inertia moments of washers:

$$J_{Drum} = \frac{1}{2} * m_{Drum} * R_d^2 \quad (14)$$

$$J_{Drum} = \frac{1}{2} * 0.0022 \text{ kg} * (0.00475 \text{ m})^2 = 0.248 * 10^{-7} \text{ kgm}^2$$

In order to determine the amount of moment of inertia, the coupling conditions between the finger and the drum are necessary.

$$\dot{x} = \dot{\theta}_1 * R_d$$

$$\dot{x} = \dot{\theta}_2 * R_2 \dot{\theta}_2 = \dot{\theta}_1 * \frac{R_d}{R_2}$$

Apply coupling conditions:

$$\frac{1}{2}J_1 * \ddot{\theta}_1^2 = \frac{1}{2}J_{Finger} * \left(\ddot{\theta}_1 * \frac{R_d}{R_2}\right)^2 + \frac{1}{2}J_{Drum} * \ddot{\theta}_1^2 \quad (15)$$

Equation shortening:

$$J_1 = J_{Finger} * \frac{R_d^2}{R_2^2} + J_{Drum} \quad (16)$$

The values for J_{Finger} and J_{Drum} are used in Eq. (17)

$$\begin{aligned} J_1 &= 9.9275 * 10^{-5} kgm^2 * \frac{(0.00475 m)^2}{(0.0085 m)^2} + 0.248 * 10^{-7} kgm^2 J_1 \\ &= 3.1 * 10^{-5} kgm^2 \end{aligned}$$

Determine load torque:

$$\begin{aligned} T_L &= F_T * R_d \\ T_L &= 8 N * 0.00475 m = 0.038 Nm \end{aligned} \quad (17)$$

Calculation of the angular acceleration

The underlying speed profile of the motor is not known. In principle, two profiles could occur, a simple triangular profile and a linear acceleration profile (ramp) running to the maximum speed. In the following calculation, a triangular profile is viewed in order to obtain an order of magnitude for the possible angular acceleration, Figure 9. It is also known that the output speed for the DC motor is 100 rpm, or 1.66 rad/s.

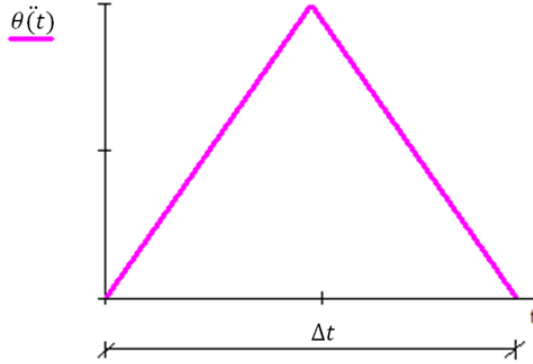


Fig. 9. Speed triangle profile.

Triangle profile:

$$\frac{\theta}{2} = \int_0^{\Delta t} \ddot{\theta} * t * dt = \left[\ddot{\theta} * \frac{t^2}{2} \right]_0^{\Delta t} = \ddot{\theta} * \frac{\Delta t^2}{2*4}$$

(18)

$$\theta = \ddot{\theta} * \frac{\Delta t^2}{4} \Rightarrow \ddot{\theta} = \frac{4*\theta}{\Delta t^2} = \frac{4*\frac{360^\circ}{180^\circ}*\pi}{1.66^2} = 9.12 \text{ rad/s}^2$$

Immediately, the required motor torque can be determined. Once for the speed triangle profile:

$$T_M = 0.038 \text{ Nm} + 3.1 * 10^{-5} \text{ kgm}^2 * 9.12 \frac{\text{rad}}{\text{s}} = 0.038 \text{ Nm}$$

It can be seen that the angular acceleration is only a small part of the motor torque to be applied. The greatest part is the load moment. The servo motor will be operated at a voltage of 5V as this is also the voltage of the Arduino/Genuino Uno Board. The DC Gearbox Motor Combo can apply a torque of approximately 79 Ncm (equivalent to 0.79 Nm), which is sufficient.

A special case is to be considered since the tendons for the little finger and the ring finger lead to a same motor. Thus, the latter has to cope with the double tendon force. Only the case with the higher angular acceleration is investigated:

$$T_M = F_T * 2 * R_d + J_1 * \ddot{\theta} = 0.076 \text{ Nm}$$

(19)

$$T_M = 8N * 2 * 0.0475 m + 3.1 * 10^{-5} kgm^2 * 9.12 \frac{rad}{s} = 0.076 Nm$$

Thus, the torque of the selected motor is sufficient.

Methodology for designing the 3D printed hand prostheses

The development and construction of the hand prosthesis is divided into three phases.

First phase

In the first phase, the requirements for the system to be developed are clarified. As a rule, a product search is also carried out in order to analyze the situation prevailing on the market and to incorporate it into the development.

This phase consists of structure planning, materials selections, feasibility study, building of robotic hand through 3D printing, mounting of mechanical parts, control of motion and testing of parts.

Second phase

In the second phase, the task position and the results from the requirements list are specified. The requirements for the product are abstracted in order to elaborate the essential problem. In several abstraction steps the problem as well as the result is characterized without influence of wishes.

The point of converting the energy into force and distance is that electrical energy is, for example, converted into force and path by means of a motor with tendons, in order to realize the bending and stretching the fingers.

Third phase

In the third design methodology, the preliminary design, with the corresponding assembly instructions, the parts list as well as the design of the components are prepared and are clarified the design conditions with regard to the installation space.

The installation space for all necessary components must be included in the hand, under hand prosthesis. The main components are five linear actuators for driving the fingers, the ATMEGA2560 Microcontroller Board to control the motors, while the accumulator are planned to be accommodated in the arm prosthesis, Figure 10.

In this phase the existing design is tested and further improved.



Fig.10. Robotic hand grasping the bottle.

Dimensions of robotic hand are: Length – 160 mm, Width – 110 mm, Height (max) – 35 mm. Length of fingers: Pinkie finger - 60 mm; Ring finger – 80 mm; Middle finger – 82 mm; Index finger – 74 mm; Thumb – 95 mm. The thickness of the middle finger is 10 mm at the end (root) of the finger, and 7 mm at the top of the finger. The thickness of the thumb is 20 mm at the end of the thumb, and 7mm – at the top of the thumb. Fingers will be moved in up and down motion with system of small pulley mechanism with motors and tendons.

Results and Discussion

Motion dynamics of robotic hand is analysed through modelling and simulation with software. The aim was to find forces necessary for the hand to grab and hold other objects, which is the final purpose. Modelling and simulation of robotic hand is done with SimWise 4d software [14]. Results of main dynamic parameters will be shown in graphical form.

In Figure 11 is shown model of robotic hand developed with software [14]. Model will be simulated to achieve grabbing of cylindrical object. Simulation scenario is to move Robotic hand and fingers to grasp and hold cylindrical body. Length of simulation is close to real motion of hand – 4 (s).

Dimensions of cylindrical object are: Height – 140 mm, diameter – 40 mm, Weight – $Q = 0.5$ kg.

Important parameters for proper grasp hold of object are coefficient of friction between fingers and object – $\mu = 0.5$, and coefficient of restitution COR, $e = 0.5$.

Based on the created model, and simulations, results are achieved for main dynamic parameters [14]: Force in tendons (F) (N) and Stress (Pa) as main parameters.

Force applied to the middle finger corresponds to the strength of the tendon to pull the finger. It is assumed that all fingers of the hand act with equal force.

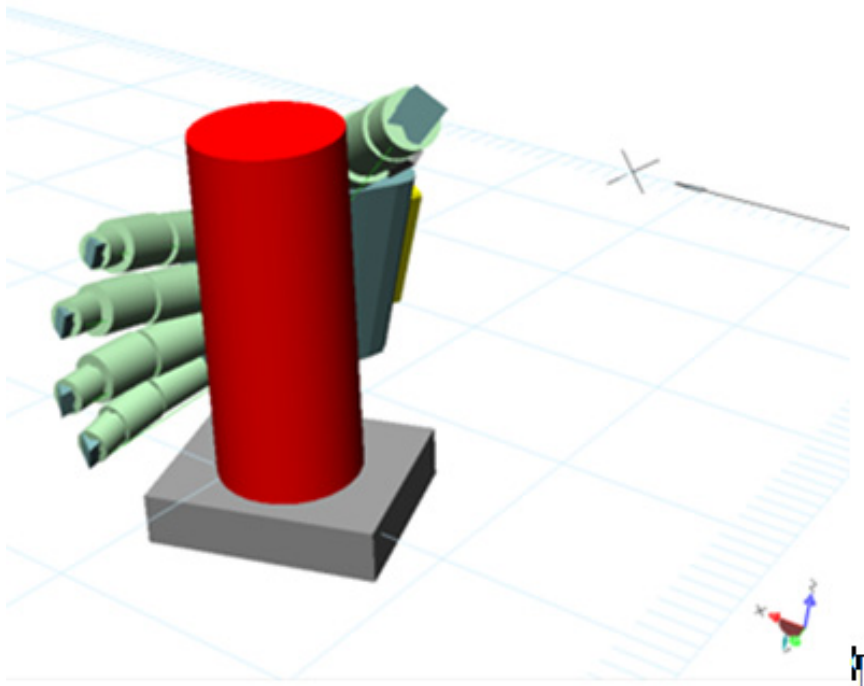


Fig.11. Model of robotic hand and simulation with other objects – grasping of cylindrical object.

Results of main dynamic parameters

In Figure 12 is represented graph of forces in tendons of index finger and middle finger necessary to grab & hold the cylindrical object. In the horizontal axe of graph is time in seconds, and in vertical axe is force in tendons in Newton (N).

Based on fig.12, the curve of force shows changes and is dynamic in nature. In time $t \approx 2$ s there is a climb of force, which denotes the time when finger grabs the cylindrical object.

The average value of coercive force for middle and index finger is $F = 3.5$ N, while maximal force is $F_{\max} = 4.4$ N, which lasts a short period of time.

Total average force applied in 5 fingers is:

$$F_{\text{total/avg}} = 5 \cdot 3.5 = 17.5 \text{ N.}$$

Mass of carrying load (cylindrical body) is $Q = 0.5$ kg.

Max force applied in 5 fingers is:

$$F_{\text{total/max}} = 5 \cdot 4.4 = 22 \text{ N.}$$

This is the force necessary for motor mounted inside the robotic hand to move the fingers. Stress analysis will be done using Finite Elements Method.

In Figure 13 is represented surface distribution of stress in middle finger and ring finger, which is achieved through Finite Elements Method (FEM) analysis, where parts of fingers are subdivided as a grid of volume FEM elements. These two fingers carry the highest load of object grab and hold.

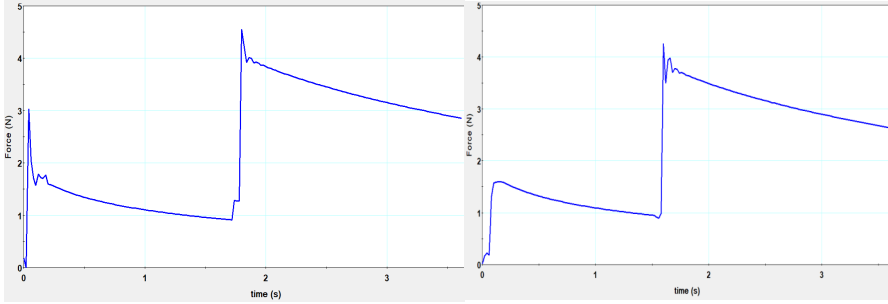


Fig.12. Graphical result of force in tendon of index and middle finger.

Based on Figure 12, in Figure 13 are shown graphs of stress in middle finger and ring finger.

According to Figure 14, the curve of stress shows changes and is dynamic in nature. In time $t \approx 2$ s there is a climb and drop of stress. Stress represents von-misses stress in the fingers parts that press and hold the cylindrical body.

Based on Figure 14, maximal value of stress is $\sigma_{max1} = 5900$ Pa in middle, and maximal value is $\sigma_{max2} = 7400$ Pa in ring finger.

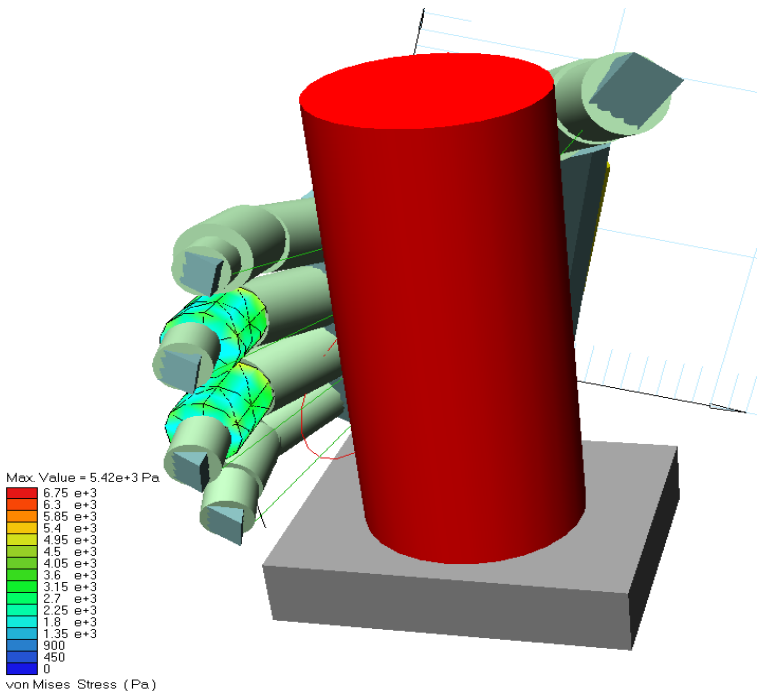


Fig.13. Stress dispersion in middle finger and ring finger.

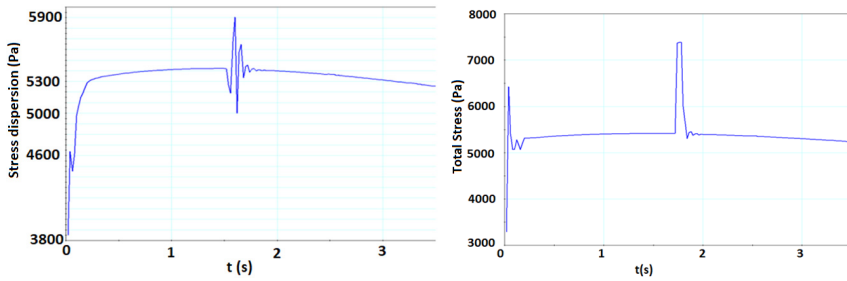


Fig.14. Graphical result of total stress in middle and ring finger.

Programming of coordinated fingers movements

Programming has included some commands and has been relatively easy considering motor-shield's use. But, here it should be mentioned that the motor of the third and fourth finger is connected to an outlet for motor-shield v1.0, and there is only room for 4 DC and 2 servo motors, Figure 15.

The tasks that are given to the coordinated movement of the fingers are: Opening and closing the hand, counting from 1 to 5, grasp the bottle and handshake.

The number of commands that were used to activate the fingers was small (Forward, Backward, Release, etc.). The biggest problem was the allocation of breaks (time delays) between the desired motions that the programme had to accomplish .

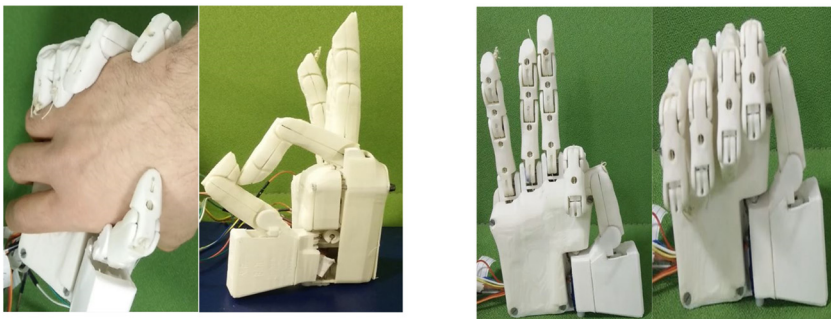


Fig.15. Programming of several tasks

Conclusion

In this research we have presented the development and analysis of robotic hand to create a cost-effective alternative to conventional dentures or prosthetics using 3D printing.

A research has been carried out to investigate the current situation in the market and, if necessary, to stimulate its own development. The hand prosthesis is also explained in terms of movements, functionality, appearance, motion dynamics analysis, and programming.

After the design is tested, a program with Arduino C++ has been written. The fingers are controlled individually or together to check the required gripping movements, which are necessary for everyday life. For everyday use, however, there is a need for further work. It is possible to cooperate with a prosthesis builder to made the arm extension from silicone and test it in order to be able to carry the prosthesis. The load, for the design of servomotors, has also been tested. Only very large objects with a diameter of 80 mm could not be grasped due to object's smooth surface and lack of sufficient friction between the object and the fingers.

Although this is a prototype model, there is still a lot of development potential in future. This study shows that the basic tasks of a hand can be performed with this robotic hand. A further approach would be incorporation of the EMG (ElectroMyoGraphy) sensor. As a result, the linear motors and the fingers could be controlled by the muscles of the arm.

Main contributions of the paper are: the methodology of design of robotic hand, materials used, the search for best ergonomic model of mounting of motors and sensors, and the forms of calculation of grip and release forces based on simulations with best software of the field.

Acknowledgments

Authors wished (would like) to Thank Ministry of Education, Science and Technology of the Republic of Kosovo for financing and support of this project.

References

- [1] Niels Birbaumer and Leonardo G. Cohen: Brain–computer interfaces: Communication and restoration of movement in paralysis, *The Journal of Physiology*, Volume 579, Issue 3, pages 621–636, March 2007.
- [2] Loredana Zollo, Stefano Roccella, Eugenio Guglielmelli, M. Chiara Carrozza, and Paolo Dario: Biomechatronic Design and Control of an Anthropomorphic Artificial Hand for Prosthetic and Robotic Applications, *IEEE/ASME Transactions on Mechatronics*, Vol. 12, No. 4, August 2007.
- [3] J. Zhao, Z. Xie, L. Jiang, H. Cai, H. Liu, and G. Hirzinger: A fivefingereed underactuated prosthetic hand control scheme, 1st IEEE/RAS-EMBS Int. Conf.Biomed.Robot. Biomechatron., Pisa, Italy, 2006.
- [4] Akitoshi Harada, Takashi Nakakuki and Mitsutaka Hikita: Robot Finger Design for Myoelectric Prosthetic Hand and Recognition of Finger Motions via Surface EMG, *Proceedings of the 2010 IEEE International Conference on Automation and Logistics August 16-20 2010, Hong Kong and Macau*.
- [5] Nozomu Araki, Kenji Inaya, Yasuo Konishi and Kunihiro Mabuchi: An Artificial Finger Robot Motion Control Based on Finger Joint Angle Estimation from EMG Signals for a Robot Prosthetic Hand System, *Proceedings of the 2012 International Conference on Advanced Mechatronic Systems, Tokyo, Japan, September 18-21, 2012*.
- [6] Panagiotis Artemiadis: *Neuro Robotics – From Brain Machine Interfaces to Rehabilitation Robotics*, Springer, 2014.
- [7] Parag G. Patil, Dennis A. Turner: The Development of Brain-Machine Interface Neuroprosthetic Devices, *Neurotherapeutics*, Volume 5, Issue 1, January 2008, Pages 137-146.
- [8] Dennis J. McFarland, Jonathan R. Wolpaw: Brain Computer Interface Operation of Robotic and Prosthetic Devices, *Computer*, Issue No.10 - October (2008 vol.41), pp: 52-56.
- [9] <http://enablingthefuture.org/upper-limb-prosthetics/> [access on 24.01.2018].
- [10] <http://inmoov.fr/> [access on 24.01.2018].
- [11] <http://exiii.jp/projects/> [access on 24.01.2018].
- [12] <http://www.openhandproject.org/dextrus.php> [access on 24.01.2018].

- [13] <https://www.openbionics.com/shop/brunel-hand> [access on 24.01.2018].
- [14] MSC VisualNastran 4D User Guide, MacNeal-Shwendler Corporation, Santa Ana, 2003.
- [15] Doçi I., Hamidi B. Studying rotational motion of Luffing Boom Cranes with maximum load using simulation. *International Journal for science, techniques and innovations for the industry-MTM* 2015; 1(12):20-24.

Dizajnimi dhe programimi i dorës robotike të shtypur 3D

Arbnor Pajaziti, Ilir Doçi, dhe Endrit Toplica

Përmbledhje

Në këtë hulumtim kemi prezantuar zhvillimin dhe analizën e dorës robotike duke përdorur shtypësin 3D për të krijuar një alternativë me kosto efektive ndaj protezave konvencionale ose protetikës. Proteza e dorës studihet edhe në aspektin e lëvizjeve, të funksionalitetit, të pamjes, të analizës së dinamikës së lëvizjes dhe të programimit.

Pas dizajnit dhe testimeve, është shkruar programi me Arduino C++. Gishtat kontrollohen individualisht ose së bashku për të kontrolluar lëvizjet e nevojshme të kapjes, të cilat janë të nevojshme për jetën e përditshme. Për përdorim të përditshëm, megjithatë, ka nevojë për punë të mëtejshme. Ngarkesat, për dizajnimin e servomotorëve, janë testuar gjithashtu. Vetëm objektet shumë të mëdha me një diametër prej 80 mm nuk mund të kapeshin, pasi që nga njëra anë objekti që do të kapej kishte një sipërfaqe të lëmuar dhe për këtë arsye nuk kishte fërkim të mjaftueshëm midis objektit dhe gishtave.

Meqë është një prototip, ka ende shumë potenciale zhvillimi, por detyrat themelore të një dore mund të kryhen me këtë dorë robotike.

Një qasje tjetër do të ishte përfshirja e sensorit EMG (ElectroMyoGraphy). Si rezultat do të kishim kontrollin e motorëve linearë ashtu që gishtat të mund të kontrollohen nga muskujt e krahut.

Kontributet kryesore të punimit janë: metodologjia e dizajnit të dorës robotike, materialet e përdorura, kërkimi i modelit më të mirë ergonomik, mënyra e montimit të motorëve dhe forma e llogaritjes së forcave të shtrëngimit dhe lirimit, bazuar në simulimet me softuerin më të avancuar të fushës.

**INVESTIGATIONS ON THE RESISTANCE OF
MAIZE GENOTYPES FROM KOSOVO,
ALBANIA AND AUSTRIA AGAINST
*FUSARIUM GRAMINEARUM***

**Vitore Shala-Mayrhofer^a, Sali Aliu^{b,*}, Valbona Hobdari^c,
Fetah Elezi^c, Blerina Rexhepi^b, Ana Koci^c,
Hans-Peter Kaul^a, Marc Lemmens^d**

Abstract

The aim of this study is to investigate maize genotypes for resistance to *Fusarium graminearum* in order to select resistant genotypes for their use in Austria, Kosovo and Albania. A large variability in *Fusarium* ear rot resistance was detected during this research study, ranging from diseased ear areas of 3.1% to 27.6% in the year 2013 and of 3.3% to 36.3% in 2014. Highly significant differences in the mean disease level are also presented between the countries: the highest disease level that was measured in the year 2013 in Kosovo (31.9%), followed by Albania and Austria (with 9.7% and 7.1%,

^a Division of Agronomy, Department of Crop Science, University of Natural Resources and Life Sciences, Vienna, Konrad-Lorenz-Straße 24, 3430 Tulln, Austria.

^b Department of Crop Science, Faculty of Agriculture and Veterinary, University of Prishtina, Str. Bill Clinton n.nr., 10000 Prishtina, Kosova.

* Corresponding author: sali.aliu@uni-pr.edu

^c Institute of PlantGenetic Resources, Agricultural University of Tirana, Siri Kodra Str., 1001 Tirana, Albania

^d Institute of Biotechnology in Plant Production, Department of Agrobiotechnology, IFA-Tulln, University of Natural Resources and Life Sciences, Vienna, Konrad-Lorenz-Straße 20, 3430 Tulln, Austria

respectively). In 2014, the mean disease level was 35.7% in Kosovo, and 5.6% in Albania.

The genotype by country interaction proved to be also highly significant in both years. Resistance ranking in Austria was significantly different from the ranking in both other countries. These differences also resulted in yield losses (from 19.5% to 24.6%). Based on the two year results the best genotypes were the landrace LMP-1 from Kosovo and the Austrian hybrid SBL-1.

Key words: *Fusarium* ear rot, resistance, *Zea mays*, genotypes, *Fusarium graminearum*

Introduction

Maize is one of the most important cereal crops in Kosovo and Albania and a major component of animal feeds. Maize (*Zea mays* L.) is considered to be a major source of food for livestock and humans due to its relatively high content of proteins, oil, starch and some other important vitamins such as vitamin B and B12. [1,2] The seeds for cultivation are largely imported from the neighbouring countries and up to date no hybrids for multiplication are available. The average yield is 4.5 t ha⁻¹ [3], and does not fulfil the domestic demands of Kosovo. The plant genetic resources are considered as the main source for the conservation of the biological diversity. [4] As a consequence, the selection of suitable maize hybrids for the production region Kosovo is of extreme importance in order to increase crop yield and quality. [3] The members of the genus *Fusarium* are among the most important plant pathogens in the world. In recent years the genus has acquired additional importance as many *Fusarium* species have been shown to produce mycotoxins causing both animal and human diseases. [5] In addition, fungal diseases of maize – in particular *Fusarium* ear rot (FER) – represent a central problem. Several *Fusarium* species have been described to be widespread as pathogens on maize in temperate climate and semi-tropical areas, including all European maize-growing areas. They cause root, stem and ear rot, with severe reductions in crop yield, often estimated between 10% and 30%. [6] Symptoms of FER are a white to pink- or salmon-coloured mould. Symptoms usually start on the tip of the ear but can also be present anywhere on the ear, or even scattered over the ear. Usually the decay begins with insect-damaged kernels. Infected kernels are often tan or brown, or have white streaks.

The most important source of infection is crop debris from the previous crop on the soil surface on which the fungi over winter. [7] FER is caused by several species of the genus *Fusarium*. They are responsible for at least two kind of maize ear rot, roughly differentiated as red ear rot or red fusariosis, and pink ear rot or pink fusariosis. The predominant species causing Fusarium red ear rot are *F. Graminearum* (teleomorph *Gibberellazeae*), *F. culmorum*, *F. cerealis* (syn. *F. crookwellense*) and *F. avenaceum*. The species frequently isolated from maize pink ear rot are essentially the widespread anamorphs of the rather rare *Gibberellafujikuroi*, namely *F. verticillioides* (syn. *F. moniliforme*), *F. proliferatum* and *F. Subglutinans*. [6] Natural infection is initiated by a mixture of the local *Fusarium* spp., but usually one species predominates. [8] *Fusarium* species can produce dangerously high amounts of mycotoxins under favourable climatic conditions on crops. [9] Mycotoxins are secondary metabolites of various fungi, which contaminate feed and food, and represent one of the most serious consequences of *Fusarium* infection. Some of them have a notable impact on human and animal health. The *Fusarium* toxins of primary concern are trichothecenes, fumonisins and zearalenone (ZON). The major type-A trichothecenes are T-2 toxin (produced by *F. sporotrichioides*), HT-2 toxin (produced by *F. sporotrichioides* and *F. acuminatum*) and diacetoxyscirpenol (mainly produced by *F. equiseti*). Type-B trichothecenes of major concern are deoxynivalenol (DON; produced by *F. graminearum* and *F. culmorum*) and nivalenol (produced by *F. graminearum*, *F. culmorum*, *F. poae*, *F. cerealis*) as well as their acetylated derivatives 3- and 15-acetyl-deoxynivalenol (3ADON and 15ADON; produced by *F. graminearum*) and Fusarenone-X (produced by *F. graminearum*, *F. poae* and *F. cerealis*) (Logrieco et al., 2002). ZON is mainly produced by *F. graminearum*, *F. culmorum*, *F. equiseti* and *F. cerealis*, while fumonisins B₁ and B₂ are produced by *F. proliferatum* and *F. verticillioides*. These toxigenic *Fusarium* species isolated from maize are in accordance with previous data from Serbia [10] and Croatia [11], but also from other countries in Europe (6) such as Austria [12], France [13], Germany [14] and Switzerland [15]. It has been reported that the composition of *Fusarium* species causing FER is also highly dependent on the year, location, hybrid and the weather conditions. [12, 13, 4] In Austria (12) found out that *F. graminearum* were dominated in the relatively humid vegetation periods. Based on economic and environmental aspects host plant resistance is considered to be the most appropriate method to control it

(8). *Fusarium* ear rot is present in Kosovo. A study performed in 2009 and 2010 to analyse the incidence and identity of *Fusarium* species isolated from naturally infected maize kernels, as well as the mycotoxin contamination, showed that the disease incidence of *Fusarium* ear rot (from 1 – 40% diseased ears) on maize in Kosovo is high, causing thereby contamination with deoxynivalenol (DON), DON-3-glucoside, 3-acetyl-DON, 15-acetyl-DON, zearalenone, zearalenone-4-sulfate, moniliformin, fumonisin B₁ and fumonisin B₂ produced by *F. graminearum*) and Fusarenone-X (produced by *F. graminearum*, *F. poae* and *F. cerealis*). [6,16] The disease is also present in Albania (17), but very little research has been done specifically into the actual situation in this country. The main objective of the present study was to describe and analyze in three locations included Austria, Kosova and Albania studies to test explicitly different maize genotypes against *Fusarium* ear rot, which is one of the main factors to control food and feed quality, reduce costs and losses as well as for the selection of the suitable maize hybrids for Kosovo and Albania.

Material and methods

Experimental side and management

The research took place during the vegetative periods in the year 2013 (in Austria, Kosovo and Albania) and 2014 (in Kosovo and Albania).

Austria (AT): The experiment was conducted on the experiment fields of the University of Natural Resources and Life Sciences Vienna (BOKU) in Tulln. Tulln is a city at the Danube in Lower Austria with Pannonian climate and lies 180 m above sea level with a mean annual temperature of about 11°C and a mean annual precipitation of 650mm. The soil type is a chernozem and the previous crop was wheat.

Kosovo (KS): The experiment was implemented on the experiment fields of the Faculty of Agriculture and Veterinary, University of Prishtina, by the Department of Crop Science, which is 1 km away from the capital city Prishtina. The climate in this region is continental, the altitude 557 m, mean annual temperature and mean annual precipitation are 10,4°C and 680 mm. During the experimental years, the average temperatures were 9,75°C in 2013 and 8,8°C in 2014. Average rainfall was 566 mm in 2013 and 649 mm in 2014 (18). The soil type is a vertisol. Forage crops were cultivated as pre-crops. The

fertilisation was done with 450 kg ha^{-1} of NPK (15:15:15, in %) and 110 kg ha^{-1} of urea (46% N). No pesticides were used.

Albania (AL):The experiment was implemented on the experimental fields of the Agricultural University of Tirana in Valias, 3.4 km from the University. The climate is mediterranean, the altitude is 40 m. In 2013, the average amount of rainfall was 69,88 mm and the average temperatures was 16,4°C. The yearly participation around 974 mm. In 2014, the mean temperature was 15,4°C and the total amount of rainfall was 1021 mm (Agricultural University of Tirana, Department of Agro-Environment). The soil type is a fluvisol.The fertilisation was done with 500 kg NPK (15:15:15, in %), 200 kg ha^{-1} ammonium nitrate (27 % N) and 300 kg ha^{-1} of urea (46% N). The previous crops were wheat. No pesticides were used.

A set of 18 important maize hybrids was selected: eight from Kosovo, eight from Albania and two from Austria. The maize hybrids included were from FAO 354 and FAO 620 groups (Table 1).

Table1.Genotypes, locations and origin of genotypes used for investigation in Austria, Kosovo and Albania on 2013 and 2014.

Genotypes	Austria (AT)	Kosovo (KS)	Albania (AL)
Landraces	None	LMP-1, 2 and 3	RA 12; FE 12; FP 12
Hybrids	SBL 1; SBL 3	BC-678; 418; 354; 572; BC-Pajdash (FAO 354-678)	SNH-9503; 2506; 2504; 9607; 8605 (FAO540-620)
Origin of hybrids	Austria	Croatia	Italy

Field analysis

The field experiments were set up in a randomized complete block design with three replications. Plots consisted of a minimum of 100 plants (excluding border rows). In each replication at least 90 plants were assessed for natural FER infection. Tenplants were treated with *F. graminearum* incrustated tooth picks which were produced in Austria. Stab inoculation was done using a home-made stab with one nail (diameter 3 mm, 1.5 cm long) which was punched in the centre of the ear through the husks. Thereafter the tooth pick was placed in the wound. Artificial inoculation at all locations was done 1 week after 50% anthesis. [8] The disease severity of FER (percentage of diseased ear

area) was visually assessed on dehusked ears after ripening before the harvest directly on the field. [19]

Ear yield

For the analysis of yield, data were collected at biological maturity from tenplants with infection and tenplants without infection from each plot. The yield was noted isg ear⁻¹and yield losses (%) were calculated from the difference between infected and healthy plants.

Results

Our investigation for the two years studied gave three different values for yield in three locations. At the location in AT for year 2013 for natural infection, on higher values was determined by maize genotypes BC678 (1711 g per 10 ear⁻¹), while with lower values were characterized maize genotype FP12 (760 g per 10 ear⁻¹). In the second and third location for 2013 in KS and AL for natural infection, with higher yield was characterized maize genotype SBL03 (1351 g per 10 ear⁻¹) in KS and AL (1407 g per 10 ear⁻¹). In 2014, in the location of Kosovo for natural infection the average value was 1918 g per 10 ear⁻¹. While in Albania in f the year 2014 the average value for artificial infection was 1815 g per 10ear⁻¹. While for Kosovo it was 1953 g per 10 ear⁻¹. Results are presented in Table 2.

Based on the results achieved on the percentage of diseased ear area (disease severity) after artificial inoculation with *Fusarium graminearum*, we found a high variability in the resistance between genotypes and a highly significant genotype by location interaction. The resistance variability detected was large, ranging from diseased ear areas of 3.1% to 27.6% in the year 2013 and of 3.3% to 36.3% in 2014. Highly significant differences in the mean disease level were present between the countries. The highest disease level was measured in Kosovo in both years (32.0% in 2013 and 35.7% in 2014), followed by Albania (9.7% in 2013, 5.6% in 2014) and Austria (7.1% in 2013). Resistance ranking in Austria was significantly different from the ranking in both other countries. Based on results achieved over both years and over all countires the best genotypes were the landrace LMP-1 from Kosovo (5.4%) and the Austrian hybrid SBL1 (6.1%).

Table 2. The overall average values for two years of yield for all maize genotypes (g ear⁻¹)

Genotype	AT 2013		KS 2013		AL2013		KS 2014		AL 2014	
	Artificial infection	Natural infection								
LMP1	840.89	885.19	960.63	989.6	715.33	738.53	1165.60	1166.3	1149.80	1169.80
LMP2	950.00	969.60	759.93	794.93	722.97	751.60	1183.03	1214.73	1238.33	1258.93
LMP3	1287.78	1330.58	691.93	736.43	846.43	872.13	1285.33	1316.03	1699.67	1722.57
BC-678	1682.86	1711.06	1130.20	1166.4	1128.27	1156.40	1766.73	1787.53	1862.0	1884.40
BC-418	1513.33	1531.93	1019.70	1069.2	1281.23	1310.63	2324.60	2375.30	1444.33	1462.70
BC-354	1134.90	1181.1	968.97	1015.07	1275.73	1299.23	1858.33	1901.63	1269.93	1293.73
BC-572	1257.05	1304.45	1132.10	1178.50	1173.20	1205.40	2567.63	2624.33	1394.67	1404.47
BCPAJ	1573.95	1619.25	1130.20	1175.70	1314.23	1343.63	2187.37	2221.17	1782.50	1801.60
SNH-9503	1237.33	1263.43	1027.70	1068.80	1421.57	1445.4	1811.70	1853.90	1544.33	1563.33
SNH-2506	1372.42	1379.82	1022.37	1062.27	1262.13	1287.23	1677.97	1711.77	1503.10	1519.80
SNH-2504	1549.33	1561.53	917.70	968.30	1299.70	1328.5	1831.77	1870.97	1289.83	1308.80
SNH-9607	1655.33	1660.23	954.23	1001.73	1344.80	1367.00	2001.13	2038.43	1693.63	1712.63
SNH-8605	1632.75	1695.45	1131.17	1172.87	1224.13	1245.80	2454.30	2505.90	1776.43	1782.33
RA	646.56	679.96	1221.70	1255.10	1162.6	1190.40	1651.0	1684.80	811.67	830.07
FE12	785.00	801.60	1102.73	1144.13	1289.83	1310.33	2127.17	2169.47	960.50	969.00
FP12	749.33	759.53	1125.47	1174.07	748.20	771.70	2103.27	2141.39	796.03	8000.30
SBL01	1333.25	1352.85	1327.40	1351.30	689.90	710.10	2297.30	2320.80	1640.13	1650.33
SBL03	1145.75	1154.75	1070.10	1111.10	1384.47	1406.77	2215.37	2248.57	1332.07	1331.27
X	1241.545	1269.01	1038.568	1079.75	1126.92	1152.26	1917.2	1952.94	1399.38	1814.78

Table 3. Percentage of diseased ear area with *Fusarium* ear rot (%) and yield losses (%) for different maize genotypes in Kosovo (KS), Albania (AL) and Austria (AT) in 2013 and 2014

Genotype	Diseased ear area (%)						Yield loss (%)						
	2013			2014			2013			2014			
	KS	AL	AT	Mean	KS	AL	Mean	KS	AL	AT	AL	KS	Mean
MPI	2.9	7.2	10.5	6.9	3.2	3.3	5.4	29.3	23.2	44.3	20.0	0.8	23.5
SBL1	4.2	3.9	1.1	3.1	20.5	0.6	6.1	23.9	20.2	19.6	10.2	23.5	19.5
RA12	15.2	8.3	6.9	10.1	16.9	0.3	9.5	33.4	27.8	45.3	18.4	33.8	31.7
BCPajdash	17.7	6.8	5.1	9.9	19.6	1.5	10.1	45.5	29.4	12.4	19.1	47.0	30.7
BC418	27.3	5.8	2.7	11.9	28.8	2.7	13.5	49.5	10.5	18.6	18.4	50.7	29.5
LMP2	19.9	12.4	12.3	14.8	20.5	2.6	13.5	35.0	28.7	45.3	20.6	31.7	32.3
FP12	30.9	4.4	6.2	13.8	33.3	2.3	15.4	41.4	20.5	10.2	4.0	38.2	22.9
BC354	35.5	7.9	1.1	14.8	37.7	1.0	16.6	46.1	23.5	46.2	23.8	43.3	36.6
SNH8605	33.3	12.7	3.5	16.5	39.0	2.2	18.2	41.7	21.7	16.5	5.9	51.6	27.5
SBL3	25.0	9.9	22.3	19.1	34.1	1.5	18.5	41.0	22.3	9.0	-0.8	33.2	21.0
SNH2504	41.1	13.8	4.1	19.7	47.0	2.0	21.6	50.6	28.8	12.2	18.2	39.2	29.8
FE12	40.6	8.7	10.7	20.0	45.8	3.1	21.8	48.6	23.5	16.6	8.8	42.3	28.0
LMP3	39.7	6.8	13.1	19.9	40.2	13.6	22.7	44.5	25.7	42.8	22.9	30.7	33.3
SNH9503	37.3	12.7	9.6	19.9	43.9	12.2	23.1	41.1	23.9	26.1	19.0	42.2	30.5
SNH9607	42.2	19.8	8.5	23.5	43.3	9.1	24.6	47.5	22.2	4.9	2.3	37.3	22.8
BC678	51.6	6.5	1.8	20.0	51.7	20.9	26.5	36.2	28.2	28.2	22.4	20.8	27.2
BC572	52.8	10.1	5.3	22.7	54.7	16.6	27.9	46.4	32.2	19.2	9.8	56.7	32.9
SNH2506	62.2	16.6	4.0	27.6	63.2	5.5	30.3	39.9	25.1	7.4	16.7	33.8	24.6
mean	32.2	9.7	7.1	16.3	35.7	5.6	18.1	41.2	24.3	23.6	14.4	36.5	28.0
LSD_{0.05}	2.3	0.04	0.04		6.5	0.01		0.82	0.17	0.21	0.23	0.21	

The most sensitive genotype with the highest disease level was established in Kosovo on hybrid SNH 2506 (30.3%). The differences between hybrids and location were statistically verified ($LSD_{0.05} = 6.6$) and are summarized in Table 3. The final grain yield ($t\ ha^{-1}$) in maize is considered to be a combined effect of various yield components, like number of ear bearing plants, number of ears per plant, number of grains per ear, weight of grains per ear and 1000 grain weight. The significant differences among the maize genotypes for yield losses (%) were also determined and are summarized in Table 2 as well. Based on the results of ANOVA, the maize genotypes are differed in yield losses. The mean yield losses across maize genotypes were 28.0%. It is evident from our results at three sites in 2013, that the maximum yield loss was determined for maize genotypes BC354 (38.6%). The loss was +10.6% higher than the overall mean. The average value of yield loss for 2013 was 29.7%. The genotypes with the highest yield losses in 2013 in Kosovo was SNH2504 with 50.6%, in Albania BC 572 (32.2%) and in Austria BC 354 (46.2%). While in 2014 in Kosovo it was genotype BC572 (56.7%) and in Albania LMP-3 with 22.9% yield losses. For 2013 the highest average value of yield loss was obtained in Kosovo (41.2%), followed by Albania (24.3%) and Austria (23.6). Also in 2014 higher yield losses occurred in Kosovo (36.5%) followed by Albania (14.4%). Overall average yield losses in 2014 (over both countries) were 25.5%, which was 4.2% lower than in the year 2013.

The experimental average values of diseased ear area with *Fusarium* for the years 2013 and 2014 were 16.3 and 18.1%, respectively. In 2013 the highest percentage of ear area was found with maize genotype SNH 2506 (+11.0%), while the lowest value was determined for the maize genotype SBL-1 (-13.0%). For 2014 the highest value characterized the maize genotype BC 678 (+15.0%), while the lowest value was found with LMP-1 (17%).

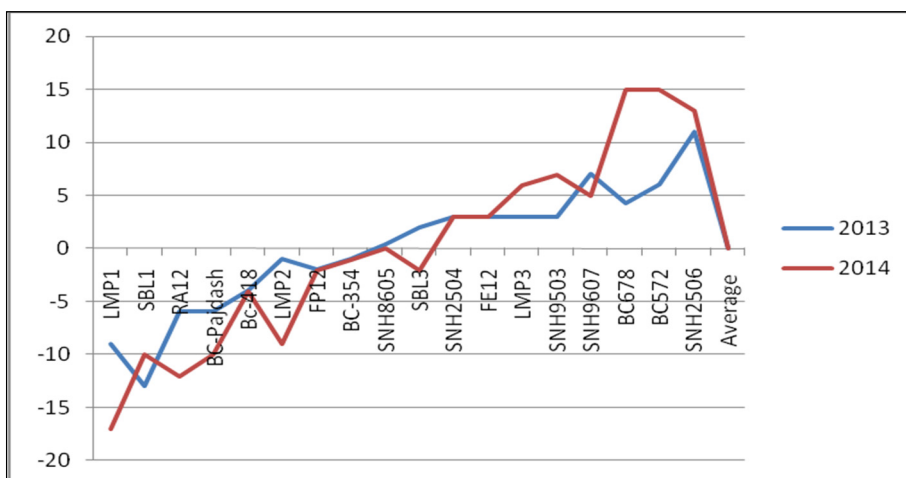


Fig.1. Average deviations from experimental values of disease severity

Discussion

Maize is predominantly attacked by *F. graminearum*, *F. moniliforme*, *F. proliferatum* and *F. subglutinans*. These species differ in their climatic distribution and in the optimum climatic conditions required for their persistence (20). This review deals with the influence of climate on the production and dispersal of inoculate, growth, competition, mycotoxin production and pathogenicity. The level of incidence of *Fusarium* ear rot is highly depended on the year, location, hybrid and weather conditions (8). This was visible in our two years study by the variability in resistance between genotypes after inoculation but also natural infection (diseased ear area ranking from 3.1% to 36.3%) and genotype by location interaction: in Kosovo (32%), followed by Albania (9.7%) and Austria (7.1%) differences in diseased ear were highly significant. Resistance ranking in Austria was significantly different from the ranking in both other countries. Based on results achieved over both years the best genotypes were the landrace LMP-1 from Kosovo (5.4%) and the Austrian hybrid SBL-1 (6.1%). Based on morphological characters, the most frequently *Fusarium* spp. identified on maize kernels in local farmers in Albania were *Fusarium subglutinans*, *Fusarium verticillioides*, *Fusarium proliferatum* and *Fusarium graminearum*. These toxigenic *Fusarium* species isolated from maize are in accordance with previous research in other countries

in Europe (6,21,13, and 14), in Switzerland (15) and Kosovo (16). The level of incidence and the composition of *Fusarium* species are also highly dependent on the year, location, and hybrid and by weather conditions (12, 15, and 14). From some investigations is found out that *Fusarium graminearum* were dominated in the relatively humid vegetation periods (12). Especially in the unusually warm vegetation period a significant increase in the incidence of *Fusarium proliferatum* could be observed. But the occurrence of the chief moniliformin producer *Fusarium subglutinans* remained largely uninfluenced by any climatic variation. While in North Switzerland the most frequently *Fusarium* species identified were *Fusarium graminearum*, *Fusarium verticillioides*, *Fusarium subglutinans*, *Fusarium proliferatum* and *F. crookwellense* in South Switzerland *Fusarium verticillioides* was the dominated *Fusarium* species identified (15). The white maize landrace is characterised with a long history and with higher value for different purpose. This preliminary information suggests the hypothesis that the local maize populations that are selected and adapted to the agro-ecological conditions for centuries from our farmers, are more tolerant to environmental stress. The success of genetic improvement of maize yield depends on several factors such as initial sources of genes (initial parental material), improvement method, types of the gene actions involved in yield control, inheritance and genetic control of related traits such as capacity of production (22). The most sensitive genotype with the highest disease level in Kosovo was hybrid SNH 2506 (30.3%). Although today more and more maize breeding programmes at both public and private institution worldwide are initiated and expanded to develop resistance in breeds and hybrids for both human and animal consumption (23), for these two countries this is just the start. Identifying the most sensitive maize genotypes gives the possibility to eliminate such genotypes for practical use. Thereby, the FER resistance could be immediately increased and the risk for toxin contamination effectively reduced.

Conclusions

In conclusion we found a large variability of the resistance against *Fusarium graminearum* between genotypes after inoculation or natural infection within the countries and highly significant differences between maize genotypes. The investigated hybrids and maize populations come from different institutions and involve distinct genetic and physiological backgrounds. In order to obtain reliable data for FER resistance, investigations in different environments (locations and/or years) are required. The used landraces (especially those from Kosovo) seem to possess genetically resistance resources which could be used for further breeding activities in order to find genotypes more resistant against FER. We recommend to continue the investigation with more landraces that the Faculty of Agriculture in Prishtina and the Centre for Genetic Recourses in Tirana preserve since several years and at different locations in these countries in order to get reliable data for the disease resistance. The investigation suggests that the local maize population LMP-1 represents a highly valuable genetic material for resistance that could be successively used for further breeding.

Acknowledgements

The work presented in this paper is part of the project “**Research Cooperation and Networking between Austria, Kosovo and the Western Balkan Region**” supported by the Austrian Ministry of Research and operated by the Centre for Social Innovation.

References

- [1] Aliu S., Rusinovci I., Fetahu Sh., and E. Simeonovska. Genetic diversity and correlation estimates for grain yield and quality traits in some Kosovo local maize (*Zea mays* L.) populations. *Acta Agriculturae Slovenica*, 2012, 99, 121-128.
- [2] Elezi F., Ibraliu A., B. Gixhari. Collecting maize landraces in Albania. *International Journal of Ecosystems and Ecology Sciences (IJEES)*, 2014, 4, 57-60.
- [3] Aliu S., Fetahu, S. And L. Rozman. Variation of physiological traits and yield components of some maize hybrid (*Zea mays* L.)

- in agro ecological conditions of Kosovo. *Acta Agriculturae Slovenica*, 2010, 95, 35–41.
- [4] Elezi F., Hajkola, K. And A. Ibraliu. Morphological characterization of some maize landraces. *Albanian Journal of Agricultural Science*, 2013, 12, 3.
- [5] Nelson P.E., Toussoun T.A. and W.F.O. Marasas. *Fusarium species: an illustrated manual for identification*. The Pennsylvania State University Press, University Park, Pennsylvania, 1983, USA.
- [6] Logrieco A., Mulè, G., Moretti, A. and A. Bottalico. Toxigenic *Fusarium* species and mycotoxins associated with maize ear rot in Europe. *European Journal of Plant Pathology*, 2002, 108, 597–609.
- [7] Shurtleff M.C. *Compendium of corn diseases*. 3rd ed., The American Phytopathological Society Press, St. Paul, Minnesota, 1986, USA.
- [8] Mesterházy Á., Lemmens, M. and M. Ried. Breeding for resistance to ear rots caused by *Fusarium* spp. in maize – a review. *Plant Breeding*, 2012, 131, 1–19.
- [9] Munkvold. G.P. Epidemiology of *Fusarium* diseases and their mycotoxins in maize ears. *European Journal of Plant Pathology*, 2003, 109, 705–713.
- [10] Lević J. T., Stanković, S.Ž., Krnjaja, V.S. and A.S. Bočarov-Sančić. *Fusarium* species. The occurrence and the importance in agriculture of Serbia. Proceedings of the National Academy of Sciences, MS Novi Sad, 2009, 116, 33–48.
- [11] Ivić D., Domijan, A.M., Peraica, M., Milicević, T. and B. Cvjetković. *Fusarium* spp. contamination of wheat, maize, soybean, and pea grain in Croatia. *Arhiv za Higijenu Rada i Toksikologiju*, 2009, 435–442.
- [12] Lew H., Adler, A., Edinger, W., Brodacz, W., Kiendler, E. and J. Hinterholzer. *Fusarium* species and their toxins in Austrian maize. *Die Bodenkultur*, 2001, 52, 199–207.
- [13] Folcher L., Jarry, M., Weissenberger, A., Gerault, F., Eychenne, N., Delos, M. and C. Regnault-Roger. Comparative activity of agrochemical treatments on mycotoxin levels with regard to corn borers and *Fusarium* mycoflora in maize (*Zea mays* L.) fields. *Crop Protection*, 2009, 28, 302–308.
- [14] Goertz A., Zuehlke, S., Spitteller, M., Steiner, U., Dehne, H.W., Waalwi, D., de Vreis, I. and E.C. Oerke. *Fusarium* species and mycotoxin profiles on commercial maize hybrids in

- Germany. *European Journal of Plant Pathology*, 2010, 128, 101–111.
- [15] Dorn B., Forrer, H.R., Schürch, S. and S. Vogelgsang. *Fusarium* species complex on maize in Switzerland: occurrence, prevalence, impact and mycotoxins in commercial hybrids under natural infection. *European Journal of Plant Pathology*, 2009, 125, 51–61.
- [16] Shala-Mayrhofer, V., Marjakaj, R., Berthiller, F., Musolli, A., Berisha, D., Kelmendi, B. And M. Lemmens. Occurrence of *Fusarium* ear rot, morphological identification of *Fusarium* species and mycotoxin contamination on maize in Kosovo. *Food Additives & Contaminants: Part B*, 2013, 6, 237–243.
- [17] Isufi L and F. Mercuri. Inventarizimi i semundjeve dhe i demtuesve ne kulturat grure, miser, oriz e patate ne disa zona ekologjike te vendit. Buletini i Shkencave Bujqësore (Albania).1986, September 3, 95–102.
- [18] Hydro-Meteorological Institute of Kosovo. Data base for sum of Temperatures and Rainfall..HMIK.2014. Prishtina.
- [19] Reid L.M. and R.I. Hamilton. Screening maize for resistance to gibberella ear rot. Agriculture and Agri-Food Canada, *Research Branch*, 1996, Ottawa, Canada.
- [20] Doohan F.M., Brennan, J. and B.M. Cooke . Influence of climatic factors on *Fusarium* species pathogenic to cereals. *European Journal of Plant Pathology*.2003, 109, 755–768.
- [21] Domijan A-M., Peraica, M., Jurjević, Ž., Ivić, D. And B. Cvjetković. Fumonisin B₁, fumonisin B₂, zearalenone and ochratoxin A contamination of maize in Croatia. *Food Additives and Contaminants*, 2005. 677–680.
- [22] Rezaei A., Yazdisamadi, B., Zali, A., Tallei, A., Zeinali H. and A. Rezaei. Estimate of heterosis and combining ability in maize (*Zea mays* L.) using diallel crossing method. In: Vollmann, J., Grausgruber, H. and P. Ruckebauer (Eds.): Proceedings of the 17th XVII EUCARPIA, General Congress.2004, 395–398.
- [23] Mesterházy Á. Relationship between resistance to stalk rot and ear rot of corn influenced by rind resistance, premature death and the rate of drying of the ear. *Maydica*.1983, 28, 425–437.

Studimi i rezistencës së gjenotipeve të misrit të Kosovës, Shqipërisë dhe Austrisë ndaj kërpudhës *Fusarium graminearum*

Vitore Shala-Mayrhofer, Sali Aliu, Valbona Hobdari, Fetah Elezi, Blerina Rexhepi, Ana Koci, Hans-Peter Kaul, Marc Lemmens

Përmbledhje

Objektivë e studimit ishte identifikimi i disa gjenotipeve të misrit (*Zea mays* L.) për rezistencë ndaj kërpudhës *Fusarium graminearum* në tre lokalitete; Kosovë, Austri dhe Shqipëri. Eksperimentet janë realizuar në tri lokalitete (L) sipas metodës së rastit me tri përsëritje. Në hulumtim janë përfshirë 18 gjenotipe për çdo lokalitet. Çdo fushë eksperimentale ka konsistuar në minimum prej 100 bimësh, ku 90 bimë janë analizuar për infeksion natyral dhe te inokuluar. Procedura e inokulimit të bimëve me *Fusarium spp* ishte ajo standarde për këtë natyrë të punës. Bimët e misrit janë infektuar në periudhën e lulëzimit femëror ♀ (një javë pas lulëzimit) dhe më pas infeksioni është analizuar në përfundim të periudhës së pjekurisë së plotë. Në hulumtimet tona është identifikuar variabilitet i gjerë për rezistencë ndaj *Fusarium spp*, vlera të cilat oscilojnë prej 3.1% deri 27.6% për vitin 2013 dhe 36.3 % në vitin 2014. Shkallë e lartë e paraqitjes së sëmundjes në vitin 2013 ishte në Kosovë (31.9%), e përcjellë nga Shqipëria (9.7%) dhe Austria (7.1%). Kurse gjatë vitit 2014, vlerë të lartë për shkallë të infeksionit kishte Kosova (35.7%), kurse Shqipëria ishte në shkallë më të vogël (5.6%). Në ekspresion të realizimit të vlerave përveç faktorit biotik, gjithashtu ishte prezent edhe bashkëveprimi ndërmjet gjenotipit dhe vitit (GjxV) që ishte me vlerë të lartë sinjifikante. Në lokalitetin e Austrisë gjithashtu të pranishme ishin edhe dallimet e potencuara më lart, kështu që ka rezultuar me humbje të rendimentit të misrit prej 19.5 deri 24.6%. Nga rezultatet e realizuara për dy vjet hulumtimi në tri lokalitete janë veçuar gjenotipet e populacioneve lokale të Kosovës (LMP-1) dhe gjenotipi hibrid me origjinë nga Austria SBL-1.

Guide for authors:

Paper submitted in electronic version by mail will be considered for publication in Research.

Research welcomes original research papers which may contain original articles, reviews and short Communications.

Journal covers Natural and Applied Sciences specified in series A, B etc. Articles are to be presented in English with summary in Albanian.

Paper considered for publication in **Research** must not have been previously published elsewhere. Each submitted manuscript will be reviewed, the final decision concerning its acceptance resting with the editors. The manuscript should conform to the formal standards of the Journal available on our web site

http://www.ashak.org/repository/docs/GENERAL_INFORMATION_FOR_THE_JOURNAL_770777.pdf **ashak@ashak.org**.

A single Word and PDF file containing text, tables, figures, references, etc. should be provided.

Udhëzime për autorët

Punimi i dorëzuar në formë elektronike me e-mail do të merret në shqyrtim për publikim në revistën Research-Kërkime.

Revista Research-Kërkime mirëpret punimet origjinale, revyale dhe kumtesat e shkurtra.

Revista përfshinë Shkenecat e Natyrës dhe të Zbatuara të specifikuar në seri A, B. Artikujt duhet të shkruhen në gjuhën angleze me rezyme në gjuhën shqipe.

Punimi i dorëzuar për botim në Research nuk duhet të jetë në shqyrtim ose i publikuar në ndonjë revistë tjetër. Dorëshkrimi i dorëzuar do të recensohet dhe vendimi përfundimtar i pranimit të tij iu mbetet kryeredaktorit të revistës. Dorëshkrimi duhet të jetë konform standardeve formale të revistës që është në dispozitim në ueb faqen tonë

http://www.ashak.org/repository/docs/INFORMATE_E_PERGJITHSHME_PER_REVISTEN_188742.pdf

Autorët duhet të përgatisin një kopje të punimit që përmban tekstin, tabelat, figurat, referencat etj. në versionin Word dhe në PDF

RESEARCH 23 KËRKIME

2018

Botues:
AKADEMIA E SHKENCAVE DHE E ARTEVE E KOSOVËS

Lektor:
Shefqet Riza

Redaktor teknik:
ASHAK

Realizimi kompjuterik:
ASHAK

Madhësia: 8.5 tabakë shtypi
Tirazhi: 200 copë
Formati: 16x24 cm

Shtypi:
Focus Print
Shkup

Subscription orders should be addressed to - Porositja mund të bëhet në këtë adresë:
Kosova Academy of Sciences and Arts
Akademia e Shkencave dhe e Arteve e Kosovës
Rr. "Agim Ramadani" Nr. 305, 10000 Prishtinë, Republika e Kosovës
Tel.+383(0) 38249 303; e-mail: ashak@ashak.org